

بِسْمِ اللَّهِ الرَّحْمَنِ الرَّحِيمِ

**Computational Analysis for Non-linear Flow Problems with  
Activation Energy**



By

**Sumaira Jabeen**

**Department of Mathematics  
Quaid-I-Azam University  
Islamabad, Pakistan  
2021**

**Computational Analysis for Non-linear Flow Problems with  
Activation Energy**



By

**Sumaira Jabeen**

Supervised by

**Prof. Dr. Tasawar Hayat**

**Department of Mathematics  
Quaid-I-Azam University  
Islamabad, Pakistan  
2021**

**Computational Analysis for Non-linear Flow Problems with  
Activation Energy**



By

**Sumaira Jabeen**

A THESIS SUBMITTED IN THE PARTIAL FULFILLMENT OF THE REQUIREMENT FOR  
THE DEGREE OF

**DOCTOR IN PHILOSOPHY**

IN

**MATHEMATICS**

Supervised by

**Prof. Dr. Tasawar Hayat**

**Department of Mathematics  
Quaid-I-Azam University  
Islamabad, Pakistan**

**2021**

## Author's Declaration

I **Sumaira Jabeen** hereby state that my PhD thesis titled **Computational Analysis for Non-linear Flow Problems with Activation Energy** is my own work and has not been submitted previously by me for taking any degree from the Quaid-I-Azam University Islamabad, Pakistan or anywhere else in the country/world.

At any time if my statement is found to be incorrect even after my graduate the university has the right to withdraw my PhD degree.

Name of Student:  **Sumaira Jabeen**

Date: **12-08-2021**

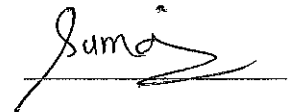
## **Plagiarism Undertaking**

I solemnly declare that research work presented in the thesis titled "**Computational Analysis for Non-linear Flow Problems with Activation Energy**" is solely my research work with no significant contribution from any other person. Small contribution/help wherever taken has been duly acknowledged and that complete thesis has been written by me.

I understand the zero tolerance policy of the HEC and **Quaid-I-Azam University** towards plagiarism. Therefore, I as an Author of the above titled thesis declare that no portion of my thesis has been plagiarized and any material used as reference is properly referred/cited.

I undertake that if I am found guilty of any formal plagiarism in the above titled thesis even afterward of PhD degree, the University reserves the rights to withdraw/revoke my PhD degree and that HEC and the University has the right to publish my name on the HEC/University Website on which names of students are placed who submitted plagiarized thesis.

Student/Author Signature: \_\_\_\_\_

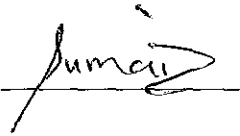


Name: **Sumaira Jabeen**

## Certificate of Approval

This is to certify that the research work presented in this thesis entitled Computational Analysis for Non-linear Flow Problems with Activation Energy was conducted by Ms. Sumaira Jabeen under the kind supervision of Prof. Dr. Tasawar Hayat. No part of this thesis has been submitted anywhere else for any other degree. This thesis is submitted to the Department of Mathematics, Quaid-I-Azam University, Islamabad in partial fulfillment of the requirements for the degree of Doctor of Philosophy in field of Mathematics from Department of Mathematics, Quaid-I-Azam University Islamabad, Pakistan.

Student Name: Sumaira Jabeen

Signature: 

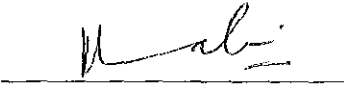
External committee:

a) External Examiner 1:

Name: Dr. Nasir Ali

Designation: Associate Professor

Office Address: Department of Mathematics & Statistics, International Islamic University, Sector H-10 Islamabad.

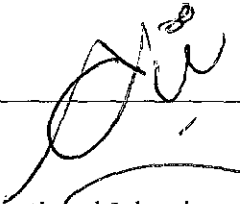
Signature: 

b) External Examiner 2:

Name: Dr. Tariq Javed

Designation: Associate Professor

Office Address: Department of Mathematics & Statistics, International Islamic University, Sector H-10 Islamabad.

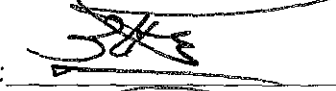
Signature: 

c) Internal Examiner

Name: Dr. Tasawar Hayat

Designation: Professor

Office Address: Department of Mathematics, QAU Islamabad.

Signature: 

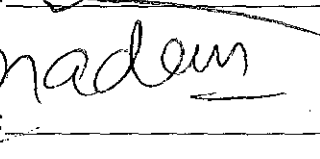
Supervisor Name:

Prof. Dr. Tasawar Hayat

Signature: 

Name of Dean/HOD:

Prof. Dr. Sohail Nadeem

Signature: 

# Computational Analysis for Non-linear Flow Problems with Activation Energy

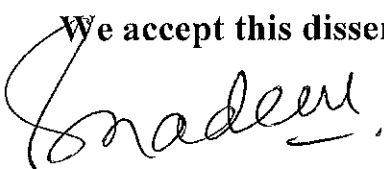
By

**Sumaira Jabeen**

CERTIFICATE

A THESIS SUBMITTED IN THE PARTIAL FULFILLMENT OF THE  
REQUIREMENTS FOR THE DEGREE OF THE  
DOCTOR OF PHILOSOPHY IN MATHEMATICS

We accept this dissertation as conforming to the required standard

1.   
\_\_\_\_\_


**Prof. Dr. Sohail Nadeem**  
(Chairman)

2.   
\_\_\_\_\_

**Prof. Dr. Tasawar Hayat**  
(Supervisor)

3.   
\_\_\_\_\_

**Dr. Nasir Ali**  
Associate Professor  
Department of Mathematics & Statistics  
International Islamic University,  
Sector H-10 Islamabad  
(External Examiner)

4.   
\_\_\_\_\_

**Dr. Tariq Javed**  
Associate Professor  
Department of Mathematics & Statistics  
International Islamic University,  
Sector H-10 Islamabad.  
(External Examiner)

**Department of Mathematics**  
**Quaid-I-Azam University**  
**Islamabad, Pakistan**  
**2021**



# Dedicated

## to

my family especially my father (Muhammad Ashraf) whose constant love, support and encouragement have put me where I am now.

## Preface

Mass transfer effects in fluid mixture are observed due to concentration variation of species in fluid. This variation occurs in a fluid when species moves from a higher concentration region to a lower concentration. Further the energy obtained by reactants before a chemical reaction can occur is referred to as activation energy. This is also called as a minimum required energy to initiate a reaction. Mass transfer phenomenon subject to activation energy is encountered in chemical and geothermal engineering, cooling of nuclear devices, mechanism comprised of (oil, water) suspension and food making.

Significance of non-Newtonian fluids is observed through its extensive biological and industrial applications. These fluids are quite prevalent in engineering processes. Examples of such fluids may include plastic molding, polymers and paper making, soaps, cosmetics, foams, lubricant, in processed food and mixture of oil etc. Mathematically the flows of these materials cannot be studied by Navier-Stokes equations. One constitutive relationship between shear stress and deformation rate for such fluids is not appropriate. Thus to overcome this issue, numerous models of non-Newtonian materials like differential, integral and rate types have been suggested in order to explain the rheological properties. Differential type fluid explores the characteristics of normal stress, shear thinning and shear thickening. Second grade/third grade and power law materials belonging to the subclasses of differential type models show normal stress/shear thinning and thickening properties. Relaxation and retardation times features are captured by rate type fluids. Rate type models include Jeffrey, Maxwell, Oldroyd, Burgers and generalized Newtonian models. In general the differential equations for non-Newtonian fluids are higher than Navier-Stokes equations. The solutions thus require more boundary conditions. This thesis consists of seven chapters.

Chapter one comprised some basic concepts which includes activation energy, nanofluid, thermal radiation, entropy, Darcy-Forchhemier flow, stratification and Cattaneo-Christov theory. Conservation laws and solution procedure are highlighted.

Chapter two reports the double stratification and activation energy in flow of tangent hyperbolic fluid. Flow is induced by nonlinear stretching sheet of variable thickness. Heat flux by Cattaneo-Christov theory is implemented. Non-linear system is computed for the convergent solutions. The data of this chapter is published in **International Journal of Numerical Methods for Heat & Fluid Flow**.

Chapter three focused on mixed convection flow of tangent hyperbolic liquid. Joule heating, double stratification, non-linear thermal radiation, Brownian motion and thermophoresis are present. Phenomenon of mass transfer is examined by activation energy along with binary chemical reaction. Computations of convergent solutions are carried out for the nonlinear mathematical system. Contents of this chapter are published in **Scientia Iranica**.

Chapter four disclosed the effects of Joule heating and entropy generation minimization for steady flow of third grade nanomaterial. A significant perspective of this attempt is to address the influences of activation energy and chemical reaction. Modified Arrhenius function is utilized to investigate the activation energy. Convergent homotopic solutions of resulting non-linear system are developed. Data of this chapter is submitted for publication in **International Communication in Heat and Mass transfer** for publication.

Chapter five addressed the entropy generation in flow of Walters-B nanomaterial. Energy equation consists of Ohmic heating, radiation and heat generation. Binary chemical reaction with modified Arrhenius energy is employed. The consequences

of thermophoresis, Brownian motion and viscous dissipation are accounted. Convergent solutions by homotopy analysis technique are constructed. Data of this chapter is published in **Scientia Iranica**.

Chapter six focused on consequences of activation energy for magneto-nanoparticles considering zero mass flux condition. Fluid flow in porous space is analyzed by using Darcy-Forchheimer model. Additionally, the significance of thermal radiation is discussed. Aspects of thermophoresis and Brownian motion are observed. Influences of convective and zero mass flux conditions at boundary are examined. Systems of partial differential equations are reduced in to ordinary differential equations by employing transformation technique. Modeled system is solved numerically and the involved parameters outcomes discussed through graphs.

Chapter seven reported the impact of entropy generation for steady flow of second grade nanomaterial with thermal radiation. Main theme of this formulation is to analyze the significance of activation energy and chemical reaction under assumed convective and zero mass flux conditions at boundary. Appropriate non-dimensional variable have been employed to get ordinary differential system. Convergent series solution is derived by using homotopic technique. The solutions are explored with respect to pertinent variables. The contents of chapters six and seven are submitted for publication in **International Communication in Heat and Mass transfer**.

# Contents

<b>1</b>	<b>Literature review and basic concepts</b>	<b>4</b>
1.1	Literature review . . . . .	4
1.2	Basic laws . . . . .	8
1.2.1	Mass conserved law . . . . .	8
1.2.2	Momentum conserved law . . . . .	9
1.2.3	Energy conserved law . . . . .	9
1.3	Solution technique . . . . .	10
<b>2</b>	<b>Flow of tangent hyperbolic liquid subject to activation energy and stratification</b>	<b>11</b>
2.1	Introduction . . . . .	11
2.2	Mathematical formulation . . . . .	11
2.3	Solutions . . . . .	15
2.4	Convergence analysis . . . . .	15
2.5	Analysis . . . . .	17
2.6	Conclusions . . . . .	21
<b>3</b>	<b>Chemical reaction in flow of hyperbolic tangent fluid</b>	<b>23</b>
3.1	Introduction . . . . .	23
3.2	Modeling . . . . .	23
3.3	Solution expressions . . . . .	28
3.4	Convergence . . . . .	28
3.5	Discussion . . . . .	29

3.6	Conclusions . . . . .	36
<b>4</b>	<b>Entropy generation minimization and activation energy in flow of third grade fluid</b>	<b>38</b>
4.1	Introduction . . . . .	38
4.2	Statement . . . . .	38
4.2.1	Physical quantities of interest . . . . .	41
4.2.2	Investigation of entropy generation . . . . .	42
4.3	Solutions by homotopy analysis method . . . . .	43
4.4	Convergence analysis . . . . .	44
4.5	Discussion . . . . .	45
4.5.1	Entropy rate analysis and Bejan number . . . . .	49
4.6	Conclusions . . . . .	54
<b>5</b>	<b>Entropy generation optimization and activation energy in flow of Walters-B nanomaterial</b>	<b>56</b>
5.1	Introduction . . . . .	56
5.2	Modeling . . . . .	56
5.2.1	Entropy generation examination . . . . .	60
5.3	Solution methodology . . . . .	61
5.4	Convergence analysis . . . . .	61
5.5	Discussion . . . . .	62
5.5.1	Entropy rate analysis . . . . .	66
5.6	Conclusions . . . . .	68
<b>6</b>	<b>Characteristics of activation energy on Darcy-Forchheimer flow with zero mass flux condition</b>	<b>69</b>
6.1	Introduction . . . . .	69
6.2	Formulation . . . . .	69
6.3	Discussion . . . . .	72
6.4	Conclusion . . . . .	77

<b>7 Irreversibility analysis for second grade nanomaterial with zero mass flux at stretching boundary</b>	<b>79</b>
7.1 Introduction . . . . .	79
7.2 Flow analysis . . . . .	79
7.2.1 Physical Quantities of interest . . . . .	82
7.2.2 Entropy generation analysis: . . . . .	83
7.3 Solutions by homotopy analysis method . . . . .	84
7.4 Convergence . . . . .	84
7.5 Analysis . . . . .	86
7.6 Conclusion . . . . .	93

# Chapter 1

## Literature review and basic concepts

This chapter comprised the literature review of concepts including activation energy, non-Newtonian fluid, nanofluid, thermal radiation, entropy, Cattaneo-Christov theory, Darcy-Forchheimer flow, stratification and some basic definitions of flow.

### 1.1 Literature review

Phenomena's related to oil reservoir and geothermal engineering followed the chemically charged system having species in chemical reaction with Arrhenius activation energy. It is necessary to formulate theoretical results other than experimental approach, to calculate the influence of activation energy about fluid flow. Interaction between chemical reaction and mass transfer is complicated. This type of interaction can be seen in production and implementation of reactant species at diverse rates, mutually in mass transport and inside the fluid. Minimum amount of energy required for chemical reaction termed as activation energy, can be calculated by employing Arrhenius calculations that elaborates how a proportion constant varies through temperature. Activation energy of mostly elements when reacted with other elements are resulted as zero. A fixed amount (threshold rate) of activation energy is needed for any element to react in a chemical system. This energy limit is characterized as a barrier between two different forms of energy. To initiate any reaction, this range must be reached. To continue the reaction process, there must have other energy limits of elements which are needed translational energy that is larger or at least equal to activation energy. That's why largest energy obstacle is



the activation energy. By using Maxwell distribution, the elements having energy greater than that energy obstacle will pass through the threshold value. So one can say that largest energy of obstacle is the activation energy. The obstacle shape as well as drilling of elements are also ignored but the number of elements having sufficient energy to carry on the reaction is entirely rely on energy. Because of this exponential function of temperature is included. Usually such chemical reaction is categorized by a biochemical variation and as a result multiple products are formed with distinct properties as compared to reactant species. Since these reactions are essential for manufacturing process in several industrial applications. Such forms of reactions are frequently occurred in reactors and restrict up to grade of mass transfer attained. In order to get maximum output, it is vital to make a reaction more vigorous, reduces the quantity of reagents and energy inputs. Effectiveness of chemical reaction in binary reaction model for vertical pipe along activation energy is investigated by Bestman et al. [1]. Maleque [2] explored the impact of activation energy on MHD flow in occurrence of viscous dissipation and heat source/sink. Current contributions can be seen through the studies [3-10] and references therein.

Thermal radiation involves electromagnetic radiations transmitted due to the thermal motion of the fluid particles almost in entire directions. Process of thermal radiation is observed in heating of the bodies by diverse means like solar light, fire and radiator. Heat transfer with radiation has extensive industrial applications including atomic reactor security, boiler design, heat exchangers, power stations and much propulsion equipment's for missiles, aircraft, in space automobiles and satellites. Radiative heat change in energy equation is measured by Rosseland calculation. Few recent efforts about this aspect can be observed through the refs. [11-20].

Stratification is a process of developing layers through temperature and concentration variation or influence of different fluids. Through simultaneous effects of heat and mass transfer, it is important to analyze the effectiveness of thermal and solutal stratification concerned with stratification of fluid medium in view of heat convection and mass transfer because of convective motion of nanofluids. Study of mixed convection with double stratification is observed in diverse industrial and engineering applications. This phenomenon has dominant role on polymer extrusion, in hydraulic flow of thermal fluids, geothermal reservoirs, volcanic flows and geological systems. Number of studies have been attempted yet through involvement of this

phenomena [21-30].

Fluid transport through a porous media is gain substantial attention among the researchers because of their presence in several processes related to geophysics, pharmacy and chemical industry. Such processes include water flow in reservoirs, energy and grain storage units, Crude oil extraction and solar thermal collectors. Classical Darcy's law is usually employed to model and develop the problem involving porous media. This law states that the sum of pressure gradient and gravitational force is proportional to the mean velocity of fluid particles. Darcy's law is applicable on the problem of lower velocity and minor porosity. It is ineffective in the situation where inertial and boundary effects can occur at higher rate of fluid flow. Contrarily, for higher Reynolds number it is not suitable to ignore the inertial effects. To overcome this issue, Forchheimer [31] added a velocity term in the expression of Darcian velocity to predict the influences of inertia and boundary. Muskat [32] named this term as "Forchheimer term" which always holds for high Reynolds number. Mukhopadhyay et al. [33] studied the radiative flow in a Darcy-Forchheimer porous medium with forced convection. Stretched flow of Maxwell material in Porous media with heterogeneous and homogeneous reactions is discussed by Sadiq et al. [34]. Darcy-Forchheimer flow of third grade liquid subject to non-Fourier heat flux theory analyzed numerically by Hayat et al. [35]. Some recent contributions in this regard can be seen through refs. [36-40].

In branch of thermodynamics, entropy of any system is defined as the quantity of inaccessible energy. It corresponds to the irreversibilities in studied system which is mainly used in thermodynamically design setups. Higher entropy loss consumes energy and influence the efficiency of system. Entropy defines the way according to which physical quantities easily separated from its constituents. When thermal energy is supplied to the system, internal energy increased and as a result thermal entropy of system enhanced. Irreversible processes are defined as the systems in which surroundings of related system are not able to reach at its initial state. Entropy also defines about the consumption of energy in a system. System changes due to gradient. Its sometimes refer as temperature gradient that represents energy transfer or may be a concentration gradient that represents mass transfer. Gradient of system mostly causes irreversibility within a system. Sine entropy relates to the disorderedness of the system due to which energy decreased and lead to decrease in potential of work. Pioneering work on this

phenomenon is done by Bejan [41]. Later on, he discussed entropy generation in process of heat loss during motion of fluid [42]. Moreover, several researchers done in this regards to inspect such phenomena under certain assumptions. Recently, Liu et al. [43] elaborated irreversibility's within curved channel in EMHD flow. Dissipative flow phenomena in a Williamson fluid over rotating disk with entropy generation is analyzed by Qayyum et al. [44]. Akbarzadeh et al. [45] explained irreversibilities in a turbulent nanofluid flow by considering solar stoves through crenelated absorber plates. Bizhaem et al. [46] deliberated heat exchange and irrversibilities of laminar flow in helical tube. In this problem, numerical technique is used to solve two phase fluid mixture problem. Recent research in this respect can be observed through [47-50].

Extensive applications of developing nanotechnology in class of thermal engineering give rise to a new branch of heat transfer fluids termed as nanofluids. In formation of nanofluid, fibers, solid particles or tubes having length of order 1-50 nm are dispersed in heat transfer fluid like oil, water and ethylene glycol. These fluids are considered as base fluids. Because of small size and mostly larger surface area of particles, nanofluids possess immense properties including greater thermal conductivity, negligible blockage in flow channels, homogeneity and long-term constancy. Nanofluids have such a substantial features due to which its helpful in several applications regarding heat mechanism like microelectronics, automotive, power stations, fuel chambers, pharmacological methods, hybrid electric engines, cooling engine automobile, caloric controlling, local refrigerator, in crushing process, mining and boiler gas outlet, temperature control and in nuclear field. Nanomaterials acquire a special auditory characteristic that's convenient in ultrasonic demonstration. Additional influence includes shear transformation of an instant compression ray and this property becomes more operative as concentration enhances. Information of the rheological implementation of nanofluids is said to be more influential in view of their stability for convection applications. Pioneering work on nanofluid was done by Choi [51]. Recently, Waini et al. [52] studied the hybrid nanomaterial flow and heat mechanism over a highly nonlinear porous sheet. Sheikholeslami [53] employed numerical approach to analyze the nanofluid flow pattern inside a porous medium. Al<sub>2</sub>O<sub>3</sub>- water nanofluid is utilized in this study. Ely [54] discussed the exact solution of nanomaterials in a porous media along heat source/sink. Further, relevant research can be seen through studies [55-60].

In recent era, the research related to flows of non-Newtonian fluid has attained much atten-

tion due to its substantial uses in industrial and engineering processes. Applications includes making of petroleum, paper production, polymer extraction and in cosmetics. These fluids cannot be categorized as viscous fluid because non-Newtonian fluids are not fully analyzed by single equation. Moreover, the relation between shear rate and strain rate is non-linear. Due to this, various constitutive equations have been presented so far in literature. Non-Newtonian fluids are characterized in two classes in which one is viscoelastic fluids and other termed as shear thinning/thickening fluids. Numerous features of non-Newtonian fluids are examined by researchers. Few recent efforts under this aspect can be observed through the refs. [61-66].

Heat transfer phenomenon has numerous biological and industrial applications including space and nuclear reactor cooling, energy production, biomedical processes, magnetic targeting in drug making and energy transfer in tissues etc. Heat flux model proposed by Fourier [67] named as heat conduction law was the initiative to analyze the mechanism of heat transfer in several practical aspects. As a result of this law, parabolic heat equation is formed which reflects that considered system is instantly affected by initially generated disturbance. This outcome is contradiction to principle of heat conduction. To resolve this problem, numerous amendments have been made in Fourier's law of heat conduction. Amongst these Cattaneo [68] suggested heat conduction law by introducing thermal relaxation time. Such modification generated hyperbolic equation that permits the transport of energy by means of wave transmission. Further, Christov [69] introduced the time and convected derivative in flow of Maxwell fluid considering Cattaneo's model to retain invariant structure. This relation is referred as Cattaneo-Christov heat flux. Recently, this definition of heat flux is adopted in the discussion of flows through studies [70-76].

## 1.2 Basic laws

### 1.2.1 Mass conserved law

Continuity equation in absence of any source/sink is,

$$\frac{\partial \tilde{\rho}}{\partial t} + \nabla \cdot (\tilde{\rho} \tilde{\mathbf{V}}) = 0, \quad (1.1)$$

where  $\tilde{\rho}$  represents fluid density,  $\tilde{\mathbf{V}}$  the velocity and  $t$  denotes time. For ( $\tilde{\rho}$ ) constant, the flow is termed as **incompressible** flow and Eq. (1.1) takes the form,

$$\nabla \cdot \tilde{\mathbf{V}} = 0. \quad (1.2)$$

### 1.2.2 Momentum conserved law

Equation for the motion of fluid is

$$\tilde{\rho} \left( \frac{\partial \tilde{\mathbf{V}}}{\partial t} + \tilde{\mathbf{V}} \cdot \nabla \tilde{\mathbf{V}} \right) = \nabla \cdot \boldsymbol{\tau} + \tilde{\rho} \mathbf{b}. \quad (1.3)$$

In above equation, the terms on the left side are basically the representation of inertial forces while terms on right side denotes body and fluids surface force.

Cauchy stress tensor  $\boldsymbol{\tau}$  for an incompressible fluid is

$$\boldsymbol{\tau} = -\tilde{p}\mathbf{I} + \mu \dot{\mathbf{A}}_1, \quad (1.4)$$

in which  $\mu$  denotes dynamic viscosity.

### 1.2.3 Energy conserved law

Mathematically energy equation can be written as follows

$$\tilde{\rho} c_p \frac{d\tilde{T}}{dt} = \check{k} \nabla^2 \tilde{T} + tr(\boldsymbol{\tau} \mathbf{L}) + \frac{1}{\sigma} \check{\mathbf{J}} \cdot \check{\mathbf{J}} \quad (1.5)$$

where

$$\check{\mathbf{J}} = \sigma (\mathbf{V} \times \mathbf{B}) \quad (1.6)$$

in which  $c_p$  stands for specific heat,  $\tilde{T}$  the fluid temperature,  $\check{k}$  the thermal conductivity,  $\boldsymbol{\tau}$  represents Cauchy stress tensor,  $d/dt$  the material derivative and  $\mathbf{L}$  the velocity gradient.

### **1.3 Solution technique**

Formulated system of equations for flow are categorized as non-linear. It is quite difficult to obtain the solution of such systems. Several techniques are introduced yet to solve highly non-linear simulation including perturbation, Adomian decomposition and homotopy perturbation method. Different limitations are associated with aforementioned techniques. In this thesis, the problems will be solved by employing homotopy analysis technique [77-85]. This method gives freedom to choose parameters, initial guesses and base functions.

## Chapter 2

# Flow of tangent hyperbolic liquid subject to activation energy and stratification

### 2.1 Introduction

This chapter addresses flow of tangent hyperbolic material over a surface of variable thickness. Nonlinear stretching is discussed. Activation energy and double stratification concepts are highlighted. Cattaneo-Christov heat flux is utilized. Convergent solutions for nonlinear system is developed. Velocity, temperature and concentration are examined in detail.

### 2.2 Mathematical formulation

Unsteady stagnation point flow of tangent hyperbolic material towards stretched surface is modeled here. Non-linear stretching velocity is accounted. Non-Fourier heat flux theory is employed for heat transfer. Influence of both thermal and solutal stratification is considered. Effect of activation energy is examined. Heat production due to chemical reaction are observed. Stretching sheet with variable thickness is accounted. Stretching and free stream velocities respectively are  $u = U_w(x) = U_0(x + b)^{\hat{n}}$  and  $U_e(x) = U_1(x + b)^{\hat{n}}$ . Conservation laws for mass,

momentum and energy give

$$\frac{\partial \tilde{u}}{\partial x} + \frac{\partial \tilde{v}}{\partial y} = 0, \quad (2.1)$$

$$\tilde{u} \frac{\partial \tilde{u}}{\partial x} + \tilde{v} \frac{\partial \tilde{u}}{\partial y} = U_e \frac{dU_e}{dx} + \nu(1 - \tilde{n}) \frac{\partial^2 \tilde{u}}{\partial y^2} + \sqrt{2} \nu \Gamma \tilde{n} \frac{\partial \tilde{u}}{\partial y} \frac{\partial^2 \tilde{u}}{\partial y^2}, \quad (2.2)$$

$$\rho c_p V \cdot \nabla \tilde{T} = -\nabla \cdot q, \quad (2.3)$$

$$\tilde{u} \frac{\partial \tilde{C}}{\partial x} + \tilde{v} \frac{\partial \tilde{C}}{\partial y} = D \frac{\partial^2 \tilde{C}}{\partial y^2} - K_r^2 (\tilde{C} - \tilde{C}_\infty) \left[ \frac{\tilde{T}}{\tilde{T}_\infty} \right]^n \exp \left[ \frac{-E_a}{k_1 \tilde{T}} \right], \quad (2.4)$$

in which Cattaneo-Christov heat flux satisfies

$$q + \lambda (V \cdot \nabla q - q \cdot \nabla V + (\nabla \cdot V) q) = -\check{k} \nabla \tilde{T}, \quad (2.5)$$

where  $\check{k}$  denotes thermal conductivity and  $\check{\lambda}$  represents the relaxation time. It is observed that for  $\check{\lambda} = 0$ , Eq. (2.5) reduces to Fourier's expression. The view of incompressibility situation yields Eq. (2.5)

$$q + \lambda (V \cdot \nabla q - q \cdot \nabla V) = -\check{k} \nabla \tilde{T}. \quad (2.6)$$

By Eqs. (2.3) and (2.6) we arrive at

$$\begin{aligned} \left( \tilde{u} \frac{\partial \tilde{T}}{\partial x} + \tilde{v} \frac{\partial \tilde{T}}{\partial y} \right) &= \frac{\check{k}}{\rho c_p} \left( \frac{\partial^2 \tilde{T}}{\partial x^2} + \frac{\partial^2 \tilde{T}}{\partial y^2} \right) - \check{\lambda} \left\{ \tilde{u} \frac{\partial \tilde{u}}{\partial x} \frac{\partial \tilde{T}}{\partial x} + \tilde{v} \frac{\partial \tilde{v}}{\partial y} \frac{\partial \tilde{T}}{\partial y} + \tilde{u} \frac{\partial \tilde{v}}{\partial x} \frac{\partial \tilde{T}}{\partial y} \right. \\ &\quad \left. + \tilde{v} \frac{\partial \tilde{u}}{\partial y} \frac{\partial \tilde{T}}{\partial x} + 2\tilde{u}\tilde{v} \frac{\partial^2 \tilde{T}}{\partial x \partial y} + \tilde{u}^2 \frac{\partial^2 \tilde{T}}{\partial x^2} + \tilde{v}^2 \frac{\partial^2 \tilde{T}}{\partial y^2} \right\}, \end{aligned} \quad (2.7)$$

with conditions

$$\begin{aligned} \tilde{u} &= U_w(x) = U_0(x+b)^{\tilde{n}}, \quad \tilde{v} = 0, \quad \tilde{T} = \tilde{T}_w = \tilde{T}_0 + \check{a}(x+b), \\ \tilde{C} &= \tilde{C}_w = \tilde{C}_0 + \check{e}(x+b) \quad \text{at} \quad y = A_1(x+b)^{\frac{1-\tilde{n}}{2}} \end{aligned} \quad (2.8)$$

$$\begin{aligned} \tilde{u} &\rightarrow U_e(x) = U_1(x+b)^{\tilde{n}}, \quad \tilde{T} \rightarrow \tilde{T}_\infty = \tilde{T}_0 + \check{b}(x+b), \\ \tilde{C} &\rightarrow \tilde{C}_\infty = \tilde{C}_0 + \check{d}(x+b) \quad \text{as} \quad y \rightarrow \infty \end{aligned} \quad (2.9)$$

In above expressions  $\tilde{u}$  and  $\tilde{v}$  depict velocity components in  $x$  and  $y$  directions,  $\Gamma$  the material time constant,  $\tilde{n}$  the power law index,  $\nu$  kinematic viscosity,  $\rho$  fluid density,  $c_p$  specific



heat,  $\mu$  the dynamic viscosity,  $\tilde{T}_0$  reference temperature,  $\check{k}$  thermal conductivity,  $(\check{a}, \check{b}, \check{c}, \check{d})$  the dimensional constants. Further  $\tilde{T}_w$  and  $\tilde{C}_w$  are the constant temperature and solute concentration near the surface while  $\tilde{T}_\infty$  and  $\tilde{C}_\infty$  represent ambient temperature and concentration. Term  $\left[\frac{\tilde{T}}{\tilde{T}_\infty}\right]^n \exp\left[\frac{-E_a}{k_1\tilde{T}}\right]$  in Eq. (2.4) is referred to as the modified Arrhenius function. Here  $k_1 = 8.61 \times 10^{-5} eV/K$  represents the Boltzmann constant,  $n$  the dimensionless constant or rate constant having range  $-1 < n < 1$ ,  $K_r$  the chemical reaction parameter and  $E_a$  the activation energy.

Consider,

$$\begin{aligned}\psi &= \sqrt{\frac{2}{\hat{n}+1}} \nu U_0 (x+b)^{\hat{n}-1} F(\xi) \quad , \quad \xi = y \sqrt{\frac{\hat{n}+1}{2}} \frac{U_0}{\nu} (x+b)^{\hat{n}-1}, \\ \tilde{\Theta} &= \frac{\tilde{T} - \tilde{T}_\infty}{\tilde{T}_w - \tilde{T}_0} \quad , \quad \tilde{\Phi} = \frac{\tilde{C} - \tilde{C}_\infty}{\tilde{C}_w - \tilde{C}_0}.\end{aligned}\tag{2.10}$$

The stream function ( $\psi$ ) satisfying  $\tilde{v} = -\frac{\partial\psi}{\partial x}$  and  $\tilde{u} = \frac{\partial\psi}{\partial y}$  yields

$$\tilde{u} = U_0 (x+b)^{\hat{n}} F'(\xi) \quad , \quad \tilde{v} = -\sqrt{\frac{\hat{n}+1}{2}} \nu U_0 (x+b)^{\hat{n}-1} (F(\xi) + \xi \frac{\hat{n}-1}{\hat{n}+1} F'(\xi))\tag{2.11}$$

Mass conservation is automatically satisfied and Eqs. (2.2) to (2.8) are transformed to

$$(1 - \tilde{n})F'''' + \tilde{n}W e \sqrt{\frac{\hat{n}+1}{2}} F'' F'''' + \frac{2\hat{n}}{\hat{n}+1} A^2 - \frac{2\hat{n}}{\hat{n}+1} (F')^2 + FF'' = 0,\tag{2.12}$$

$$\begin{aligned}\tilde{\Theta}'' + \text{Pr} F \tilde{\Theta}' + \gamma \text{Pr} \left(\frac{\hat{n}-3}{2}\right) F F' \tilde{\Theta}' - \frac{\hat{n}+1}{2} F^2 \tilde{\Theta}'' + \\ \text{Pr}(S_{\tilde{\theta}} + \tilde{\Theta})(\gamma F F'' - \frac{2\hat{n}}{\hat{n}+1} \gamma F'^2 - \frac{2}{\hat{n}+1} F') = 0,\end{aligned}\tag{2.13}$$

$$\tilde{\Phi}'' + Sc F \tilde{\Phi}' - \frac{2}{\hat{n}+1} Sc \left(S_{\tilde{\phi}} F' + F' \tilde{\Phi}\right) - \sigma \frac{2}{\hat{n}+1} Sc [1 + \tilde{\Theta}\beta]^n \exp\left[\frac{-\hat{E}}{1 + \tilde{\Theta}\beta}\right] = 0,\tag{2.14}$$

$$\begin{aligned}F(\delta) &= \delta \frac{1-\hat{n}}{1+\hat{n}}, \quad F'(\delta) = 1, \quad F'(\infty) = A \\ \tilde{\Theta}(\delta) &= 1 - S_{\tilde{\theta}}, \quad \tilde{\Theta}(\infty) = 0, \\ \tilde{\Phi}(\delta) &= 1 - S_{\tilde{\phi}}, \quad \tilde{\Phi}(\infty) = 0.\end{aligned}\tag{2.15}$$

In above expression  $\delta = A\sqrt{\frac{U_0(\hat{n}+1)}{2v}}$  is the surface thickness parameter and prime represents differentiation with respect to  $\delta$ . We define  $F(\xi) = \check{f}(\xi - \delta) = \check{f}(\eta)$  and obtain

$$(1 - \tilde{n})\check{f}''' + \tilde{n}We\sqrt{\frac{\hat{n}+1}{2}}\check{f}''\check{f}''' + \frac{2\hat{n}}{\hat{n}+1}A^2 - \frac{2\hat{n}}{\hat{n}+1}(\check{f}')^2 + \check{f}\check{f}'' = 0, \quad (2.16)$$

$$\begin{aligned} & \check{\theta}'' + \text{Pr}\check{f}\check{\theta}' + \gamma\text{Pr}\left(\frac{\hat{n}-3}{2}\right)\check{f}\check{f}'\check{\theta}' - \frac{\hat{n}+1}{2}\check{f}^2\check{\theta}'' \\ & + \text{Pr}(S_{\check{\theta}} + \check{\theta})(\gamma\check{f}\check{f}'' - \frac{2\hat{n}}{\hat{n}+1}\gamma\check{f}'^2 - \frac{2}{\hat{n}+1}\check{f}') = 0, \end{aligned} \quad (2.17)$$

$$\check{\phi}'' + Scf\check{\phi}' - \frac{2}{\hat{n}+1}Sc\left(S_{\check{\phi}}f' + f'\check{\phi}\right) - \sigma\frac{2}{\hat{n}+1}Sc[1 + \check{\theta}\beta]^n \exp\left[\frac{-\hat{E}}{1 + \check{\theta}\beta}\right] = 0, \quad (2.18)$$

$$\begin{aligned} \check{f}(\eta) &= \delta\frac{1-\hat{n}}{1+\hat{n}}, & f'(\eta) &= 1, & \check{\theta}(\eta) &= 1 - S_{\check{\theta}}, & \check{\phi}(\eta) &= 1 - S_{\check{\phi}} \quad \text{at } \eta = 0, \\ f'(\eta) &= A & \check{\theta}(\eta) &= 0 & \check{\phi}(\eta) &= 0 & \text{at } \eta \rightarrow \infty. \end{aligned} \quad (2.19)$$

where  $We$  denotes the Weissenberg number,  $A$  the ratio of velocities,  $\hat{n}$  the velocity index,  $\gamma$  the relaxation parameter,  $\text{Pr}$  the Prandtl number,  $(S_{\check{\theta}}, S_{\check{\phi}})$  the thermal and solutal stratified parameters,  $Sc$  the Schmidt number,  $\beta$  the temperature ratio parameter,  $\hat{E}$  dimensionless activation energy and  $\sigma$  the dimensionless chemical reaction parameter. These parameters are defined as:

$$\begin{aligned} We &= \Gamma\sqrt{\frac{2U_0^3(x+b)^{3\hat{n}-1}}{v}}, & A &= \frac{U_\infty}{U_0}, & \text{Pr} &= \frac{\mu c_p}{\check{k}U_0(x+b)^{\hat{n}-1}}, \\ \gamma &= \lambda U_0(x+b)^{\hat{n}-1}, & Sc &= \frac{v}{D}, & S_{\check{\theta}} &= \frac{\check{b}}{\check{a}}, & \beta &= \frac{\check{T}_w - \check{T}_0}{\check{T}_\infty}, \\ S_{\check{\phi}} &= \frac{\check{d}}{\check{e}}, & \hat{E} &= \frac{E_a}{k_1\check{T}_\infty}, & \sigma &= \frac{K_r^2}{U_0}(x+b)^{1-\hat{n}}. \end{aligned} \quad (2.20)$$

Heat transfer rate is given as

$$\tilde{N}u_x = \frac{(x+b)\check{q}_w}{\check{k}(\check{T}_w - \check{T}_0)}, \quad (2.21)$$

where wall heat flux is

$$\check{q}_w = -\check{k} \frac{\partial \check{T}}{\partial y} + \lambda \left( \check{u} \check{v} \frac{\partial \check{T}}{\partial x} + \check{v}^2 \frac{\partial \check{T}}{\partial y} \right), \quad (2.22)$$

In dimensionless form,

$$\tilde{N}u_x \text{Re}_x^{-\frac{1}{2}} = - \left( \frac{\hat{n} + 1}{2} \right)^{\frac{1}{2}} \left( \frac{\delta^2 (1 - \hat{n})^2}{2(1 + \hat{n})} \text{Pr} \gamma + 1 \right) \check{\theta}'(0). \quad (2.23)$$

## 2.3 Solutions

Homotopy solutions are under consideration. The suitable initial approximations  $(\check{f}_0, \check{\theta}_0, \check{\phi}_0)$  and associated linear operators  $(\check{\mathcal{L}}_{\check{f}}, \check{\mathcal{L}}_{\check{\theta}}, \check{\mathcal{L}}_{\check{\phi}})$  are

$$\check{f}_0(\eta) = A\eta + (1 - A)(1 - e^\eta) + \delta \frac{1 - \hat{n}}{1 + \hat{n}}, \quad (2.24)$$

$$\check{\theta}_0(\eta) = (1 - S_{\check{\theta}})e^{-\eta}, \quad (2.25)$$

$$\check{\phi}_0(\eta) = (1 - S_{\check{\phi}})e^{-\eta}, \quad (2.26)$$

$$\check{\mathcal{L}}_{\check{f}}(\eta) = \frac{d^3 \check{f}}{d\eta^3} - \frac{d\check{f}}{d\eta}, \quad \check{\mathcal{L}}_{\check{\theta}}(\eta) = \frac{d^2 \check{\theta}}{d\eta^2} - \check{\theta}, \quad \check{\mathcal{L}}_{\check{\phi}}(\eta) = \frac{d^2 \check{\phi}}{d\eta^2} - \check{\phi}, \quad (2.27)$$

$$\check{\mathcal{L}}_{\check{f}} \left[ \tilde{X}_1 + \tilde{X}_2 e^\eta + \tilde{X}_3 e^{-\eta} \right] = 0, \quad (2.28)$$

$$\check{\mathcal{L}}_{\check{\theta}} \left[ \tilde{X}_4 e^\eta + \tilde{X}_5 e^{-\eta} \right] = 0, \quad (2.29)$$

$$\check{\mathcal{L}}_{\check{\phi}} \left[ \tilde{X}_6 e^\eta + \tilde{X}_7 e^{-\eta} \right] = 0. \quad (2.30)$$

with  $\tilde{X}_i$  ( $i = 1 - 7$ ) as the arbitrary constants.

## 2.4 Convergence analysis

Homotopy analysis method is employed to find convergent series solution. Convergence region is controlled through plots of curves  $\check{h}_{\check{f}}$ ,  $\check{h}_{\check{\theta}}$  and  $\check{h}_{\check{\phi}}$ . Thus  $\check{h}$ -curves are plotted in Fig. 2.1. Here permissible ranges of parameters  $\check{h}_{\check{f}}$ ,  $\check{h}_{\check{\theta}}$  and  $\check{h}_{\check{\phi}}$  are  $-0.75 \leq \check{h}_{\check{f}} \leq -0.2$ ,  $-1.0 \leq \check{h}_{\check{\theta}} \leq -0.1$  and  $-0.6 \leq \check{h}_{\check{\phi}} \leq -0.1$ . Table 2.1 also ensures that 20<sup>th</sup> order approximations are sufficient for momentum equations whereas 25<sup>th</sup> order of approximations are required for energy and

concentration expressions.

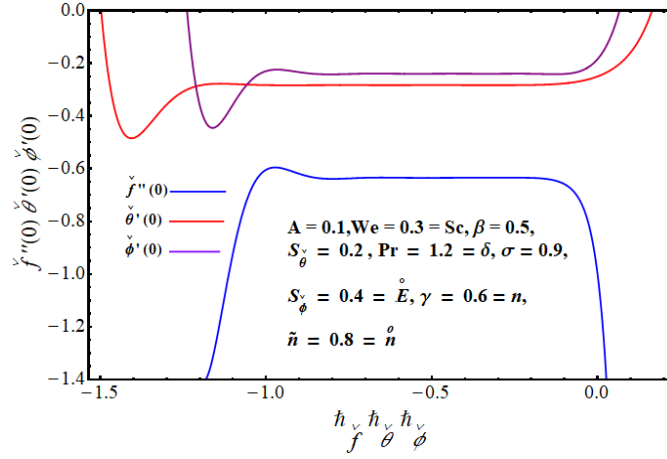


Fig. 2.1:  $\hbar$ -curve for  $\check{f}''(0), \check{\theta}'(0), \check{\phi}'(0)$

**Table 2.1:** HAM solutions convergence for  $A = 0.1, We = 0.3 = Sc, \beta = 0.5, S_\theta = 0.2, Pr = 1.2 = \delta, S_\phi = 0.4 = \hat{E}, \gamma = 0.6 = n, \hat{n} = 0.8 = \tilde{n}$ .

Order of approximations	$-\check{f}''(0)$	$-\check{\theta}'(0)$	$-\check{\phi}'(0)$
1	0.8795	0.2631	0.2748
2	0.7994	0.2719	0.2841
3	0.7456	0.2776	0.2858
4	0.7090	0.2813	0.2840
6	0.6839	0.2835	0.2815
12	0.6353	0.2838	0.2789
15	0.6339	0.2831	0.2781
20	0.6346	0.2829	0.2787
25	0.6346	0.2831	0.2784
30	0.6346	0.2831	0.2784
50	0.6346	0.2831	0.2784

## 2.5 Analysis

Our interest here is to predict the influences of sundry variables on physical quantities. Thus we displayed Figs. 2.2-2.16 here. Fig. 2.2 predict influence of Weissenberg number  $We$  on velocity  $\check{f}'(\eta)$ . Clearly momentum layer and velocity are reduced for higher  $We$ . Infact through an increase in relaxation time the fluid thickness increases and so a reduction of fluid velocity occurs. Fig. 2.3 depicts that how velocity  $\check{f}'(\eta)$  affected with power law index  $\tilde{n}$ . Hence velocity  $\check{f}'(\eta)$  and related boundary layer are decreased through  $\tilde{n}$ . Obviously larger values of power law index enhances fluid viscosity which opposes the motion of fluid particles. Change in velocity  $\check{f}'(\eta)$  by increasing the ratio parameter  $A$  is shown in Fig. 2.4. Here velocity and associated layer thickness are enhances for larger ratio parameter  $A$ . Fig. 2.5 witnesses impact of velocity index  $\hat{n}$  on  $\check{f}'(\eta)$ . This parameter is also recognized as motion parameter or shape parameter. Rise in velocity index  $\hat{n}$  leads to an increase of velocity  $\check{f}'(\eta)$ . Shape of surface is strongly influenced by numerical values of  $\hat{n}$ . For flat surface  $\hat{n} = 1$  and there is occurrence of uniform thickness case. When  $\hat{n} > 1$ , the thickness of surface shrinks and outer concave shape is noticed. For  $\hat{n} < 1$ , the thickness enhances and outer convex image of surface is observed. Since  $\hat{n}$  is also declared as motion parameter thus Fig. 2.6 and 2.7 are shown to predict the behavior of  $\hat{n}$  along surface thickness  $\delta$ . Velocity  $\check{f}'(\eta)$  is enhanced for larger surface thickness parameter  $\delta$  when  $\hat{n} > 1$ , i.e for this case accelerated motion is examined. Beside this decelerated motion of fluid particles occurs for larger values of  $\delta$  when  $\hat{n} < 1$  (see Fig. 2.7).

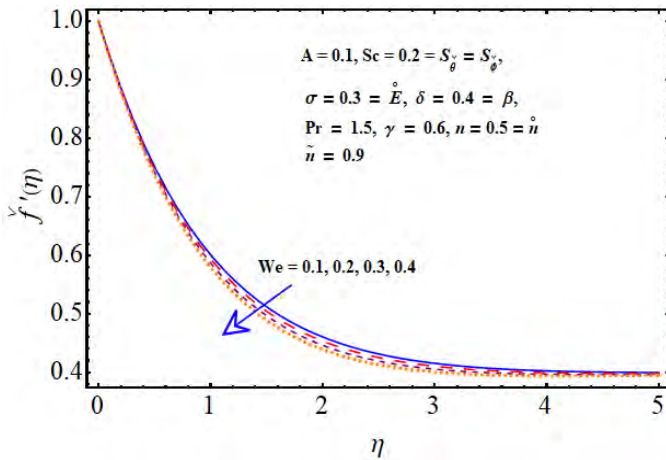


Fig. 2.2:  $\check{f}'(\eta)$  for  $We$  effect

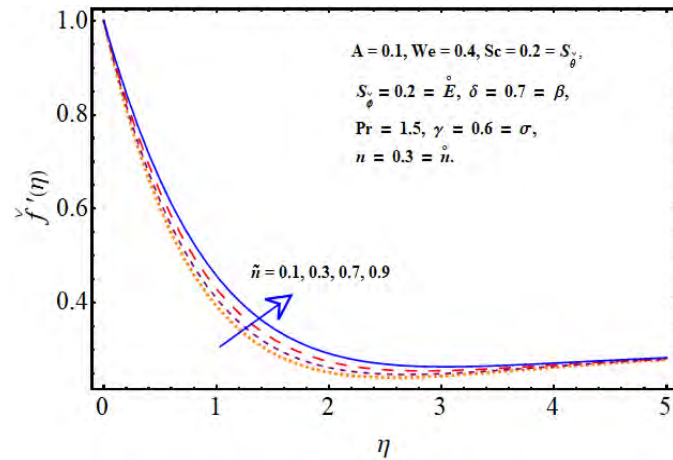


Fig. 2.3:  $\check{f}'(\eta)$  for  $\tilde{n}$  effect

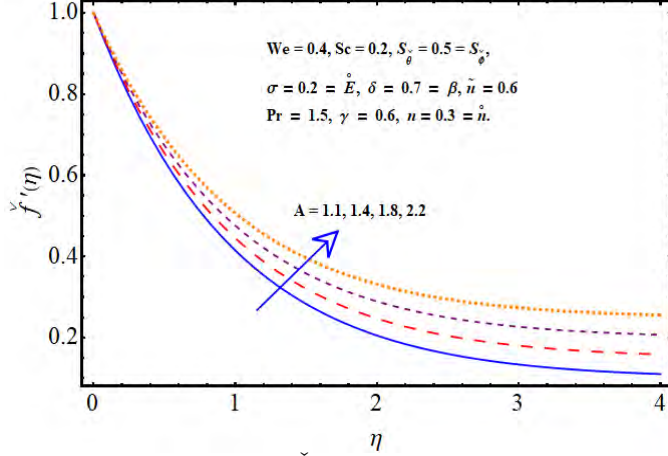


Fig. 2.4:  $\check{f}'(\eta)$  for  $A$  effect

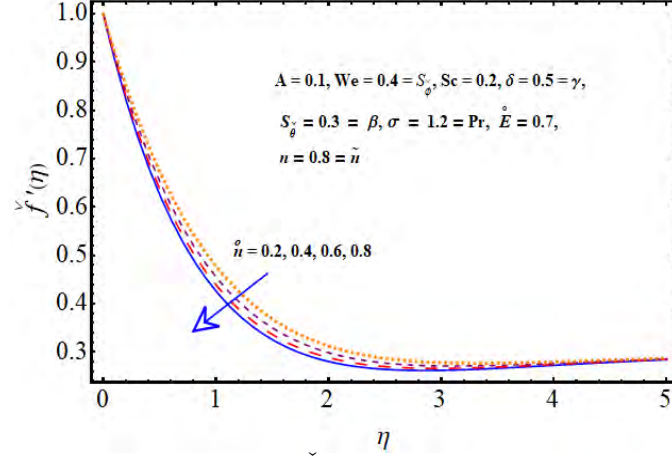


Fig. 2.5:  $\check{f}'(\eta)$  for  $\hat{n}$  effect

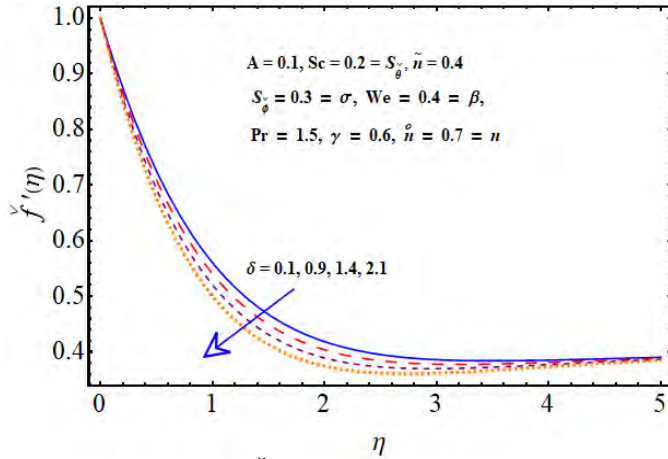


Fig. 2.6:  $\check{f}'(\eta)$  for  $\delta(\hat{n} < 1)$  effect

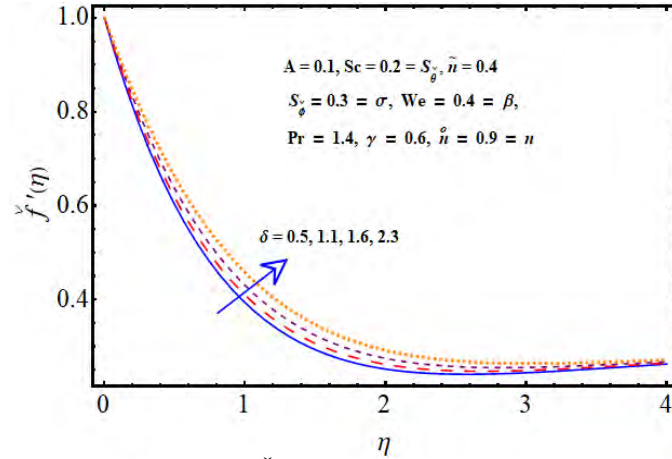


Fig. 2.7:  $\check{f}'(\eta)$  for  $\delta(\hat{n} > 1)$  effect

Fig. 2.8 explores the variation of temperature field  $\check{\theta}(\eta)$  for Prandtl number  $Pr$ . Thermal diffusivity is reduced when Prandtl number enhances. As a consequence the temperature and thermal layer have been decreased. Temperature against thermal relaxation parameter  $\gamma$  is shown in Fig. 2.9. Larger variation in thermal relaxation parameter induces decay in  $\check{\theta}(\eta)$ . Infact large  $\gamma$  confirms that fluid particles acquire more time to transfer heat to its adjacent particles and thus temperature reduces. However there is an increase of heat transfer rate for higher  $\gamma$ . Fig. 2.10 discloses that how temperature  $\check{\theta}(\eta)$  affected with the change in velocity index  $\hat{n}$ . Higher  $\hat{n}$  lead to temperature  $\check{\theta}(\eta)$  enhancement. Impact of  $S_{\hat{\theta}}$  on  $\check{\theta}(\eta)$  is in Fig. 2.11.  $\check{\theta}(\eta)$  decays with an increase in  $S_{\hat{\theta}}$ . Obviously difference in temperature is decreased gradually

between the ambient temperature  $\tilde{T}_\infty$  and surface temperature  $\tilde{T}_w$ .

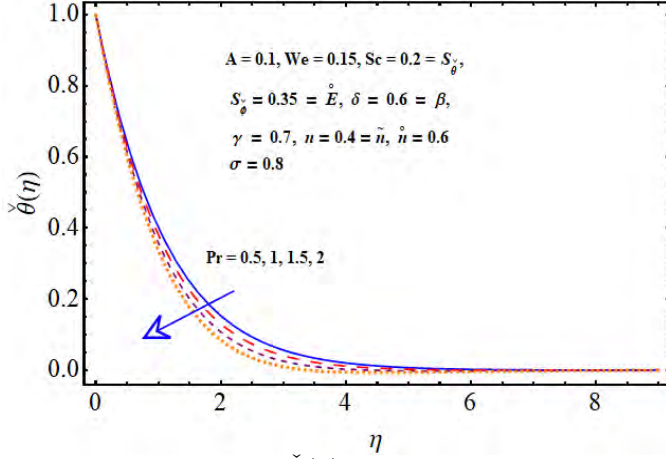


Fig. 2.8:  $\check{\theta}(\eta)$  for Pr effect

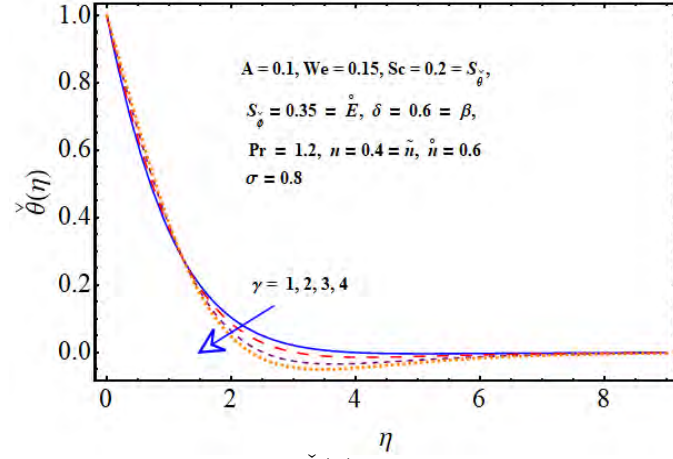


Fig. 2.9:  $\check{\theta}(\eta)$  for  $\gamma$  effect

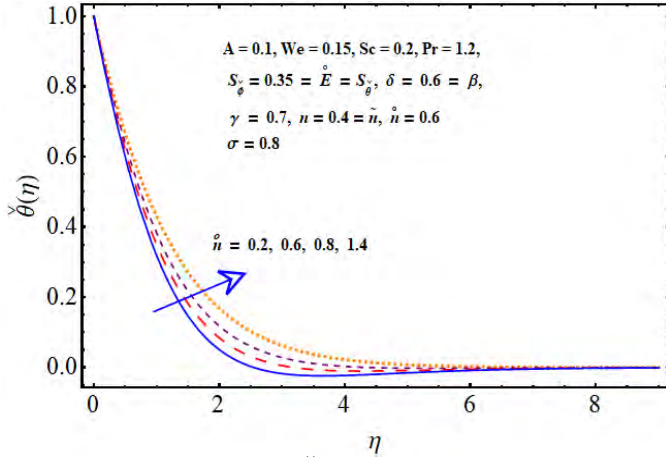


Fig. 2.10:  $\check{\theta}(\eta)$  for  $\hat{n}$  effect

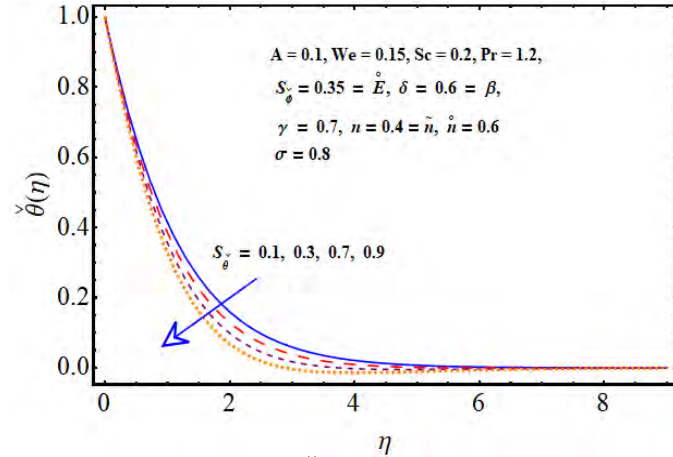


Fig. 2.11:  $\check{\theta}(\eta)$  for  $S_g$  effect

Outcome of dimensionless chemical reaction parameter  $\sigma$  on concentration field  $\check{\phi}(\eta)$  is presented in Fig. 2.12. An increment in  $\sigma$  causes decrease in concentration  $\check{\phi}(\eta)$  and associated layer thickness. Higher chemical rate enhance the mass transport in fluid and consequently concentration decreases. However opposite effects are observed for concentration in case of activation energy parameter  $\dot{E}$  (Fig. 2.13). Concentration distribution  $\check{\phi}(\eta)$  is an increasing function of  $\dot{E}$ . Fig. 2.14 displayed  $\check{\phi}(\eta)$  for Schmidt number. There is an increase in  $j(\eta)$  for higher  $Sc$ . Note that Schmidt number is ratio of momentum diffusivity to mass diffusivity. Hence larger Schmidt number declared small mass diffusivity and thus concentration  $\check{\phi}(\eta)$  enhances. Analysis of velocity index  $\hat{n}$  on  $\check{\phi}(\eta)$  is plotted in Fig. 2.15. Here concentration distri-

bution is increased for higher  $\hat{n}$ . Impact of solutal stratification  $S_{\check{\phi}}$  on concentration distribution  $\check{\phi}(\eta)$  is presented in Fig. 2.16.  $\check{\phi}(\eta)$  decays for larger values of  $S_{\check{\phi}}$ . Solutal stratification occurs due to minor variation in surface and ambient concentration.

Influences of various embedded parameters on Nusselt number is demonstrated in Table 2.2. It displays variation in heat transfer rate against some parameters of interest. Tabulated values witness that heat transfer rate decreases for thermal relaxation parameter  $\gamma$  and for dimensionless thermally stratified parameter  $S_{\check{\theta}}$ , while it enhances for Prandtl number  $Pr$  and  $\delta$ .

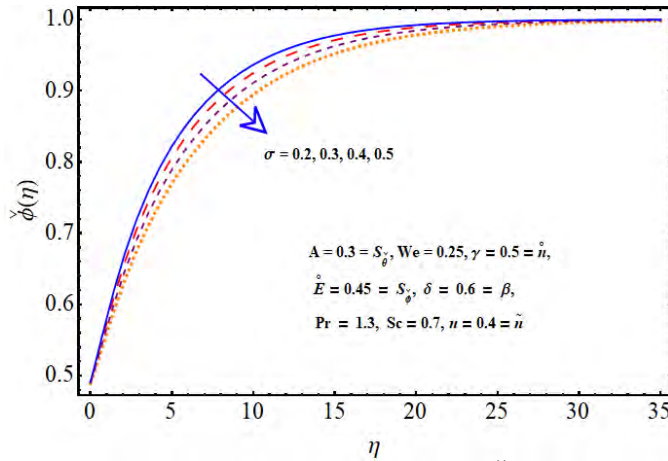


Fig. 2.12: Variation of  $\sigma$  on  $\check{\phi}(\eta)$

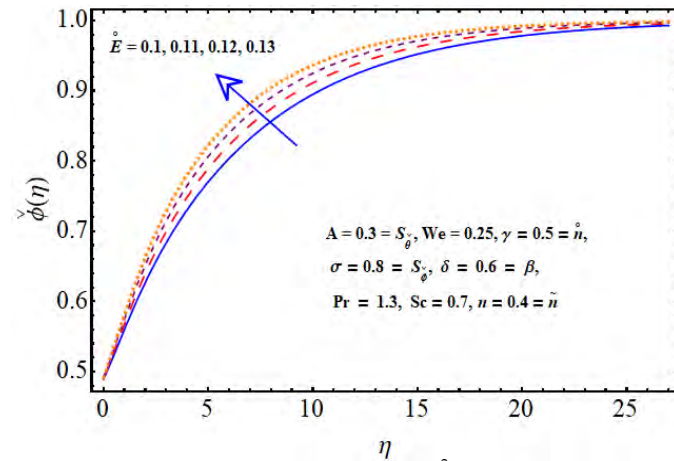


Fig. 2.13: Variation of  $\hat{E}$  on  $\check{\phi}(\eta)$

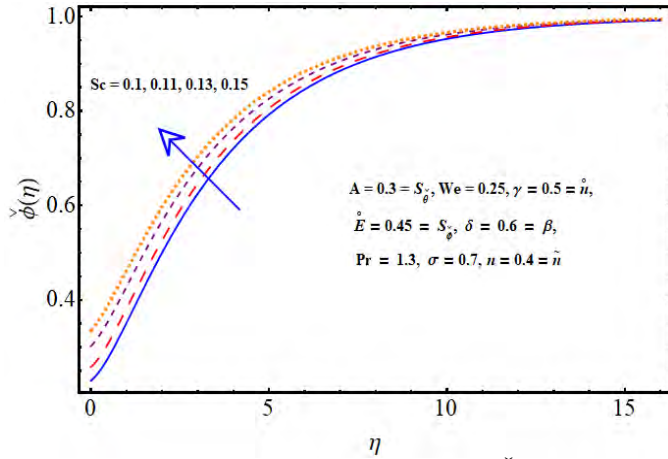


Fig. 2.14: Variation of  $Sc$  on  $\check{\phi}(\eta)$

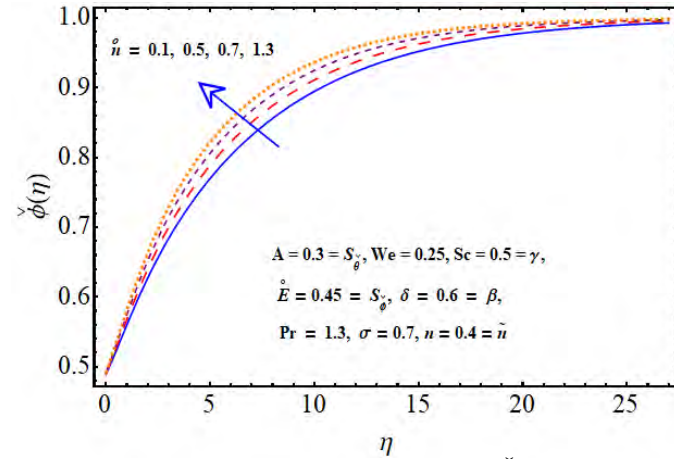


Fig. 2.15: Variation of  $\hat{n}$  on  $\check{\phi}(\eta)$



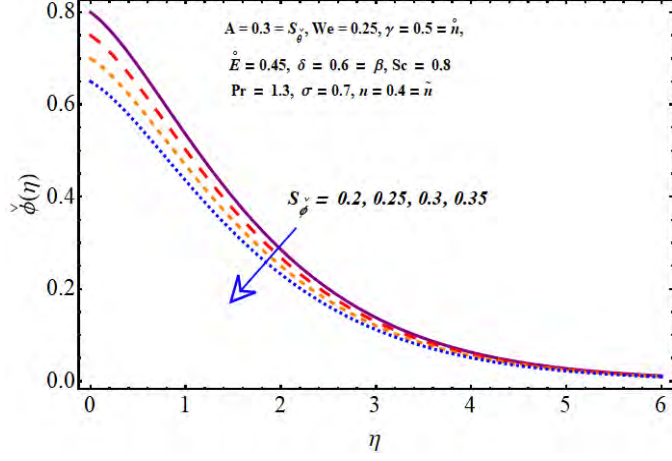


Fig. 2.16: Variation of  $S_j$  on  $\check{\phi}(\eta)$

**Table 2.2:** Description of Nusselt number.

Pr	$\delta$	$\gamma$	$S_\delta$	$\tilde{Nu}_x \text{Re}_x^{-\frac{1}{2}}$
1	0.5	1.6	0.3	0.2084664
1.1				0.2544226
1.2				0.3026473
1	0.6	1.6	0.3	0.2492009
	0.7			0.2893210
	0.8			0.3293889
1	0.5	1.7	0.3	0.2781875
		1.8		0.2288348
		1.9		0.1920219
1	0.5	1.6	0.4	0.1800328
			0.5	0.1541903
			0.6	0.1291780

## 2.6 Conclusions

Key findings here are as follows:

- An increment in surface thickness parameter leads to enhancement of velocity when  $\hat{n} > 1$ .
- Influence of velocity index  $\hat{n}$  on concentration and velocity are qualitatively similar.

- Conjugate parameter yields enhancement of temperature and thermal boundary layer thickness.
- Temperature is significantly decreased for stratified parameter  $S_{\bar{\theta}}$ .
- Temperature has direct relation with velocity law index  $\hat{n}$ .
- Heat transfer rate enhances for Prandtl number  $Pr$  and thermal relaxation parameter  $\gamma$ .
- Velocity is decreased for larger Weissenberg number  $We$ .
- Concentration distribution is reduced for increment in chemical reaction parameter  $\sigma$ .
- Stronger activation energy parameter  $\hat{E}$  resulted in an increase of concentration distribution.
- Velocity for power law index  $\tilde{n}$  and velocity law index  $\hat{n}$  is opposite.

## Chapter 3

# Chemical reaction in flow of hyperbolic tangent fluid

### 3.1 Introduction

Mixed convection stretched flow of tangent hyperbolic liquid is explored in this chapter. Joule heating, double stratification, non-linear thermal radiation, Brownian motion and thermophoresis are considered. Phenomenon of mass transfer is examined by activation energy along with binary chemical reaction. Computations of convergent solutions are carried out for the nonlinear mathematical system. Graphical representation is employed for outcome of sundry variables on velocity, temperature and concentration of nanoparticles. Moreover, Nusselt number, coefficient of drag force and mass transfer rate are examined. Here velocity decays for larger Weissenberg number. Concentration of fluid enhances for higher activation energy parameter.

### 3.2 Modeling

Unsteady flow of tangent hyperbolic nanofluid is examined here. Impermeable stretched sheet (at  $y = 0$ ) is accountable for fluid motion. Material density is assumed constant. Fluid confined the space  $y > 0$ . Sheet is stretched with velocity  $U_w(x) = ax$  in  $x$ -direction. The sheet has constant temperature ( $\tilde{T}_w$ ) and constant concentration ( $\tilde{C}_w$ ) whereas  $(\tilde{C}_\infty, \tilde{T}_\infty)$  are fluid's ambient concentration and temperature respectively. Brownian diffusion and thermophoresis

are present. Magnetic fluid is in transverse direction to flow (Fig.3.1). Effects of electric field are assumed negligible. Moreover influence of activation energy with binary chemical reaction is accounted. Thermal radiation is taken non-linear. Viscous dissipation and heat generation/absorption are absent. The relevant expressions satisfy

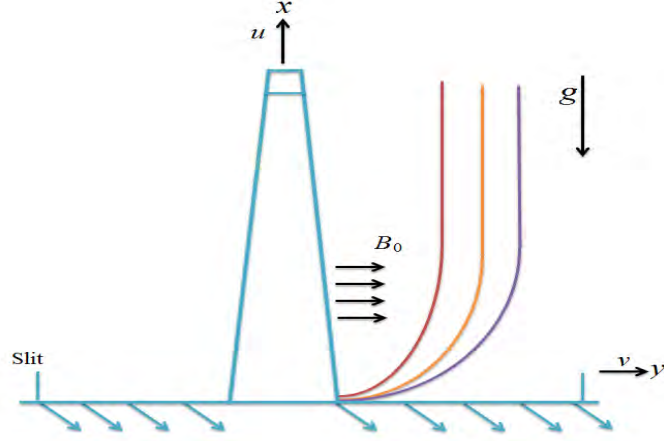


Fig. 3.1: Physical model

$$\frac{\partial \tilde{u}}{\partial x} + \frac{\partial \tilde{v}}{\partial y} = 0,$$

$$\tilde{u} \frac{\partial \tilde{u}}{\partial x} + \tilde{v} \frac{\partial \tilde{u}}{\partial y} = \nu(1 - \tilde{n}) \frac{\partial^2 \tilde{u}}{\partial y^2} + \sqrt{2} \nu \Gamma \tilde{n} \frac{\partial \tilde{u}}{\partial y} \frac{\partial^2 \tilde{u}}{\partial y^2} - \sigma \frac{B_0^2}{\rho_f} \tilde{u} + g[\beta_{\tilde{T}}(\tilde{T} - \tilde{T}_\infty) + \beta_{\tilde{C}}(\tilde{C} - \tilde{C}_\infty)], \quad (3.1)$$

$$\begin{aligned} \left( \tilde{u} \frac{\partial \tilde{T}}{\partial x} + \tilde{v} \frac{\partial \tilde{T}}{\partial y} \right) &= \frac{\check{k}}{(\rho c_p)_f} \left( \frac{\partial^2 \tilde{T}}{\partial y^2} \right) + \tau D_B \left( \frac{\partial \tilde{T}}{\partial y} \right) \left( \frac{\partial \tilde{C}}{\partial y} \right) + \\ &\tau \frac{D_{\tilde{T}}}{\tilde{T}_\infty} \left( \frac{\partial \tilde{T}}{\partial y} \right)^2 + \sigma \frac{B_0^2}{(\rho c_p)_f} \tilde{u}^2 - \frac{1}{(\rho c_p)_f} \frac{\partial \check{q}_r}{\partial y}, \end{aligned} \quad (3.2)$$

$$\tilde{u} \frac{\partial \tilde{C}}{\partial x} + \tilde{v} \frac{\partial \tilde{C}}{\partial y} = D_B \left( \frac{\partial^2 \tilde{C}}{\partial y^2} \right) + \frac{D_{\tilde{T}}}{\tilde{T}_\infty} \left( \frac{\partial^2 \tilde{T}}{\partial y^2} \right) - K_r^2 (\tilde{C} - \tilde{C}_\infty) \left[ \frac{\tilde{T}}{\tilde{T}_\infty} \right]^n \exp \left[ \frac{-E_a}{k_1 \tilde{T}} \right]. \quad (3.3)$$

The relevant boundary conditions are

$$\tilde{u} = U_w(x) = ax, \quad \tilde{v} = 0, \quad \tilde{T} = \tilde{T}_w = \tilde{T}_0 + \check{a}x, \quad \tilde{C} = \tilde{C}_w = \tilde{C}_0 + \check{c}x \quad \text{at } y = 0,$$

$$\tilde{u} \rightarrow 0, \quad \tilde{T} \rightarrow \tilde{T}_\infty = \tilde{T}_0 + \check{b}x, \quad \tilde{C} \rightarrow \tilde{C}_\infty = \tilde{C}_0 + \check{d}x \quad \text{as } y \rightarrow \infty. \quad (3.4)$$

Here  $\tilde{u}$  and  $\tilde{v}$  depict the velocity components parallel to  $x$  and  $y$ -axes,  $\Gamma$  material constant,  $\tilde{n}$  power law index,  $\nu$  kinematic viscosity,  $\rho$  fluid density,  $c_p$  specific heat,  $\mu$  the dynamic viscosity,  $D_{\tilde{T}}$  the thermophoresis coefficient,  $U_w$  the stretching velocity,  $D_B$  the Brownian coefficient,  $\tau$  the heat capacity of nanoparticles,  $\check{\sigma}$  the electrical conductivity,  $\tilde{T}_0$  the reference temperature,  $\check{k}$  the thermal conductivity,  $\beta_{\tilde{T}}$  thermal expansion coefficient,  $\beta_{\tilde{C}}$  concentration expansion coefficient and  $(\check{a}, \check{b}, \check{c}, \check{d})$  the dimensional constants. Further  $\tilde{T}_w$  and  $\tilde{C}_w$  are the constant temperature and solute concentration near the surface while  $\tilde{T}_\infty$  and  $\tilde{C}_\infty$  represent ambient temperature and concentration. Term  $\left[\frac{\tilde{T}}{\tilde{T}_\infty}\right]^n \exp\left[\frac{-E_a}{k_1\tilde{T}}\right]$  in Eq. (3.4) is referred to as the modified Arrhenius function. Here  $k_1 = 8.61 \times 10^{-5} eV/K$  represents the Boltzmann constant,  $n$  is the dimensionless constant or rate constant having range  $-1 < n < 1$ ,  $K_r$  the chemical reaction parameter and  $E_a$  the activation energy.

We consider,

$$\begin{aligned} \psi &= \sqrt{av}x\check{f}(\eta), & \eta &= \sqrt{\frac{a}{\nu}}y \\ \check{\theta}(\eta) &= \frac{\tilde{T} - \tilde{T}_\infty}{\tilde{T}_w - \tilde{T}_0}, & \check{\phi}(\eta) &= \frac{\tilde{C} - \tilde{C}_\infty}{\tilde{C}_w - \tilde{C}_0}. \end{aligned} \quad (3.5)$$

We have velocity components in terms of stream function ( $\psi$ ) by  $\tilde{v} = -\frac{\partial\psi}{\partial x}$  and  $\tilde{u} = \frac{\partial\psi}{\partial y}$ . Now

$$\tilde{u} = ax\check{f}'(\eta) \quad , \quad \tilde{v} = -\sqrt{av}\check{f}(\eta), \quad (3.6)$$

Radiative heat flux through Rosseland approximation yields

$$\frac{\partial\check{q}_r}{\partial y} = \frac{-4\sigma^*}{3k^*} \frac{\partial}{\partial y} \left( \frac{\partial\tilde{T}^4}{\partial y} \right) = \frac{-16\sigma^*}{3k^*} \left[ \tilde{T}^3 \frac{\partial^2\tilde{T}}{\partial y^2} + 3\tilde{T}^2 \left( \frac{\partial\tilde{T}}{\partial y} \right)^2 \right], \quad (3.7)$$

where  $\sigma^*$  and  $k^*$  represent Stefan-Boltzmann constant and mean absorption coefficient. By

Eqs. (3.3) expression (3.9) becomes

$$\begin{aligned} \left( \tilde{u} \frac{\partial \tilde{T}}{\partial x} + \tilde{v} \frac{\partial \tilde{T}}{\partial y} \right) &= \frac{\check{k}}{(\rho c_p)_f} \left( \frac{\partial^2 \tilde{T}}{\partial y^2} \right) + \tau D_B \left( \frac{\partial \tilde{T}}{\partial y} \right) \left( \frac{\partial \tilde{C}}{\partial y} \right) + \tau \frac{D_{\tilde{T}}}{\tilde{T}_\infty} \left( \frac{\partial \tilde{T}}{\partial y} \right)^2 \\ &+ \check{\sigma} \frac{B_0^2}{\rho} \tilde{u}^2 + \frac{1}{(\rho c_p)_f} \frac{16\sigma^*}{3k^*} \left[ \tilde{T}^3 \frac{\partial^2 \tilde{T}}{\partial y^2} + 3\tilde{T}^2 \left( \frac{\partial \tilde{T}}{\partial y} \right)^2 \right], \end{aligned} \quad (3.8)$$

Continuity expression is verified and equations (3.2) to (3.10) yield

$$(1 - \tilde{n}) \check{f}''' + \check{f} \check{f}'' - (\check{f}')^2 + \tilde{n} We e \check{f}'' \check{f}''' - M^2 \check{f}' + \lambda_1 [\check{\theta} + N^* \check{\phi}] = 0, \quad (3.9)$$

$$\begin{aligned} \check{\theta}'' - \text{Pr} S_{\check{\theta}} \check{f}' + \text{Pr} (\check{f} \check{\theta}' - \check{f}' \check{\theta}) + \text{Pr} N_b \check{\theta}' \check{\phi}' + \text{Pr} N_t (\check{\theta}')^2 + M E c^2 (\check{f}')^2 + \\ \frac{4}{3} R_d \{ \check{\theta}'' [\check{\theta} (\check{\theta}_w - \check{\theta}_0) + 1]^3 + 3(\check{\theta}')^2 (\check{\theta}_w - \check{\theta}_0) [\check{\theta} (\check{\theta}_w - \check{\theta}_0) + 1]^2 \} = 0, \end{aligned} \quad (3.10)$$

$$\check{\phi}'' + \frac{N_t}{N_b} \check{\theta}'' + Sc (\check{f} \check{\phi}' - \check{f}' \check{\phi}) - Sc S_{\check{\phi}} \check{f}' - \sigma Sc [1 + \check{\theta} (\check{\theta}_w - \check{\theta}_0)]^n \exp \left[ \frac{-\hat{E}}{1 + \check{\theta} (\check{\theta}_w - \check{\theta}_0)} \right] = 0, \quad (3.11)$$

$$\begin{aligned} \check{f}'(\eta) &= 1, & \check{f}(\eta) &= 0 & \check{\theta}(\eta) &= 1 - S_{\check{\theta}}, & \check{\phi}(\eta) &= 1 - S_{\check{\phi}} & \text{at } \eta = 0, \\ \check{f}'(\eta) &\rightarrow 0, & \check{\theta}(\eta) &\rightarrow 0, & \check{\phi}(\eta) &\rightarrow 0 & \text{when } \eta \rightarrow \infty. \end{aligned} \quad (3.12)$$

where  $We$  denotes the Weissenberg number,  $M$  magnetic parameter,  $N^*$  the local buoyancy parameter,  $\lambda_1$  the mixed convection parameter,  $\text{Pr}$  the Prandtl number,  $S_{\check{\theta}}$  the thermal stratified parameter,  $S_{\check{\phi}}$  the solutal stratified parameter,  $Sc$  the Schmidt number,  $\hat{E}$  dimensionless activation energy and  $\sigma$  the dimensionless chemical reaction parameter. Furthermore,  $Ec$ ,  $R_d$ ,  $(\check{\theta}_w, \check{\theta}_0)$ ,  $N_b$ ,  $N_t$ ,  $(Gr, Gr^*)$  are the Eckert number, radiation parameter, temperature ratio parameter, Brownian motion parameter, thermophoresis parameter and the Grashof number

(temperature and concentration). Definition of these parameters are

$$\begin{aligned}
We &= \sqrt{\frac{2a^3}{v}}\Gamma x, \quad M^2 = \frac{\sigma B_0^2}{\rho a}, \quad Gr = \frac{g\beta_{\tilde{T}}(\tilde{T}_w - \tilde{T}_0)x^3}{v^2}, \quad \lambda_1 = \frac{Gr}{\text{Re}_x^2}, \\
Gr^* &= \frac{g\beta_C(C_w - C_0)x^3}{v^2}, \quad N^* = \frac{Gr^*}{Gr}, \quad R_d = \frac{4\sigma^*\tilde{T}_\infty^3}{\check{k}k^*}, \quad S_{\tilde{\theta}} = \frac{\check{b}}{\check{a}}, \\
Ec &= \frac{U_w^2}{(\tilde{T}_w - \tilde{T}_0)c_p}, \quad \tilde{\theta}_w = \frac{\tilde{T}_w}{\tilde{T}_\infty}, \quad \tilde{\theta}_0 = \frac{\tilde{T}_0}{\tilde{T}_\infty}, \quad Sc = \frac{v}{D_B}, \quad \text{Pr} = \frac{v}{\alpha}, \\
N_b &= \frac{\tau D_B}{v}\check{e}x, \quad N_t = \frac{\tau D_{\tilde{T}}}{v\tilde{T}_\infty}\check{a}x, \quad S_{\check{\phi}} = \frac{\check{d}}{\check{e}}, \quad \check{E} = \frac{E_a}{k_1\tilde{T}_\infty}, \quad \sigma = \frac{K_r^2}{a}. \quad (3.13)
\end{aligned}$$

Coefficient of drag force ( $\check{C}_{fx}$ ), heat transfer rate ( $\check{N}u_x$ ) and mass transfer rate ( $\check{S}h_x$ ) are described as:

$$\check{C}_{fx} = \frac{\check{\tau}_w}{\frac{1}{2}\rho U_w^2 x}, \quad \check{N}u_x = \frac{x\check{q}_w}{\check{k}(\tilde{T}_w - \tilde{T}_0)}, \quad \check{S}h_x = \frac{x\check{q}_m}{D_B(\check{C}_w - \check{C}_0)}. \quad (3.14)$$

where,

$$\begin{aligned}
\check{\tau}_w &= \mu \left[ (1 - \tilde{n}) \frac{\partial \tilde{u}}{\partial y} + \frac{\Gamma \tilde{n}}{\sqrt{2}} \left( \frac{\partial \tilde{u}}{\partial y} \right)^2 \right]_{y=0}, \\
\check{q}_w &= -\check{k} \left\{ \left[ 1 + \tilde{T}^3 \frac{16\sigma^*}{3\check{k}k^*} \right] \left( \frac{\partial \tilde{T}}{\partial y} \right) \right\}_{y=0}, \\
\check{q}_m &= -D_B \left( \frac{\partial \check{C}}{\partial y} \right)_{y=0}. \quad (3.15)
\end{aligned}$$

In non-dimensional form we obtain

$$\begin{aligned}
\text{Re}_x^{\frac{1}{2}} \check{C}_{fx} &= (1 - \tilde{n}) \check{f}''(0) + We \frac{\tilde{n}}{2} (\check{f}''(0))^2, \\
\text{Re}_x^{\frac{1}{2}} \check{N}u_x &= -\check{\theta}'(0) \{ 1 + R_d [1 + (\check{\theta}_w - \check{\theta}_0) \check{\theta}(0)]^3 \}, \\
\text{Re}_x^{\frac{1}{2}} \check{S}h_x &= -\check{\phi}'(0). \quad (3.16)
\end{aligned}$$

in which  $\text{Re}_x = \frac{U_w x}{v}$  is Reynold number.

### 3.3 Solution expressions

Series solution here is constructed via homotopic technique. Initial guesses  $(\check{f}_0, \check{\theta}_0, \check{\phi}_0)$  and associated linear operators  $(\check{\mathcal{L}}_{\check{f}}, \check{\mathcal{L}}_{\check{\theta}}, \check{\mathcal{L}}_{\check{\phi}})$  are

$$\begin{aligned}\check{f}_0(\eta) &= 1 - e^\eta, \\ \check{\theta}_0(\eta) &= (1 - S_{\check{\theta}})e^{-\eta}, \\ \check{\phi}_0(\eta) &= (1 - S_{\check{\phi}})e^{-\eta},\end{aligned}\tag{3.17}$$

$$\check{\mathcal{L}}_{\check{f}}(\eta) = \frac{d^3 \check{f}}{d\eta^3} - \frac{d\check{f}}{d\eta}, \quad \check{\mathcal{L}}_{\check{\theta}}(\eta) = \frac{d^2 \check{\theta}}{d\eta^2} - \check{\theta}, \quad \check{\mathcal{L}}_{\check{\phi}}(\eta) = \frac{d^2 \check{\phi}}{d\eta^2} - \check{\phi},\tag{3.18}$$

$$\check{\mathcal{L}}_{\check{f}} \left[ \tilde{X}_1 + \tilde{X}_2 e^\eta + \tilde{X}_3 e^{-\eta} \right] = 0,\tag{3.19}$$

$$\check{\mathcal{L}}_{\check{\theta}} \left[ \tilde{X}_4 e^\eta + \tilde{X}_5 e^{-\eta} \right] = 0,\tag{3.20}$$

$$\check{\mathcal{L}}_{\check{\phi}} \left[ \tilde{X}_6 e^\eta + \tilde{X}_7 e^{-\eta} \right] = 0.\tag{3.21}$$

with  $\tilde{X}_i$  ( $i = 1 - 7$ ) as the arbitrary constants.

### 3.4 Convergence

Homotopy analysis technique is helpful to find convergent series solutions and provides a chance to sketch region of convergence. This region can be controlled by setting appropriate values of  $\hbar_{\check{f}}$ ,  $\hbar_{\check{\theta}}$  and  $\hbar_{\check{\phi}}$ . Fig. 3.2 displays h-configurations. It is analyzed that ranges of parameters  $\hbar_{\check{f}}$ ,  $\hbar_{\check{\theta}}$  and  $\hbar_{\check{\phi}}$  are  $-1.5 \leq \hbar_{\check{f}} \leq -0.5$ ,  $-1.3 \leq \hbar_{\check{\theta}} \leq -0.4$  and  $-1.4 \leq \hbar_{\check{\phi}} \leq -0.7$ . Numerically obtained solution convergence is presented in Table 3.1. Here 20<sup>th</sup> order of approximation are enough for momentum equation while energy and concentration equations converge at 25<sup>th</sup> order of approximation.



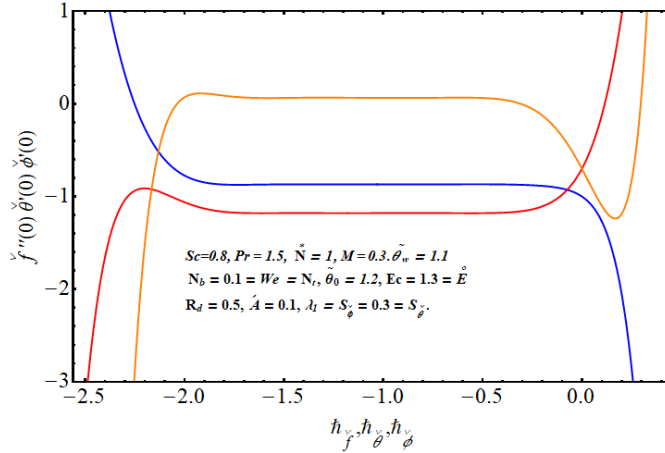


Fig.3.2:  $h$ -plots in view of  $f''(0)$ ,  $\theta'(0)$ , and  $\phi'(0)$

**Table 1:** HAM solutions convergence when  $\tilde{n} = A' = 0.1 = We$ ,  $\lambda_1 = 0.3 = M = Sc$ ,  $S_\theta = 0.3 = S_\phi$ ,  $Pr = 1.5$ ,  $R_d = 0.5$ ,  $Ec = 1.3 = \hat{E}$ ,  $Sc = 0.8$ ,  $N^* = 1$ ,  $N_b = 0.1 = N_t$ ,  $\check{\theta}_w = 1.1$  and  $\check{\theta}_0 = 1.2$ .

Order of approximations	$-\check{f}''(0)$	$-\check{\theta}'(0)$	$\check{\phi}'(0)$
1	0.87717	1.0384	0.074223
2	0.88392	1.1535	0.075501
3	0.87568	1.1784	0.069273
4	0.86657	1.1822	0.065361
6	0.86657	1.1830	0.065025
12	0.86901	1.1795	0.064510
15	0.86902	1.1798	0.064469
20	0.86903	1.1793	0.064242
25	0.86903	1.1794	0.064303
30	0.86903	1.1794	0.064303
50	0.86903	1.1794	0.064303

### 3.5 Discussion

Here velocity, temperature and concentration are discussed through Figs. 3.3-3.16. Fig. 3.3 predicts Weissenberg number  $We$  variation on  $\check{f}'(\eta)$ . Clearly velocity and momentum layer are

less through  $We$ . In fact the Weissenberg number is ratio of relaxation time to particular time of fluid. Hence for more relaxation time the fluid thickness increases and consequently fluid velocity reduces. Fig. 3.4 indicates variation of velocity  $\check{f}'(\eta)$  by increasing local buoyancy parameter  $N^*$ . Clearly velocity and related layer thickness are increased through larger  $N^*$ . Fig. 3.5 illustrates impact of magnetic parameter  $M$  on  $\check{f}'(\eta)$ . A rise in  $M$  leads to a decrease of velocity field  $\check{f}'(\eta)$ . Obviously larger magnetic parameter  $M$  increase Lorentz force (also termed as resistive force) which opposes fluid movement and so velocity reduces. Influence of mixed convection parameter  $\lambda_1$  is pictured in Fig. 3.6. Velocity is enhanced through  $\lambda_1$ . Higher values of mixed convection enhances buoyancy forces and thus velocity and corresponding momentum layer increases.

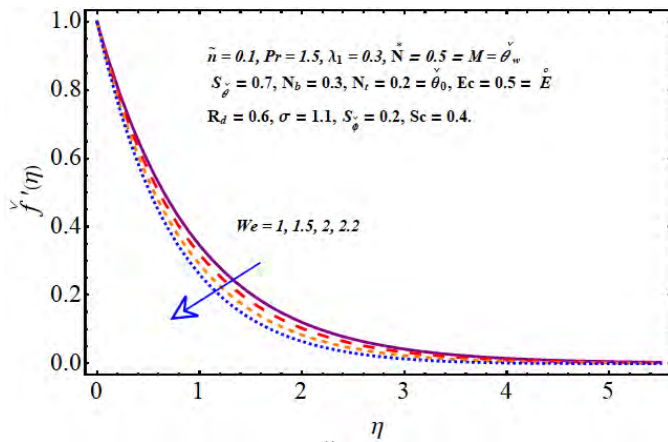


Fig. 3.3:  $\check{f}'(\eta)$  via  $We$

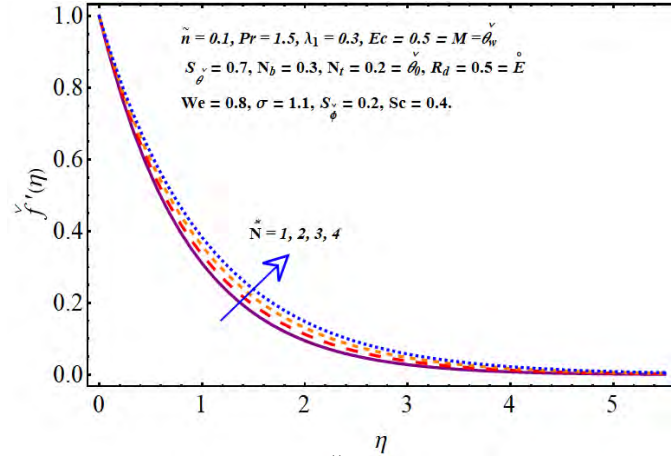


Fig. 3.4:  $\check{f}'(\eta)$  via  $N^*$

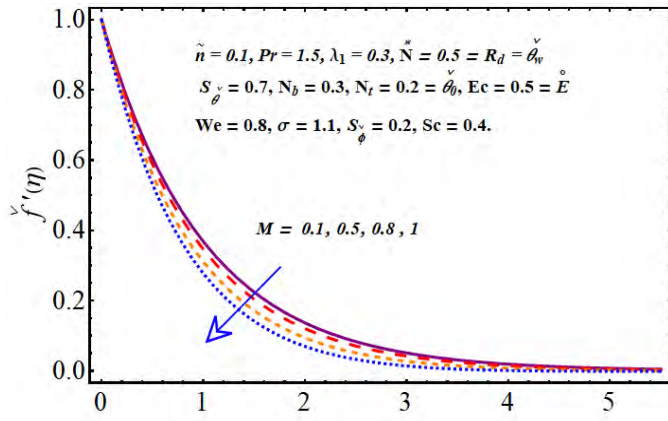


Fig. 3.5:  $\check{f}'(\eta)$  via  $M$

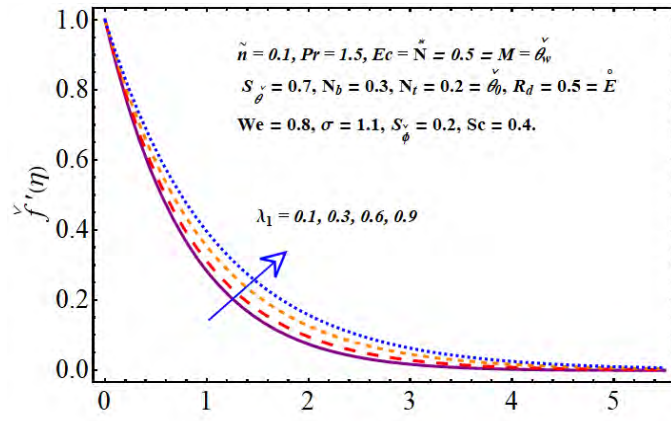


Fig. 3.6:  $\check{f}'(\eta)$  via  $\lambda_1$

Fig. 3.7 explores variation of temperature field for magnetic parameter  $M$ . Here temperature is increased for larger magnetic parameter. Fig. 3.8 witnesses that temperature and thermal layer are enhanced for higher Eckert number  $Ec$ . Graphical illustration of  $N_b$  for  $\check{\theta}(\eta)$  is presented in Fig. 3.9. Temperature rises in response to larger variation of  $N_b$ . Since motion of fluid particle is unsystematic in reaction of higher Brownian motion parameter that leads to increase in heat production. Fig. 3.10 explores variation of temperature for radiation parameter  $R_d$ . Larger  $R_d$  give rise to rate of heat transfer since heat production enhanced the radiation process. Impact of thermal stratified variable  $S_{\check{\theta}}$  on temperature  $\check{\theta}(\eta)$  is reflected in Fig. 3.11. Thermal field decays with an increase in  $S_{\check{\theta}}$  as the difference in temperature is decreased gradually between the ambient temperature  $\check{T}_{\infty}$  and surface temperature  $\check{T}_w$ .

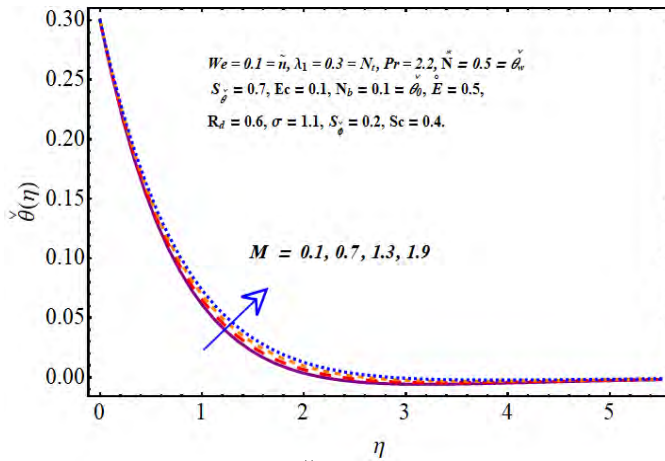


Fig. 3.7:  $\check{\theta}(\eta)$  against  $M$

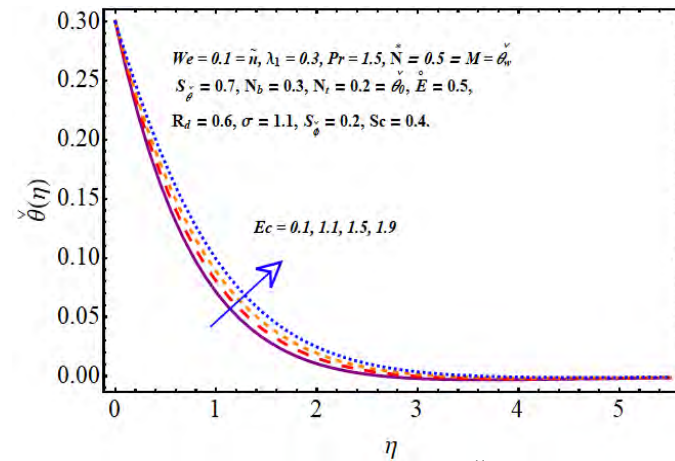


Fig. 3.8:  $Ec$  impact on  $\check{\theta}(\eta)$

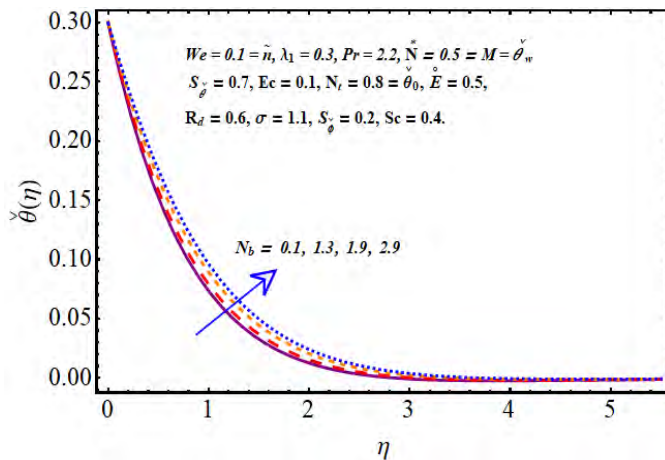


Fig. 3.9:  $N_b$  impact on  $\check{\theta}(\eta)$

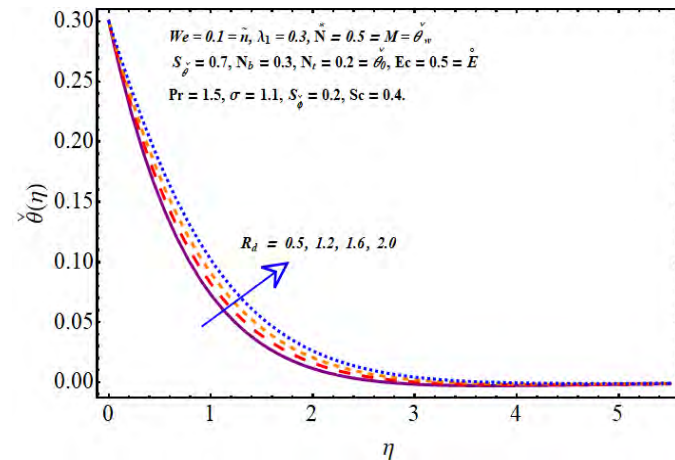


Fig. 3.10:  $R_d$  impact on  $\check{\theta}(\eta)$

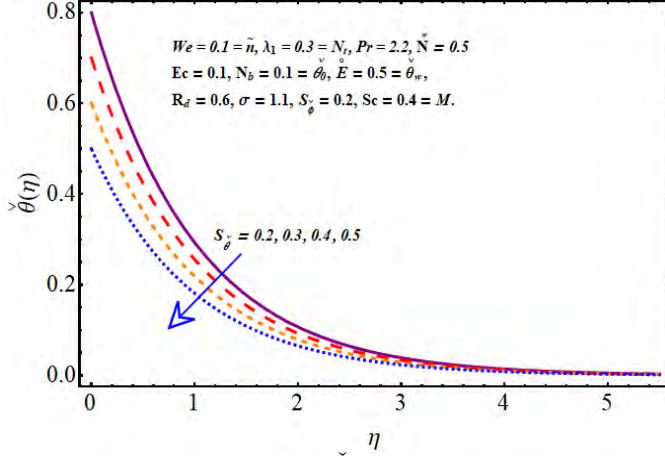


Fig. 3.11:  $\check{\theta}(\eta)$  via  $S_{\check{\phi}}$

Fig. 3.12 clarifies outcome of  $\sigma$  on concentration of nanoparticles. As predicted, the decline in nanoparticle concentration is noticed for larger  $\sigma$ . Variation of activation energy  $\check{E}$  on nanoparticles concentration is reflected in Fig. 3.13. As expected concentration is enhanced through  $\check{E}$ . Outcome of Schmidt number  $Sc$  on  $\check{\phi}(\eta)$  is displayed in Fig. 3.14. Here concentration decayed for higher  $Sc$ . Concentration stratification parameter  $S_{\check{\phi}}$  on  $\check{\phi}(\eta)$  is displayed in Fig. 3.15. It seems that larger values of  $S_{\check{\phi}}$  corresponds to lesser nanoparticles concentration  $\check{\phi}(\eta)$ . Fig. 3.16 elucidates marginal increase in nanoparticles concentration when thermophoresis parameter  $N_t$  varies from  $N_t = 0.2$  to  $N_t = 0.35$ .

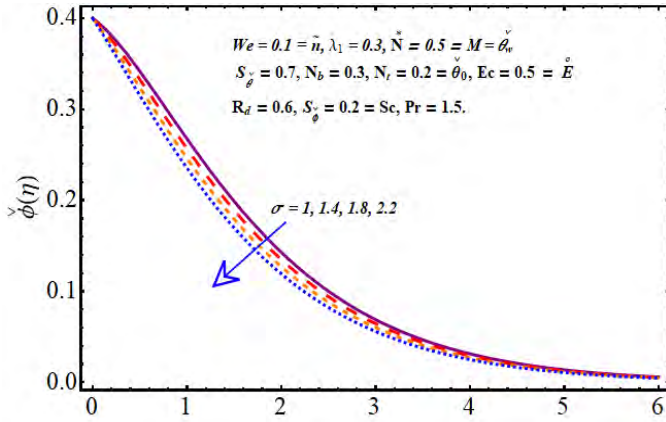


Fig. 3.12:  $\check{\phi}(\eta)$  via  $\sigma$

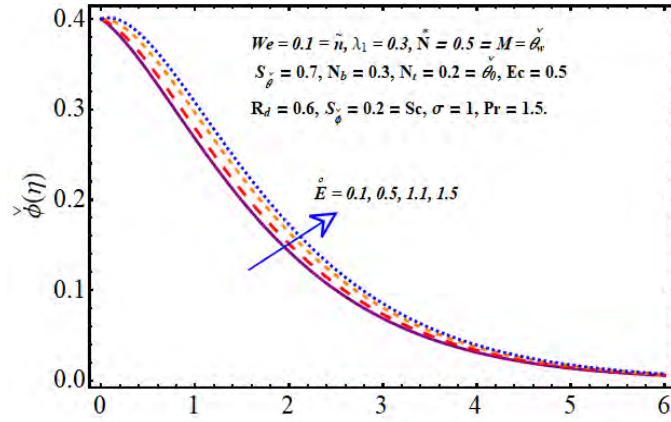


Fig. 3.13:  $\check{\phi}(\eta)$  via  $\check{E}$

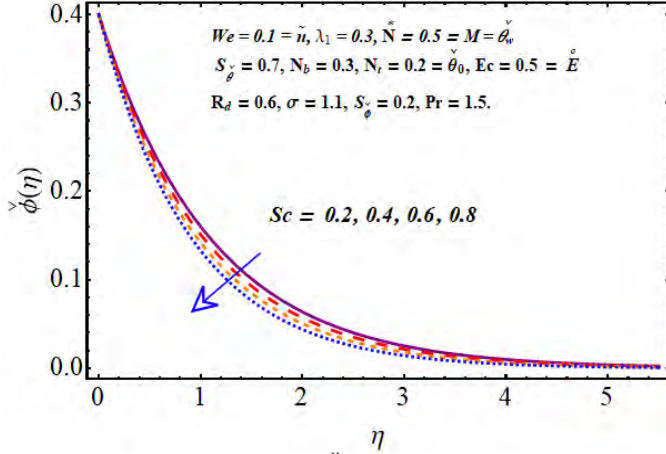


Fig. 3.14:  $\check{\phi}(\eta)$  via  $Sc$

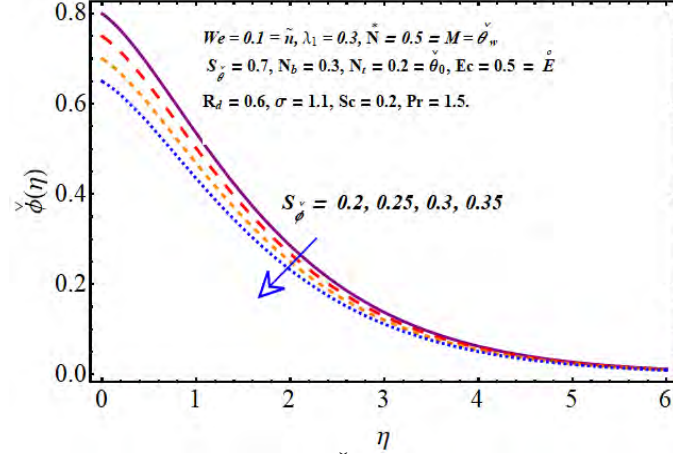


Fig. 3.15:  $\check{\phi}(\eta)$  via  $S_\phi$

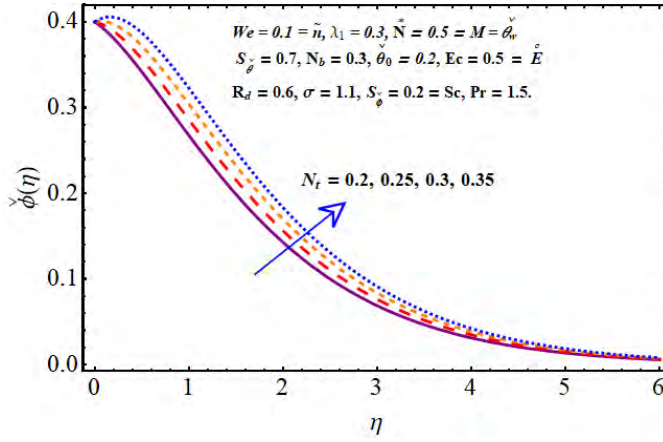


Fig. 3.16:  $\check{\phi}(\eta)$  via  $N_t$

Influences of various embedded variables on skin-friction coefficient, Nusselt number and Sherwood number are demonstrated in Tables 3.2-3.4. Table 3.2 declares that coefficient of drag force is affected by mixed convection parameter  $\lambda_1$  and non-dimensional activation energy  $\check{E}$ . Coefficient of drag force is decreased by these parameters. Skin-friction coefficient has increased behavior for higher  $\tilde{n}$ ,  $We$ ,  $M$  and  $N^*$ . Table 3.3 displays variation in heat transfer rate against some parameters of interest. Tabulated values witness that heat transfer rate decreases for Eckert number  $Ec$ , dimensionless thermally stratified parameter  $S_\vartheta$ , Brownian diffusion parameter  $N_b$  and thermophoresis parameter  $N_t$  while it enhances for Prandtl number  $Pr$  and  $R_d$ . Further mass transfer rate is decreased via higher Schmidt number  $Sc$  and Brownian diffusion coefficient  $N_b$  however it increases for other parameters mentioned in Table 3.4.

**Table 3.2:** Numerical description of skin friction coefficient.

$\tilde{n}$	$We$	$M$	$\lambda_1$	$N^*$	$\hat{E}$	$-\text{Re}_x^{\frac{1}{2}} \tilde{C}_{fx}$
0.1	0.1	0.3	0.3	1	1.3	0.8688595
	0.2					0.9131529
	0.3					0.9673078
0.1	0.2	0.3	0.3	1	1.3	0.8701973
	0.3					0.8759865
	0.4					0.8783699
0.1	0.1	0.4	0.3	1	1.3	0.9030014
		0.5				0.9458779
		0.6				0.9977259
0.1	0.1	0.3	0.4	1	1.3	0.8039160
			0.5			0.7507146
			0.6			0.7290100
0.1	0.1	0.3	0.3	1.2	1.3	0.4763013
				1.3		0.5473585
				1.4		0.6347946
0.1	0.1	0.3	0.3	1	1.4	0.6814829
					1.5	0.5666427
					1.6	0.5298977

**Table 3.3:** Numerical description of Nusselt number.

Pr	$R_d$	$Ec$	$S_{\dot{\theta}}$	$N_b$	$N_t$	$Re_x^{\frac{1}{2}} \tilde{Nu}_x$
1	0.5	1.6	0.3	0.1	0.1	0.2084664
	1.1					0.2544226
	1.2					0.3026473
1	0.6	1.6	0.3	0.1	0.1	0.2492009
	0.7					0.2893210
	0.8					0.3293889
1	0.5	1.7	0.3	0.1	0.1	0.2781875
	1.8					0.2288348
	1.9					0.1920219
1	0.5	1.6	0.4	0.1	0.1	0.1800328
			0.5			0.1541903
			0.6			0.1291780
1	0.5	1.6	0.3	0.2	0.1	0.1929118
				0.3		0.1779978
				0.4		0.1644246
1	0.5	1.6	0.3	0.2	0.2	0.1849759
					0.3	0.1755373
					0.4	0.1683754

**Table 3.4:** Numerical description of Sherwood number.

$Sc$	$\sigma$	$\hat{E}$	$S_{\tilde{\phi}}$	$N_b$	$N_t$	$Re_x^{\frac{1}{2}} \tilde{Sh}_x$
0.8	0.1	1.1	0.1	0.2	0.3	0.3911616
0.9						0.4536701
1						0.5391772
0.8	0.2	1.1	0.1	0.2	0.3	0.3758304
	0.3					0.3745837
	0.4					0.3651333
0.8	0.1	1.2	0.1	0.2	0.3	0.3876376
	1.3					0.3654337
	1.4					0.3559579
0.8	0.1	1.1	0.15	0.2	0.3	0.3536455
			0.2			0.3270567
			0.25			0.3119910
0.8	0.1	1.1	0.1	0.25	0.3	0.5049517
				0.3		0.5660433
				0.35		0.6292429
0.8	0.1	1.1	0.1	0.2	0.4	0.2766914
					0.5	0.1498125
					0.6	0.04072542

### 3.6 Conclusions

Thermal and concentration stratifications, non-linear thermal radiation and activation energy are explored. We have main results as follows

- Velocity field decays via larger Weissenberg number  $We$ .
- Concentration distribution reduces for an increment in solutal stratification parameter  $S_{\tilde{\phi}}$ .



- Temperature distribution significantly reduces for stronger thermal stratified parameter  $S_{\theta}$ .
- Stronger chemical reaction parameter  $\sigma$  results in an increase of concentration distribution.
- Velocity for mixed convection parameter  $\lambda_1$  varies directly.
- Concentration against activation energy variable  $\hat{E}$  is increased.
- Heat transfer rate enhances for radiation parameter  $R_d$ .
- Higher mass transfer rate is noted for thermophoresis parameter  $N_t$ .

## Chapter 4

# Entropy generation minimization and activation energy in flow of third grade fluid

### 4.1 Introduction

Present chapter discloses the effects of Joule heating and entropy generation minimization for steady flow of third grade nanomaterial. Particular attention is given to address the influences of activation energy and chemical reaction. Modified Arrhenius function is utilized to investigate the activation energy. Appropriate non-dimensional variables have been utilized in obtaining ordinary differential systems. Convergent homotopic solutions of resulting non-linear system are constructed. Graphical results are discussed for velocity, temperature and concentration. Flow behavior is analyzed through Nusselt number, coefficient of drag force and mass transfer rate.

### 4.2 Statement

Mixed convective flow of third grade nanofluid is examined here. Impermeable stretched sheet at  $y = 0$  is accountable for fluid motion. Material density is assumed constant and fluid confined the region  $y > 0$ . Sheet is stretched with velocity  $U_w(x) = ax$  in  $x$ -direction (see Fig.

4.1). The sheet preserved at constant temperature ( $\tilde{T}_w$ ) and constant concentration ( $\tilde{C}_w$ ) of nanoparticles whereas ( $\tilde{C}_\infty, \tilde{T}_\infty$ ) being fluid's ambient concentration and temperature. The Brownian diffusion and thermophoresis properties are retained. Motion of fluid and magnetic field ( $B_0$ ) are perpendicular to each other. Effects of electric field are assumed negligible. Moreover influence of activation energy with binary chemical reaction is considered. A phenomenon of entropy generation is reviewed for involved parameters. Thermal radiation and heat generation/absorption are taken absent. Under these considerations, the velocity, temperature and concentration equations are

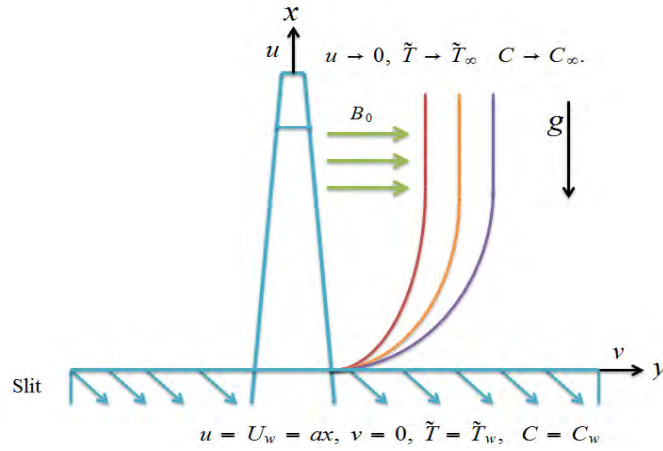


Fig. 4.1: Flow geometry.

$$\frac{\partial \tilde{u}}{\partial x} + \frac{\partial \tilde{v}}{\partial y} = 0, \quad (4.1)$$

$$\begin{aligned} \tilde{u} \frac{\partial \tilde{u}}{\partial x} + \tilde{v} \frac{\partial \tilde{v}}{\partial y} = & v \frac{\partial^2 \tilde{u}}{\partial y^2} + \frac{\alpha_1^*}{\rho_f} \left( \tilde{u} \frac{\partial^3 \tilde{u}}{\partial y^2 \partial x} + \frac{\partial \tilde{u}}{\partial x} \frac{\partial^2 \tilde{u}}{\partial y^2} + v \frac{\partial^3 \tilde{u}}{\partial y^3} + 3 \frac{\partial \tilde{u}}{\partial x} \frac{\partial^2 \tilde{u}}{\partial y \partial x} \right) + 2 \frac{\alpha_2^*}{\rho_f} \left( \frac{\partial \tilde{u}}{\partial y} \frac{\partial^2 \tilde{u}}{\partial y \partial x} \right) \\ & + \frac{6\beta^*}{\rho_f} \left( \frac{\partial \tilde{u}}{\partial y} \right)^2 \frac{\partial^2 \tilde{u}}{\partial y^2} - \check{\sigma} \frac{B_0^2}{\rho_f} \tilde{u} + g[\beta_{\tilde{T}}(\tilde{T} - \tilde{T}_\infty) + \beta_{\tilde{C}}(\tilde{C} - \tilde{C}_\infty)], \end{aligned} \quad (4.2)$$

$$\begin{aligned} \left( \tilde{u} \frac{\partial \tilde{T}}{\partial x} + \tilde{v} \frac{\partial \tilde{T}}{\partial y} \right) = & \frac{\check{k}}{(\rho c_p)_f} \left( \frac{\partial^2 \tilde{T}}{\partial y^2} \right) + \frac{\mu}{(\rho c_p)_f} \left( \frac{\partial \tilde{u}}{\partial y} \right)^2 + \frac{\alpha_1^*}{(\rho c_p)_f} \left( \tilde{u} \frac{\partial \tilde{u}}{\partial y} \frac{\partial^2 \tilde{u}}{\partial x \partial y} + \tilde{v} \frac{\partial \tilde{u}}{\partial y} \frac{\partial^2 \tilde{u}}{\partial y^2} \right) \\ & + \frac{2\beta^*}{(\rho c_p)_f} \left( \frac{\partial \tilde{u}}{\partial y} \right)^4 + \tau D_B \left( \frac{\partial \tilde{T}}{\partial y} \right) \left( \frac{\partial \tilde{C}}{\partial y} \right) + \tau \frac{D_{\tilde{T}}}{\tilde{T}_\infty} \left( \frac{\partial \tilde{T}}{\partial y} \right)^2 + \check{\sigma} \frac{B_0^2}{\rho_f} \tilde{u}^2 \end{aligned} \quad (4.3)$$

$$\tilde{u} \frac{\partial \tilde{C}}{\partial x} + \tilde{v} \frac{\partial \tilde{C}}{\partial y} = D_B \left( \frac{\partial^2 \tilde{C}}{\partial y^2} \right) + \frac{D_{\tilde{T}}}{\tilde{T}_\infty} \left( \frac{\partial^2 \tilde{T}}{\partial y^2} \right) - K_r^2 (\tilde{C} - \tilde{C}_\infty) \left[ \frac{\tilde{T}}{\tilde{T}_\infty} \right]^n \exp \left[ \frac{-E_a}{k_1 \tilde{T}} \right]. \quad (4.4)$$

The relevant boundary conditions are

$$\tilde{u} = U_w(x) = ax, \quad \tilde{v} = 0, \quad \tilde{T} = \tilde{T}_w \quad \tilde{C} = \tilde{C}_w \quad \text{at} \quad y = 0 \quad (4.5)$$

$$\tilde{u} \rightarrow 0, \quad \tilde{v} \rightarrow 0 \quad \tilde{T} \rightarrow \tilde{T}_\infty \quad \tilde{C} \rightarrow \tilde{C}_\infty \quad \text{when} \quad y \rightarrow \infty. \quad (4.6)$$

Here  $\tilde{u}$  and  $\tilde{v}$  represents the velocities parallel to the  $x$  and  $y$ -axes,  $\nu$  the kinematic viscosity,  $(\alpha_1^*, \alpha_2^*, \beta^*)$  the fluid parameters,  $\rho$  the fluid density,  $c_p$  the specific heat,  $\mu$  the dynamic viscosity,  $D_{\tilde{T}}$  the thermophoresis coefficient,  $U_w$  the stretching velocity,  $D_B$  the Brownian coefficient,  $\tau$  the heat capacity of nanoparticles,  $\check{\sigma}$  the electrical conductivity and  $\check{k}$  the thermal conductivity. Further  $\tilde{T}_w$  and  $\tilde{C}_w$  are the constant temperature and solute concentration of the surface while  $\tilde{T}_\infty$  and  $\tilde{C}_\infty$  represents the ambient temperature and concentration respectively. The term  $\left[ \frac{\tilde{T}}{\tilde{T}_\infty} \right]^n \exp \left[ \frac{-E_a}{k_1 \tilde{T}} \right]$  in Eq. (4.4) is referred as the modified Arrhenius function. Here  $k_1 = 8.61 \times 10^{-5} eV/K$  represents the Boltzmann constant,  $n$  being dimensionless constant or rate constant having the range  $-1 < n < 1$ ,  $K_r$  the chemical reaction parameter and  $E_a$  called the activation energy.

We set

$$\begin{aligned} \psi &= \sqrt{av} x f(\eta), & \eta &= \sqrt{\frac{a}{\nu}} y \\ \check{\theta}(\eta) &= \frac{\tilde{T} - \tilde{T}_\infty}{\tilde{T}_w - \tilde{T}_\infty}, & \check{\phi}(\eta) &= \frac{\tilde{C} - \tilde{C}_\infty}{\tilde{C}_w - \tilde{C}_\infty}. \end{aligned} \quad (4.7)$$

Here  $\psi$  denotes the stream function satisfying  $\tilde{v} = -\frac{\partial \psi}{\partial x}$  and  $\tilde{u} = \frac{\partial \psi}{\partial y}$ . We can write

$$\tilde{u} = ax \check{f}'(\eta) \quad , \quad \tilde{v} = -\sqrt{av} \check{f}(\eta), \quad (4.8)$$

Expressions (4.2)-(4.6) are converted as follows:

$$\check{f}''' + \check{f} \check{f}'' - (\check{f}')^2 + \check{\epsilon}_1 (2\check{f}' \check{f}''' - \check{f} \check{f}^{iv}) + (3\check{\epsilon}_1 + 2\check{\epsilon}_2) \check{f}''^2 + 6\beta_1 \text{Re} \check{f}''' \check{f}''^2 - M^2 \check{f}' + \lambda_1 [\check{\theta} + N^* \check{\phi}] = 0, \quad (4.9)$$

$$\check{\theta}'' + \text{Pr} \check{f} \check{\theta}' + \text{Pr} Ec [ \check{f}''^2 + \check{\varepsilon}_1 \check{f}' \check{f}''^2 - \check{\varepsilon}_1 \check{f} \check{f}'' \check{f}''' + 2\beta_1 \text{Re} \check{f}''^4 ] + \text{Pr} N_b' \check{\theta}' \check{\phi}' + \text{Pr} N_t (\check{\theta}')^2 + M Ec^2 (\check{f}')^2 = 0, \quad (4.10)$$

$$\check{\phi}'' + \frac{N_t}{N_b} \check{\theta}'' + \text{Pr} Le f \check{\phi}' - \text{Pr} Le \sigma^2 (1 + \check{\delta} \check{\theta})^n \exp \left[ \frac{-\check{E}}{1 + \check{\delta} \check{\theta}} \right] \check{\phi} = 0, \quad (4.11)$$

$$\begin{aligned} f'(\eta) &= 1, & f(\eta) &= 0 & \check{\theta}(\eta) &= 1, & \check{\phi}(\eta) &= 1 & \text{at } \eta &= 0, \\ f'(\eta) &\rightarrow 0, & \check{\theta}(\eta) &\rightarrow 0, & \check{\phi}(\eta) &\rightarrow 0 & \text{as } \eta &\rightarrow \infty. \end{aligned} \quad (4.12)$$

where expression (1) is trivially justified,  $(\check{\varepsilon}_1, \check{\varepsilon}_2)$  the material fluid parameters,  $\beta_1$  the third grade fluid parameter,  $M$  the magnetic parameter,  $\text{Re}$  the Reynolds number,  $N^*$  the local buoyancy parameter,  $\lambda_1$  the mixed convection parameter,  $Le$  the Lewis number,  $\check{E}$  the dimensionless activation energy and  $\sigma$  the dimensionless chemical reaction parameter. Furthermore,  $Ec$ ,  $N_b$ ,  $N_t$ ,  $\check{\delta}$ ,  $(Gr, Gr^*)$  are the Eckert number, Brownian motion parameter, thermophoresis parameter, temperature ratio parameter, Grashof number (temperature and concentration) respectively. These parameters are defined as:

$$\begin{aligned} M^2 &= \frac{\check{\sigma} B_0^2 x^2}{\mu}, & Gr &= \frac{g \beta_{\check{T}} (\check{T}_w - \check{T}_\infty) x^3}{v^2}, & \lambda_1 &= \frac{Gr}{\text{Re}_x^2}, & Le &= \frac{\alpha}{D_B}, & \check{\delta} &= \frac{(\check{T}_w - \check{T}_\infty)}{\check{T}_\infty}, \\ Gr^* &= \frac{g \beta_C (C_w - C_\infty) x^3}{v^2}, & N^* &= \frac{Gr^*}{Gr}, & \text{Pr} &= \frac{v}{\alpha}, \dots, \beta_1 &= \frac{a^2 \beta^*}{\mu}, & Ec &= \frac{U_w^2}{(\check{T}_w - \check{T}_\infty) c_p}, \\ \check{\varepsilon}_1 &= \frac{a \alpha_1^*}{\mu}, & \check{\varepsilon}_2 &= \frac{a \alpha_2^*}{\mu}, & \sigma &= \frac{K_r^2}{a}, & N_t &= \frac{(\rho c)_p D_{\check{T}}}{v(\rho c)_f}, & N_b &= \frac{(\rho c)_p D_B (C_w - C_\infty)}{v(\rho c)_f}, \\ \check{E} &= \frac{-E_a}{k_1 \check{T}_\infty}. \end{aligned} \quad (4.13)$$

#### 4.2.1 Physical quantities of interest

Coefficient of drag force ( $\check{C}_{f_x}$ ), rate of heat flux ( $Nu_x$ ) and mass transfer rate ( $Sh_x$ ) are described as:

$$\check{C}_{f_x} = \frac{\check{\tau}_w}{\rho U_w^2 x}, \quad \check{Nu}_x = \frac{x \check{q}_w}{\check{k} (\check{T}_w - \check{T}_\infty)}, \quad \check{Sh}_x = \frac{x \check{q}_m}{D_B (\check{C}_w - \check{C}_\infty)}. \quad (4.14)$$

$$\begin{aligned}
\check{\tau}_w &= \mu \left[ \mu \frac{\partial \tilde{u}}{\partial y} + \alpha_1^* \left( \tilde{u} \frac{\partial^2 \tilde{u}}{\partial x \partial y} + 2 \frac{\partial \tilde{u}}{\partial x} \frac{\partial \tilde{u}}{\partial y} + \tilde{v} \frac{\partial^2 \tilde{u}}{\partial y^2} \right) + 2\beta^* \left( \frac{\partial \tilde{u}}{\partial y} \right)^3 \right] \Big|_{y=0}, \\
\check{q}_w &= -\check{k} \left( \frac{\partial \tilde{T}}{\partial y} \right) \Big|_{y=0}, \\
\check{q}_m &= -D_B \left( \frac{\partial \tilde{C}}{\partial y} \right) \Big|_{y=0}.
\end{aligned} \tag{4.15}$$

In non-dimensional form we obtain

$$\begin{aligned}
\text{Re}_x^{\frac{1}{2}} \tilde{C}_{fx} &= \check{f}''(0) + \check{\epsilon}_1 [3\check{f}'(0)\check{f}''(0) - \check{f}(0)\check{f}'''(0)] + 2\beta_1 \text{Re}(\check{f}''(0))^3, \\
\text{Re}_x^{\frac{1}{2}} \tilde{N}u_x &= -\check{\theta}'(0), \\
\text{Re}_x^{\frac{1}{2}} \tilde{S}h_x &= -\check{\phi}'(0).
\end{aligned} \tag{4.16}$$

in which  $\text{Re}_x = \frac{U_w x}{\nu}$  is Reynold number.

#### 4.2.2 Investigation of entropy generation

Dimensionless entropy minimization equation for third grade fluid is [1]:

$$\begin{aligned}
\check{S}_G &= \underbrace{\frac{\check{k}}{\tilde{T}_\infty^2} \left( \frac{\partial \tilde{T}}{\partial y} \right)^2}_{\text{Thermal irreversibility}} + \underbrace{\frac{RD}{\tilde{C}_\infty} \left( \frac{\partial \tilde{C}}{\partial y} \right)^2 + \frac{RD}{\tilde{T}_\infty} \left( \frac{\partial \tilde{T}}{\partial y} \right) \left( \frac{\partial \tilde{C}}{\partial y} \right)}_{\text{Diffusive irreversibility}} \\
&+ \underbrace{\frac{\mu}{\tilde{T}_\infty} \left[ \left( \frac{\partial \tilde{u}}{\partial y} \right)^2 + \frac{\alpha_1^*}{\mu} \left( \tilde{u} \frac{\partial \tilde{u}}{\partial y} \frac{\partial^2 \tilde{u}}{\partial x \partial y} + v \frac{\partial \tilde{u}}{\partial y} \frac{\partial^2 \tilde{u}}{\partial y^2} \right) + \frac{2\beta^*}{\mu} \left( \frac{\partial \tilde{u}}{\partial y} \right)^4 \right]}_{\text{Fluid friction irreversibility}} \\
&+ \underbrace{\check{\sigma} \frac{B_0^2}{\tilde{T}_\infty} \tilde{u}^2}_{\text{Joule dissipation irreversibility}}.
\end{aligned} \tag{4.17}$$

Above-mentioned equation witnesses the involvement of four main sources for entropy generation irreversibility. First term on right hand side is due to conduction effect which occurs because of heat transmission in finite temperature variation referred as thermal irreversibility. Second term is called diffusive irreversibility. It is clear that entropy generation in view of diffusion is basically the sum of overlapped term with combine thermal and concentration gradients

and a pure term comprised of difference in concentration only. Third term is by reason of friction in between different fluid layers entitled as fluid friction irreversibility. Fourth term is due to Joule dissipation irreversibility. Entropy generation number is the ratio of actual entropy rate ( $\check{S}_G$ ) to the characteristic entropy rate ( $\check{S}_0$ ). Entropy generation number can be written as

$$\begin{aligned} \check{N}_G &= \frac{\check{S}_G}{\check{S}_0} = \text{Re}_x (\check{\theta}')^2 + \text{Re}_x \left( \frac{\check{\xi}}{\check{\Omega}} \right)^2 \zeta (\check{\phi}')^2 + \text{Re}_x \zeta \left( \frac{\check{\xi}}{\check{\Omega}} \right) \check{\theta}' \check{\phi}' \\ &+ \frac{\text{Re}_x}{\check{\Omega}} \text{Pr} Ec [\check{f}''^2 + \check{\epsilon}_1 \check{f}' \check{f}''^2 - \check{\epsilon}_1 \check{f} \check{f}'' \check{f}''' + 2\beta_1 \text{Re}_x \check{f}''^4] \\ &+ M^2 \frac{Br}{\check{\Omega}} (\check{f}')^2, \end{aligned} \quad (4.18)$$

in which  $\check{S}_0 = \frac{\check{k}(\Delta\check{T})}{\check{T}_\infty^2 x^2}$  is characteristic entropy rate,  $\zeta = \frac{RD\check{C}_\infty}{\check{k}}$  diffusion constant,  $Br = \frac{\mu U_w^2}{\check{k}\Delta\check{T}}$  Brinkman number,  $\check{\xi} = \frac{\Delta\check{C}}{C_\infty}$  and  $\check{\Omega} = \frac{\Delta\check{T}}{T_\infty}$  the concentration and temperature differences respectively.

Bejan number is defined as

$$Be = \frac{\text{Thermal irreversibility} + \text{Diffusive irreversibility}}{\text{Total entropy rate}}. \quad (4.19)$$

In non-dimensionalized form it can be represented as

$$Be = \left. \begin{aligned} &\frac{\text{Re}_x (\check{\theta}')^2 + \text{Re}_x \left( \frac{\check{\xi}}{\check{\Omega}} \right)^2 \zeta (\check{\phi}')^2 + \text{Re}_x \zeta \left( \frac{\check{\xi}}{\check{\Omega}} \right) \check{\theta}' \check{\phi}'}{\text{Re}_x (\check{\theta}')^2 + \text{Re}_x \left( \frac{\check{\xi}}{\check{\Omega}} \right)^2 \zeta (\check{\phi}')^2 + \text{Re}_x \zeta \left( \frac{\check{\xi}}{\check{\Omega}} \right) \check{\theta}' \check{\phi}'} \\ &+ \frac{\text{Re}_x}{\check{\Omega}} \text{Pr} Ec [\check{f}''^2 + \check{\epsilon}_1 \check{f}' \check{f}''^2 - \check{\epsilon}_1 \check{f} \check{f}'' \check{f}''' + 2\beta_1 \text{Re}_x \check{f}''^4] \\ &+ M^2 \frac{Br}{\check{\Omega}} (\check{f}')^2. \end{aligned} \right\} \quad (4.20)$$

### 4.3 Solutions by homotopy analysis method

Series solutions of above mentioned systems is obtained via homotopic analysis. Suitable initial assumptions ( $\check{f}_0, \check{\theta}_0, \check{\phi}_0$ ) and associated linear operators ( $\check{\mathcal{L}}_{\check{f}}, \check{\mathcal{L}}_{\check{\theta}}, \check{\mathcal{L}}_{\check{\phi}}$ ) are

$$\check{f}_0(\eta) = 1 - e^{-\eta}, \quad (4.21)$$

$$\check{\theta}_0(\eta) = e^{-\eta}, \quad (4.22)$$

$$\check{\phi}_0(\eta) = e^{-\eta}, \quad (4.23)$$

$$\tilde{\mathcal{L}}_{\tilde{f}}(\eta) = \frac{d^3 \tilde{f}}{d\eta^3} - \frac{d\tilde{f}}{d\eta}, \quad \tilde{\mathcal{L}}_{\tilde{\theta}}(\eta) = \frac{d^2 \tilde{\theta}}{d\eta^2} - \tilde{\theta}, \quad \tilde{\mathcal{L}}_{\tilde{\phi}}(\eta) = \frac{d^2 \tilde{\phi}}{d\eta^2} - \tilde{\phi}, \quad (4.24)$$

$$\tilde{\mathcal{L}}_{\tilde{f}} \left[ \tilde{F}_1 + \tilde{F}_2 \eta + \tilde{F}_3 e^\eta \right] = 0, \quad (4.25)$$

$$\tilde{\mathcal{L}}_{\tilde{\theta}} \left[ \tilde{F}_4 e^\eta + \tilde{F}_5 e^{-\eta} \right] = 0, \quad (4.26)$$

$$\tilde{\mathcal{L}}_{\tilde{\phi}} \left[ \tilde{F}_6 e^\eta + \tilde{F}_7 e^{-\eta} \right] = 0. \quad (4.27)$$

with  $\tilde{F}_i$  ( $i = 1 - 7$ ) as the arbitrary constants.

## 4.4 Convergence analysis

Homotopy analysis method is helpful to find the convergent solutions. It provides a chance to sketch the region of convergence. This region can be controlled by setting appropriate values of  $\tilde{h}_f$ ,  $\tilde{h}_\theta$  and  $\tilde{h}_\phi$ . For this purpose the  $\tilde{h}$ -curves are plotted in Fig. 4.2. It is analyzed that the ranges of convergence control parameters  $\tilde{h}_f$ ,  $\tilde{h}_\theta$  and  $\tilde{h}_\phi$  are  $-0.4 \leq \tilde{h}_f \leq -0.15$ ,  $-0.45 \leq \tilde{h}_\theta \leq -0.25$  and  $-0.5 \leq \tilde{h}_\phi \leq -0.35$ . Convergence of obtained solution is numerically presented in Table 4.1. From table, one can observe that at 25<sup>th</sup> order of approximation the momentum equation converges while energy and concentration equations are convergent at 20<sup>th</sup> order of approximations.

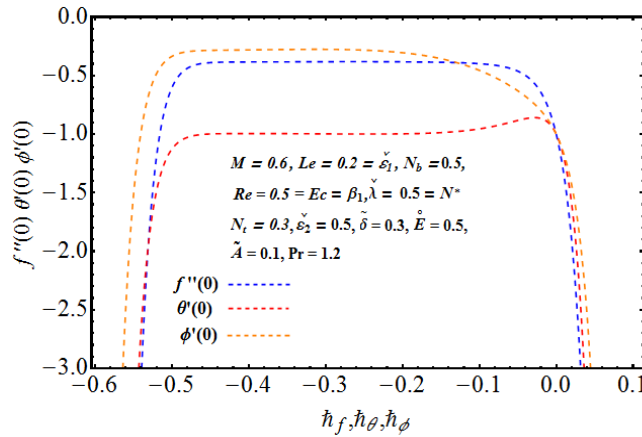


Fig. 4.2:  $\tilde{h}$ -plots in view of  $f''(0)$ ,  $\theta'(0)$ , and  $\phi'(0)$



**Table 4.1:** HAM solutions convergence when  $\sigma = 0.1 = We, \lambda_1 = 0.3 = M = Le, Pr = 1.5, Ec = 1.3 = \dot{E}, \beta_1 = 0.8 = Re, N^* = 1, N_b = 0.1 = N_t, \tilde{\epsilon}_1 = 1.1$  and  $\tilde{\epsilon}_2 = 1.2$ .

Order of approximations	$-\check{f}''(0)$	$-\check{\theta}'(0)$	$-\check{\phi}'(0)$
1	0.54350	0.76750	0.77000
2	0.46232	0.84084	0.69446
3	0.42238	0.88763	0.61467
4	0.40645	0.92394	0.54454
6	0.39258	0.94890	0.48503
12	0.38395	0.99796	0.28075
15	0.38123	0.99593	0.27679
20	0.38136	0.99601	0.27627
25	0.38368	0.99601	0.27774
30	0.38368	0.99601	0.27774
50	0.38368	0.99601	0.27774

## 4.5 Discussion

Intention here is to highlight the influence of involved variables for velocity, temperature and concentration (see Figs. 4.3-4.21). Fig. 4.3 predicts impact of magnetic parameter  $M$  for  $\check{f}'(\eta)$ . Here velocity and boundary layer thickness are decreased with larger  $M$ . It is because of fact that for larger values of magnetic parameter  $M$  the Lorentz force (also termed as resistive force) opposes the fluid's motion and as a consequence the velocity of fluid decreases. Fig. 4.4 illustrates effectiveness of mixed convection parameter  $\lambda_1$  on velocity. Here velocity is an increasing function of  $\lambda_1$ . Influence of buoyancy parameter  $N^*$  on velocity field is sketched in Fig. 4.5. Momentum boundary layer and velocity against  $N^*$  are enhanced. Impact of third grade fluid variable  $\beta_1$  on velocity field  $\check{f}'(\eta)$  is pictured in Fig. 4.6. It is noticed that velocity enhances for larger  $\beta_1$ . Physically higher values of  $\beta_1$  enhances shear thinning influences in fluid and as a result the viscosity of fluid flow decreases and so velocity  $\check{f}'(\eta)$  increases. Changes in velocity field  $\check{f}'(\eta)$  in view of material fluid parameters ( $\tilde{\epsilon}_1, \tilde{\epsilon}_2$ ) are revealed in Figs. 4.7 and 4.8. Velocity field  $\check{f}'(\eta)$  is an increasing function of material fluid parameters.

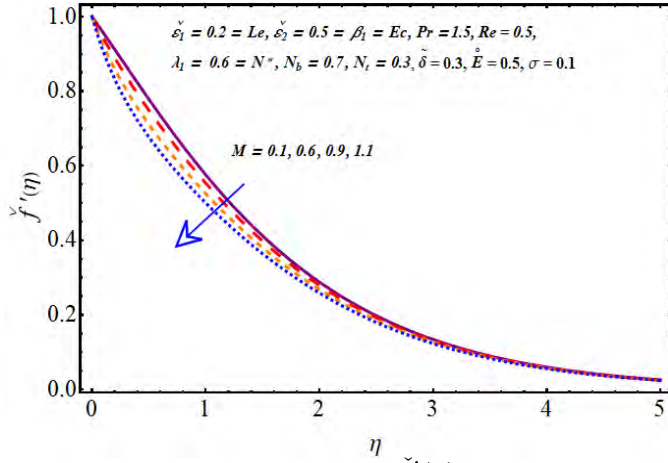


Fig. 4.3: Impact for  $\check{f}'(\eta)$  via  $M$

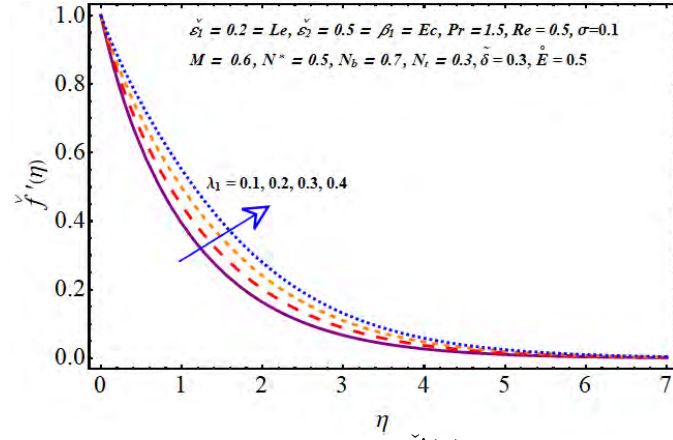


Fig. 4.4: Impact for  $\check{f}'(\eta)$  via  $\lambda_1$

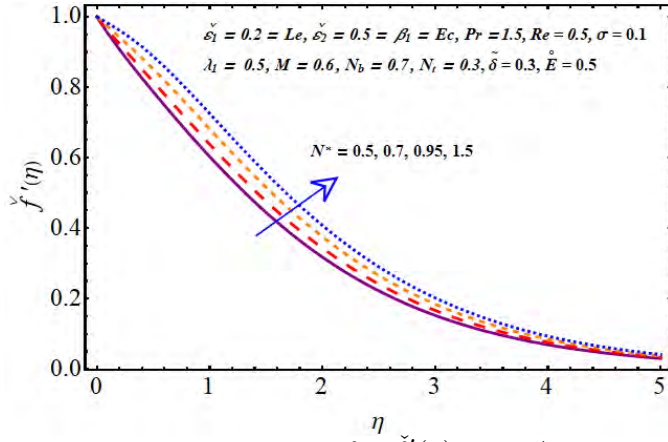


Fig. 4.5: Impact for  $\check{f}'(\eta)$  via  $N^*$

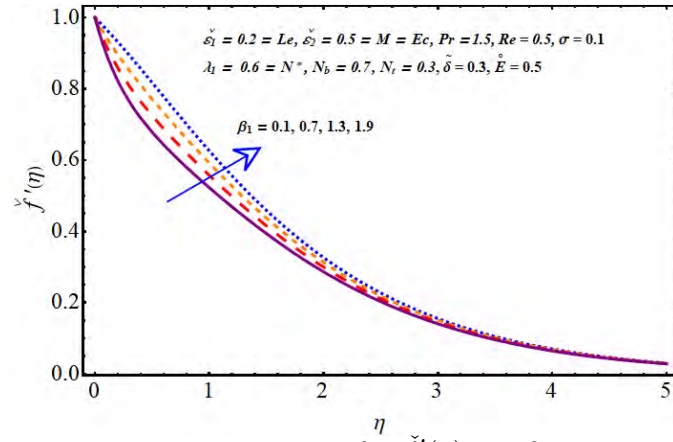


Fig. 4.6: Impact for  $\check{f}'(\eta)$  via  $\beta_1$

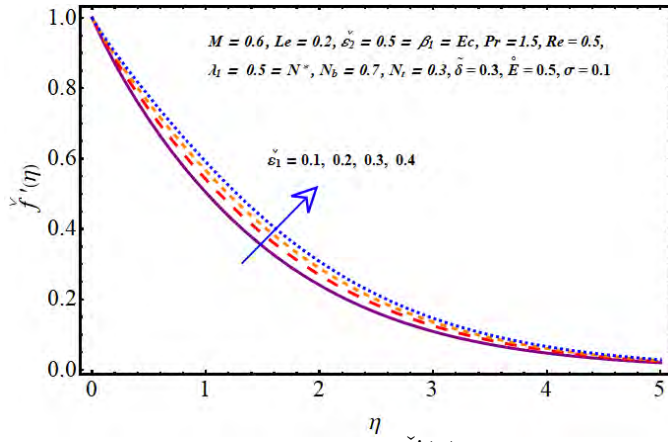


Fig. 4.7: Impact for  $\check{f}'(\eta)$  via  $\check{\epsilon}_1$

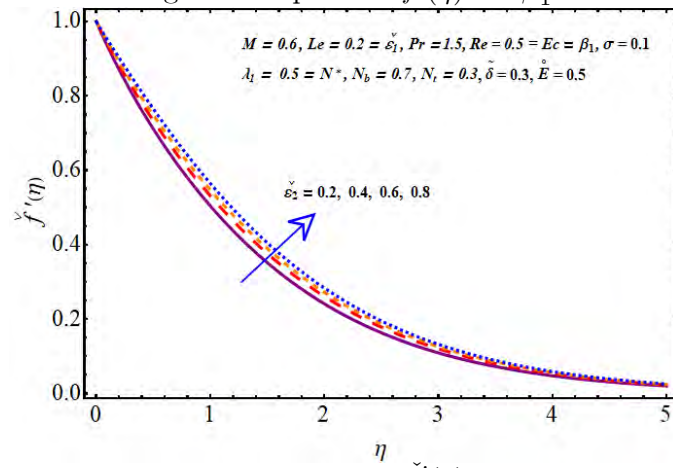


Fig. 4.8: Impact for  $\check{f}'(\eta)$  via  $\check{\epsilon}_2$

Variation in temperature  $\check{\theta}(\eta)$  in view of higher mixed convection parameter  $\check{\lambda}$  can be seen through Fig. 4.9. Clearly temperature  $\check{\theta}(\eta)$  decreases by increasing  $\lambda_1$ . Temperature  $\check{\theta}(\eta)$

variation via Brownian motion parameter  $N_b$  is demonstrated in Fig. 4.10. Temperature rises as a result of higher  $N_b$ . Graphical presentation of  $N_t$  for  $\check{\theta}(\eta)$  is reflected in Fig. 4.11. As in thermophoresis process, the heat transfer from the hotter surface to the cooler one so by increasing  $N_t$  the temperature  $\check{\theta}(\eta)$  increases. Change of temperature due to variation in Prandtl number  $Pr$  is captured in Fig. 4.12. Since higher  $Pr$  tends to decrease in thermal diffusivity so temperature and corresponding boundary layer are decreased. Fig. 4.13 explores variation of temperature  $\check{\theta}(\eta)$  for magnetic parameter  $M$ . It is found that temperature is an increasing function of magnetic parameter  $M$ . Fig. 4.14 discloses the influence of Eckert number  $Ec$  on temperature  $\check{\theta}(\eta)$ . Higher value of  $Ec$  tends to rise in viscous dissipation and accordingly the temperature increases.

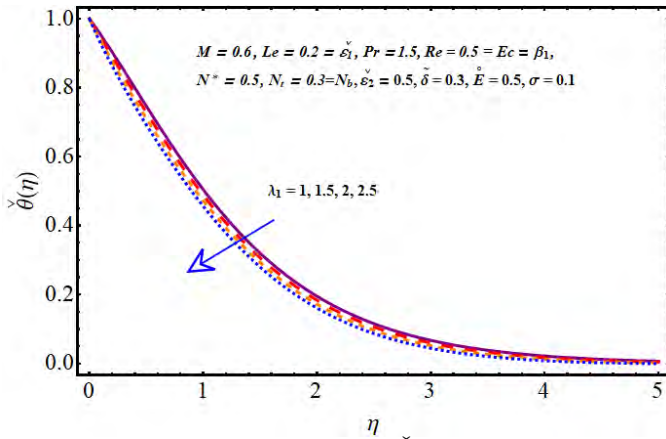


Fig. 4.9: Impact for  $\check{\theta}(\eta)$  via  $\lambda_1$

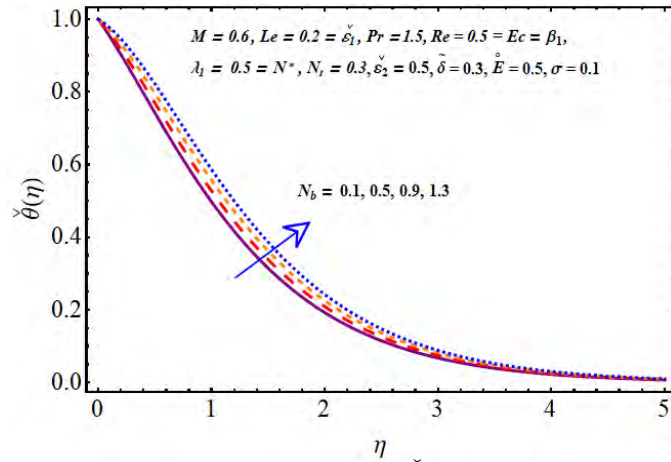


Fig. 4.10: Impact for  $\check{\theta}(\eta)$  via  $N_b$

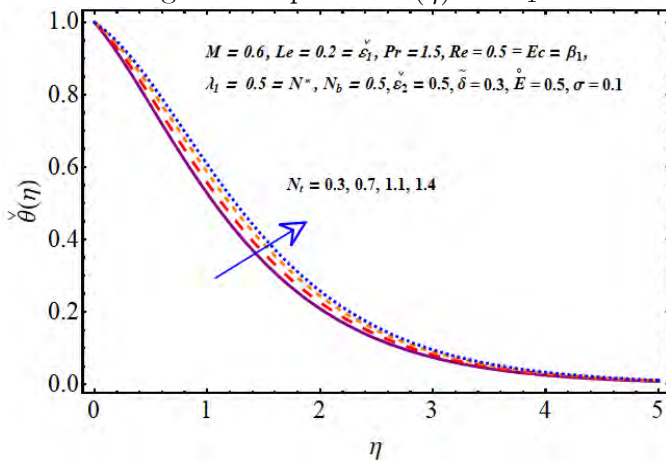


Fig. 4.11: Impact for  $\check{\theta}(\eta)$  via  $N_t$

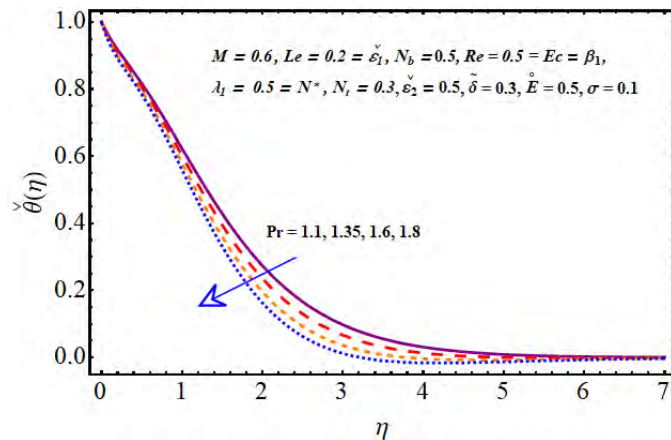


Fig. 4.12: Impact for  $\check{\theta}(\eta)$  via  $Pr$

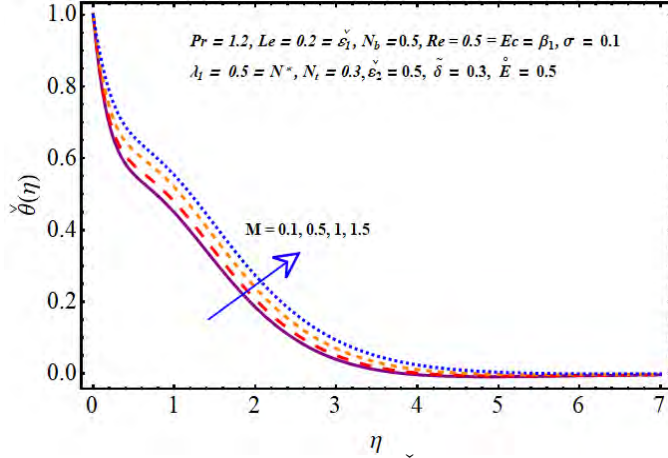


Fig. 4.13: Impact for  $\check{\theta}(\eta)$  via  $M$

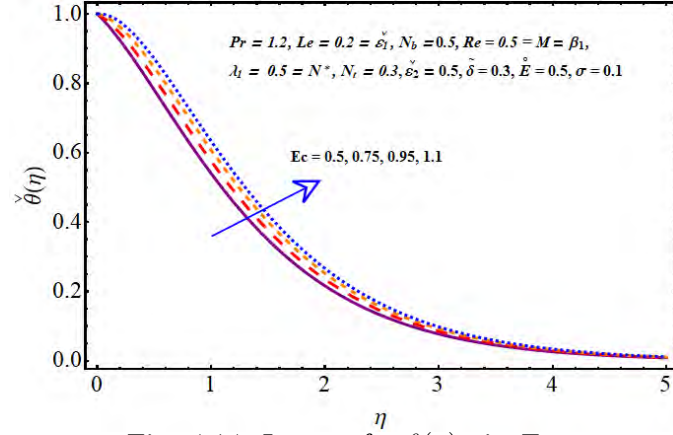


Fig. 4.14: Impact for  $\check{\theta}(\eta)$  via  $Ec$

Fig. 4.15 illustrates the variation of nanoparticles concentration in response to Brownian diffusion coefficient  $N_b$ . An increment in  $N_b$  causes decay in  $\check{\phi}(\eta)$  and related layer thickness. Fig. 4.16 elucidates the marginal growth in nanoparticles concentration as thermophoresis parameter  $N_t$  varies from  $N_t = 0.1$  to  $N_t = 0.4$ . Influence of Lewis number  $Le$  on  $\check{\phi}(\eta)$  is portrayed in Fig. 4.17. It is depicted that concentration distribution decreases for higher values of  $Le$ . Fig. 4.18 clarifies the influence of non-dimensional chemical reaction parameter  $\sigma$  on concentration of nanoparticles. As expected, the decline in nanoparticle concentration is noticed for higher  $\sigma$ . Prediction of dimensionless activation energy  $\check{E}$  on nanoparticles concentration is reflected in Fig. 4.19. Increasing behavior of concentration profile is noticed for larger  $\check{E}$ .

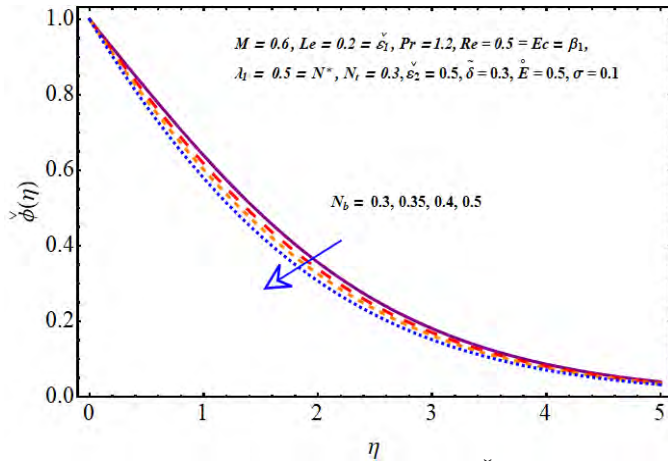


Fig. 4.15: Effect of  $N_b$  on  $\check{\phi}(\eta)$

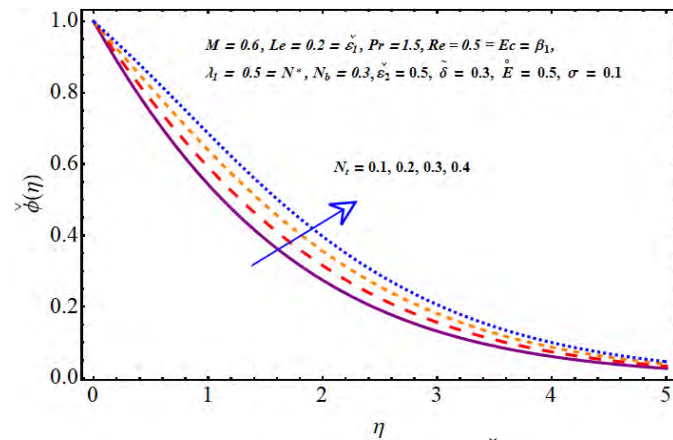


Fig. 4.16: Effect of  $N_t$  on  $\check{\phi}(\eta)$

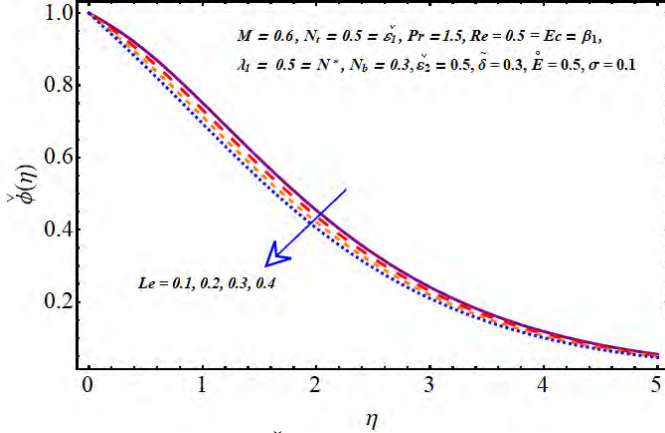


Fig. 4.17:  $\check{\phi}(\eta)$  variation via  $Le$

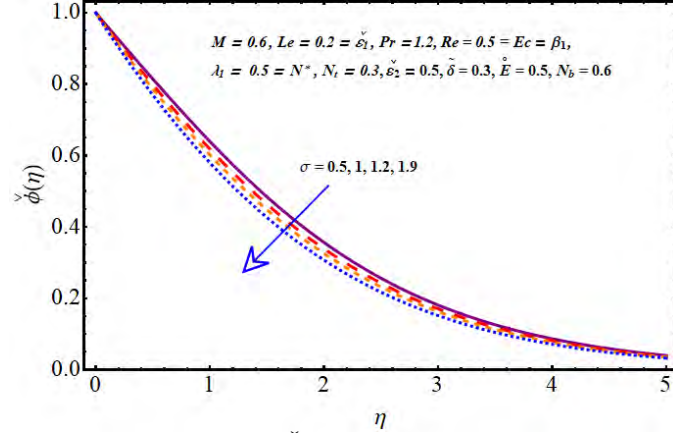


Fig. 4.18:  $\check{\phi}(\eta)$  variation via  $\sigma$

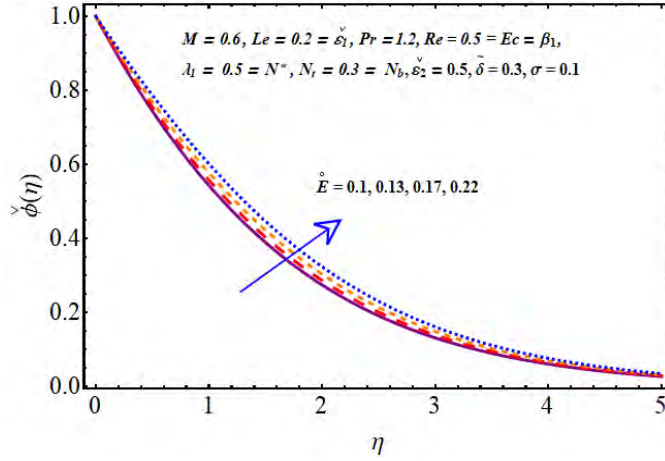


Fig. 4.19:  $\check{\phi}(\eta)$  variation via  $\hat{E}$

#### 4.5.1 Entropy rate analysis and Bejan number

Figs. 4.20 and 4.21 elucidate impact of Brinkman number  $Br$  on  $N_G(\eta)$  and Bejan number  $Be$ . It is conducted that  $N_G(\eta)$  increases for larger  $Br$ . It is due to the reason that irreversibility in fluid friction occurs by increasing  $Br$ . While Bejan number declines for higher  $Br$ . Consequences of Reynolds number  $Re$  on  $N_G(\eta)$  and  $Be$  are disclosed in Figs. 4.22 and 4.23. It is concluded from Eq. (4.17) that entropy generation minimization occurs due to all irreversibility processes and as a result  $N_G(\eta)$  enhances by increasing Reynolds number. Figs. 4.24 and 4.25 depict  $N_G(\eta)$  and  $Be$  for larger values of temperature difference parameter  $\check{\xi}$ . These Figs. reflect that  $N_G(\eta)$  and  $Be$  are increasing functions of  $\check{\xi}$ . It is because of the reason that for higher values of  $\check{\xi}$  the heat transfer dominates than fluid friction and magnetic field. Fig. 4.26

is sketched to show the effectiveness of Eckert number  $Ec$  on  $N_G(\eta)$ . Here higher  $Ec$  enhanced the entropy generation number  $N_G(\eta)$ .

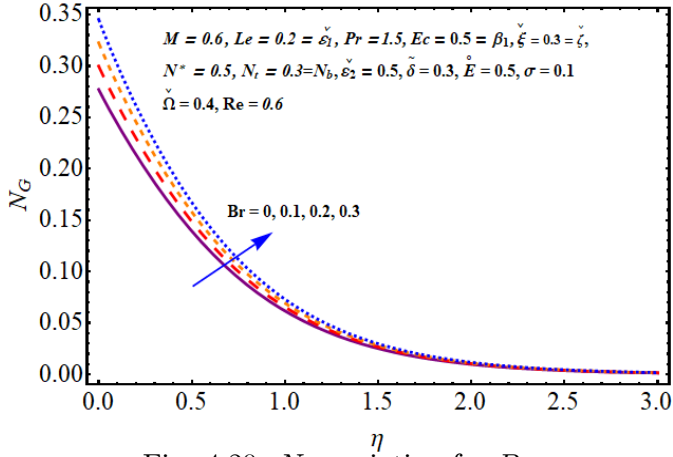


Fig. 4.20:  $N_G$  variation for  $Br$

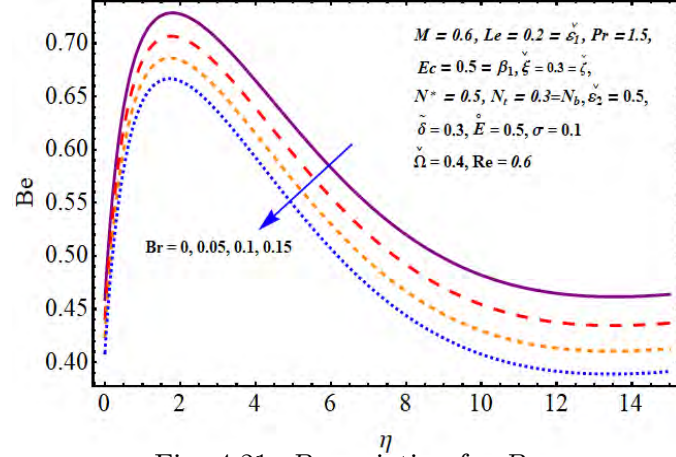


Fig. 4.21:  $Be$  variation for  $Br$

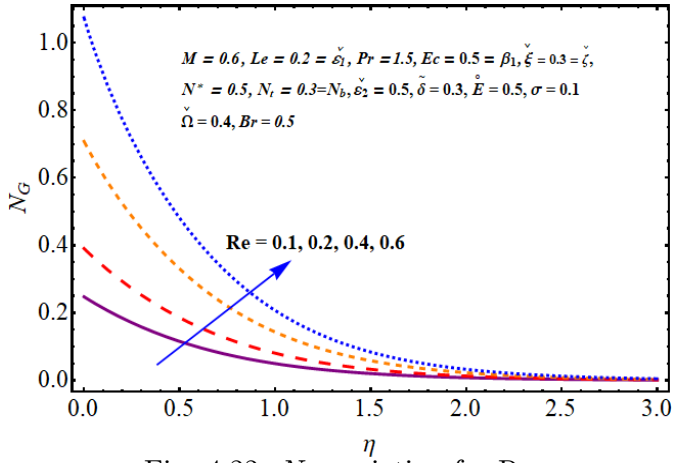


Fig. 4.22:  $N_G$  variation for  $Re$

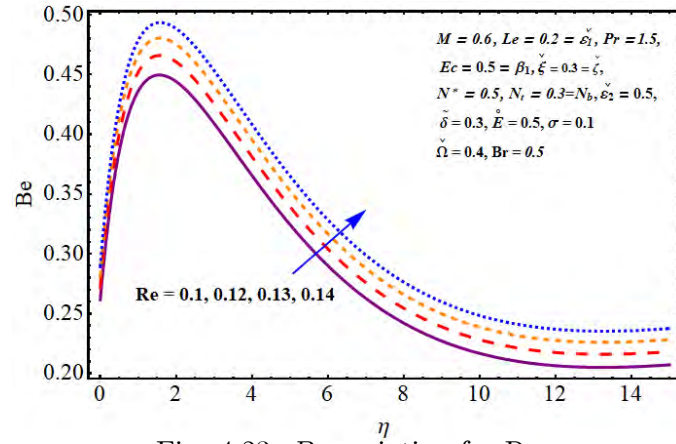


Fig. 4.23:  $Be$  variation for  $Re$

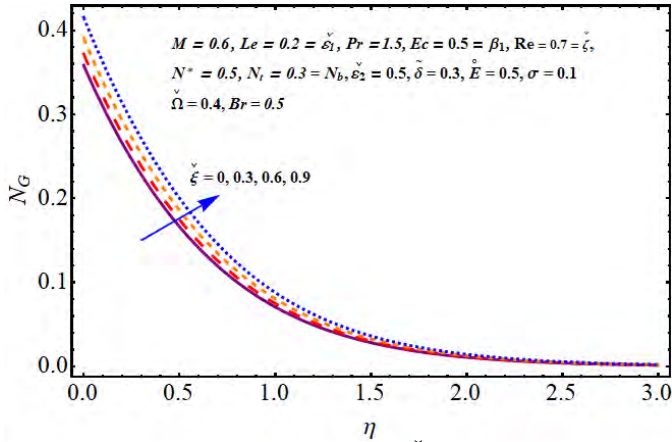


Fig. 4.24: Effect of  $\xi$  on  $N_G$

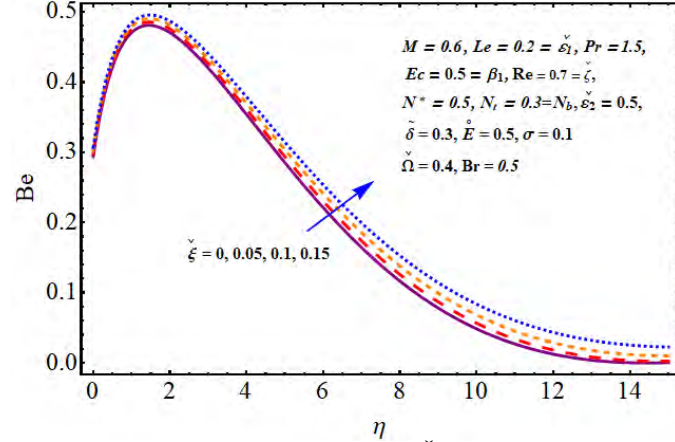


Fig. 4.25: Effect of  $\xi$  on  $Be$

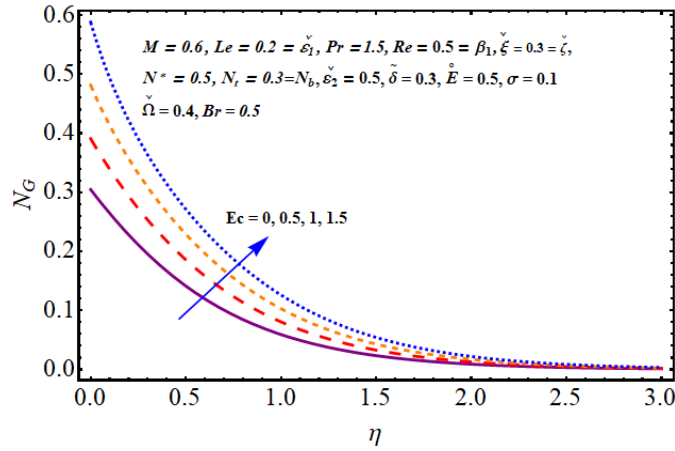


Fig. 4.26: Effect of  $Ec$  on  $N_G$

Influence of different embedded parameters on skin-friction coefficient, Nusselt number and Sherwood number are demonstrated in tables 4.2-4.4. By studying table 4.2, it is found that coefficient of drag force is affected by local buoyancy parameter  $N^*$  and non-dimensional activation energy  $\hat{E}$ . Here magnitude of skin-friction coefficient is enhanced for rising values of  $\beta_1$ ,  $M$  and  $\lambda_1$ . Table 4.3 displays variation in heat transfer rate. Higher  $Ec$  leads to decay in heat transfer rate. Heat transfer rate decreases for higher Brownian diffusion parameter  $N_b$  and thermophoresis parameter  $N_t$  while it enhances for Prandtl number  $Pr$  and magnetic parameter  $M$ . Further the rate of mass transfer is decreased for non-dimensional chemical reaction parameter  $\sigma$  and non-dimensional activation energy  $\hat{E}$  however it increases for other parameters as mentioned in table 4.4.

**Table 4.2:** Numerical description of skin friction coefficient for different parameters.

$\beta_1$	$M$	$\lambda_1$	$N^*$	$\hat{E}$	$-\text{Re}_x^{\frac{1}{2}} \tilde{C}_{fx}$
0.1	0.3	0.3	1	1.3	0.8688595
	0.3				0.9131529
	0.4				0.9673078
0.2	0.3	0.3	1	1.3	0.8701973
	0.4				0.8759865
	0.5				0.8783699
0.1	0.3	0.3	1	1.3	0.9030014
		0.5			0.9458779
		0.6			0.9977259
0.1	0.3	0.3	1.1	1.3	0.8039160
			1.2		0.7507146
			1.3		0.7290100
0.1	0.3	0.3	1	1.4	0.6347946
				1.5	0.5473585
				1.6	0.4763013



**Table 4.3:** Numerical description of Nusselt number for different parameters.

Pr	$M$	$Ec$	$N_b$	$N_t$	$Re_x^{-\frac{1}{2}} \tilde{Nu}_x$
1	0.5	1.6	0.1	0.1	0.2084664
	1.1				0.2544226
	1.2				0.3026473
1	0.6	1.6	0.1	0.1	0.2492009
	0.7				0.2893210
	0.8				0.3293889
1	0.5	1.7	0.1	0.1	0.2781875
		1.8			0.2288348
		1.9			0.1920219
1	0.5	1.6	0.2	0.1	0.1800328
			0.3		0.1541903
			0.4		0.1291780
1	0.5	1.6	0.1	0.2	0.1929118
				0.3	0.1779978
				0.4	0.1644246

**Table 4.4:** Numerical description of Sherwood number for different parameters.

$Le$	$\sigma$	$\hat{E}$	$N_b$	$N_t$	$Re_x^{-\frac{1}{2}} \tilde{Sh}_x$
0.8	0.1	1.1	0.2	0.3	0.3911616
0.9					0.4536701
1					0.5391772
0.8	0.2	1.1	0.2	0.3	0.3758304
	0.3				0.3745837
	0.4				0.3651333
0.8	0.1	1.2	0.2	0.3	0.3876376
		1.3			0.3654337
		1.4			0.3559579
0.8	0.1	1.1	0.25	0.3	0.5049517
			0.3		0.5660433
			0.35		0.6292429
0.8	0.1	1.1	0.2	0.4	0.04072542
				0.5	0.1498125
				0.6	0.2766914

## 4.6 Conclusions

Main points of present study are listed as follows:

- Velocity is in direct relation with mixed convection parameter  $\lambda_1$ .
- Velocity decays via larger magnetic parameter  $M$ .
- Concentration distribution reduces for higher chemical reaction parameter  $\sigma$ .
- Behaviors of Brownian diffusion coefficient  $N_b$  and thermophoresis parameter  $N_t$  are quite opposite for nanoparticles concentration.
- Concentration field is enhanced for larger activation energy parameter  $\hat{E}$ .
- Temperature is significantly enhanced for higher Eckert number  $Ec$ .

- Higher Brinkman number  $Br$ , Reynolds number  $Re$ , temperature difference parameter  $\check{\xi}$  and Eckert number  $Ec$  cause an increase in  $N_G$ .
- $Be$  decays approximately with higher  $Br$ .
- Influences of  $Re$  and  $\check{\xi}$  on  $Be$  are similar in a qualitative sense.

## Chapter 5

# Entropy generation optimization and activation energy in flow of Walters-B nanomaterial

### 5.1 Introduction

Entropy generation in flow of Walters-B nanomaterial is addressed. Energy equation consist of Ohmic heating, radiation and heat generation. Binary chemical reaction with modified Arrhenius energy is employed. The consequences of thermophoresis, Brownian motion and viscous dissipation are accounted. Convergent solutions by homotopy analysis technique are constructed. Intervals of convergence are explicitly identified. Results of physical quantities of interest are analyzed.

### 5.2 Modeling

Irreversibility process and activation energy with binary chemical reaction in flow of Walters-B nanomaterial bounded by a stretching surface is addressed. An incompressible liquids is conducting in presence of magnetic field with constant strength  $B_0$ . Small magnetic Reynolds number leads to omission of induced magnetic field. Here  $x$  and  $y$ -axes are parallel and normal to the surface. Heat source/ sink is considered. Surface temperature and concentration

are taken as  $\tilde{T}_w$  and  $\tilde{C}_w$  while ambient temperature and concentration are denoted by  $\tilde{T}_\infty$  and  $\tilde{C}_\infty$ . Fig. 1 describes the problem geometry. Governing mathematical equations of the system are as follow:

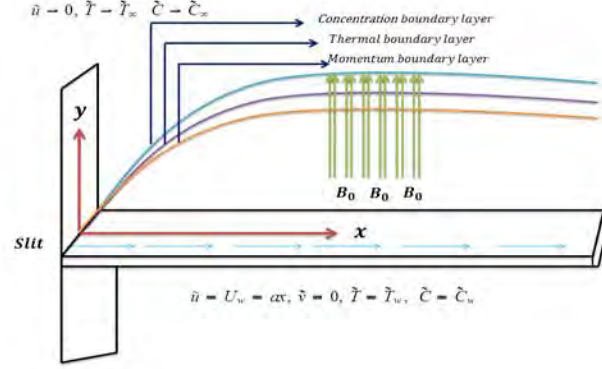


Fig. 5.1: Flow geometry

$$\frac{\partial \tilde{u}}{\partial x} + \frac{\partial \tilde{v}}{\partial y} = 0, \quad (5.1)$$

$$\tilde{u} \frac{\partial \tilde{u}}{\partial x} + \tilde{v} \frac{\partial \tilde{u}}{\partial y} = \nu \frac{\partial^2 \tilde{u}}{\partial y^2} - \frac{k_0}{\rho} \left( \tilde{u} \frac{\partial^3 \tilde{u}}{\partial x \partial y^2} + \frac{\partial \tilde{u}}{\partial x} \frac{\partial^2 \tilde{u}}{\partial y^2} + \tilde{v} \frac{\partial^3 \tilde{u}}{\partial y^3} - \frac{\partial \tilde{u}}{\partial y} \frac{\partial^2 \tilde{u}}{\partial x \partial y} \right) - \frac{\sigma B_0^2}{\rho} \tilde{u}, \quad (5.2)$$

$$\begin{aligned} \tilde{u} \frac{\partial \tilde{T}}{\partial x} + \tilde{v} \frac{\partial \tilde{T}}{\partial y} &= \frac{k}{\rho c_p} \frac{\partial^2 \tilde{T}}{\partial y^2} + \frac{\mu}{\rho c_p} \left( \frac{\partial \tilde{u}}{\partial y} \right)^2 - \frac{k_0}{\rho c_p} \left[ \frac{\partial \tilde{u}}{\partial x} \left( \frac{\partial \tilde{u}}{\partial y} \right)^2 + \tilde{u} \frac{\partial \tilde{u}}{\partial y} \frac{\partial^2 \tilde{u}}{\partial x \partial y} + \tilde{v} \frac{\partial \tilde{u}}{\partial y} \frac{\partial^2 \tilde{u}}{\partial y^2} + 2 \left( \frac{\partial \tilde{u}}{\partial y} \right)^2 \frac{\partial \tilde{v}}{\partial y} \right] \\ &+ \frac{1}{\rho c_p} \frac{16\sigma^* \tilde{T}_\infty^3}{3k^*} \frac{\partial^2 \tilde{T}}{\partial y^2} + \frac{Q_0}{\rho c_p} (\tilde{T} - \tilde{T}_\infty) + \tau \left[ D_B \frac{\partial \tilde{T}}{\partial y} \frac{\partial \tilde{C}}{\partial y} + \frac{D_{\tilde{T}}}{\tilde{T}_\infty} \left( \frac{\partial \tilde{T}}{\partial y} \right)^2 \right] + \sigma \frac{B_0^2}{\rho_f} \tilde{u}^2, \quad (5.3) \end{aligned}$$

$$\tilde{u} \frac{\partial \tilde{C}}{\partial x} + \tilde{v} \frac{\partial \tilde{C}}{\partial y} = D_B \left( \frac{\partial^2 \tilde{C}}{\partial y^2} \right) + \frac{D_{\tilde{T}}}{\tilde{T}_\infty} \left( \frac{\partial^2 \tilde{T}}{\partial y^2} \right) - K_r^2 (\tilde{C} - \tilde{C}_\infty) \left[ \frac{\tilde{T}}{\tilde{T}_\infty} \right]^n \exp \left[ \frac{-E_a}{k_1 \tilde{T}} \right], \quad (5.4)$$

subject to the conditions

$$\tilde{u} = U_w = ax, \quad \tilde{v} = 0, \quad \tilde{T} = \tilde{T}_w, \quad \tilde{C} = \tilde{C}_w \quad \text{at} \quad y = 0 \quad (5.5)$$

$$\tilde{u} \rightarrow 0, \quad \tilde{T} \rightarrow \tilde{T}_\infty, \quad \tilde{C} \rightarrow \tilde{C}_\infty \quad \text{as} \quad y \rightarrow \infty$$

Here  $(\tilde{u}, \tilde{v})$  are velocity components in  $(x, y)$  directions,  $(k_0), (k), (c_p), (\rho), (\check{\sigma}), (\sigma^*), (k^*), (Q_0), (D_B), (K_r), (E_a), (k_1),$  and  $(D_{\tilde{T}})$  denote material constant, density, electrical conductivity, specific heat, thermal conductivity, Stefan-Boltzmann constant, mean absorption coefficient, heat generation coefficient, Brownian diffusion coefficient, Boltzmann constant, the dimensionless constant or rate constant having the range  $-1 < n < 1$ , chemical reaction parameter, activation energy and thermophoretic diffusion coefficient. Considering

$$\begin{aligned} \psi &= \sqrt{avx}f(\eta), & \eta &= \sqrt{\frac{a}{v}}y \\ \theta(\eta) &= \frac{\tilde{T} - \tilde{T}_\infty}{\tilde{T}_w - \tilde{T}_\infty}, & \phi(\eta) &= \frac{\tilde{C} - \tilde{C}_\infty}{\tilde{C}_w - \tilde{C}_\infty}, \end{aligned} \quad (5.7)$$

the problems can be reduced in to the following forms

$$\check{f}''' - \check{f}'^2 + \check{f}\check{f}'' - K_0(2\check{f}'\check{f}'''' - \check{f}\check{f}'''' - \check{f}'^2) - M\check{f}' = 0, \quad (5.8)$$

$$(1 + R_d)\check{\theta}'' + \text{Pr} Ec[K_0 f f'' f''' + (f'')^2] + \text{Pr} N_b \check{\theta}' \check{\phi}' + \text{Pr} N_t (\check{\theta}')^2 + \text{Pr} \tilde{Q} \check{\theta} = 0, \quad (5.9)$$

$$\check{\phi}'' + \frac{N_t}{N_b} \check{\theta}'' + \text{Pr} Le \check{f} \check{\phi}' - \text{Pr} Le \sigma^2 (1 + \check{\delta} \theta)^n \exp \left[ \frac{-\check{E}}{1 + \check{\delta} \theta} \right] \check{\phi} = 0, \quad (5.10)$$

$$\begin{aligned} \check{f}'(\eta) &= 1, & \check{f}(\eta) &= 0 & \check{\theta}(\eta) &= 1, & \check{\phi}(\eta) &= 1 & \text{at } \eta &= 0, \\ \check{f}'(\eta) &\rightarrow 0, & \check{\theta}(\eta) &\rightarrow 0, & \check{\phi}(\eta) &\rightarrow 0 & \text{when } \eta &\rightarrow \infty. \end{aligned} \quad (5.11)$$

where

$$\begin{aligned} K_0 &= \frac{k_0 a}{\mu}, & M &= \frac{\check{\sigma} B_0^2}{\rho a}, & R &= \frac{16 \sigma^* \tilde{T}_\infty^3}{3 k k^*}, & \text{Pr} &= \frac{\mu c_p}{k}, & Ec &= \frac{U_w^2}{c_p (T_w - T_\infty)}, \\ N_b &= \frac{(\rho c)_p D_B (C_w - C_\infty)}{v(\rho c)_f}, & N_t &= \frac{(\rho c)_p D_T (T_w - T_\infty)}{v(\rho c)_f}, & \tilde{Q} &= \frac{Q_0}{a \rho c_p}, & Le &= \frac{(k/\rho c_p)}{D_B}, \\ \check{E} &= \frac{-E_a}{k_1 \tilde{T}_\infty}, & \check{\delta} &= \frac{(\tilde{T}_w - \tilde{T}_\infty)}{\tilde{T}_\infty}, & \sigma &= \frac{K_r^2}{a}. \end{aligned}$$

In above expressions the definitions  $(M)$ ,  $(Pr)$ ,  $(N_t)$ ,  $(Le)$ ,  $(R)$ ,  $(Ec)$ ,  $(\tilde{Q})$ ,  $(N_b)$ ,  $(K_0)$ ,  $(\tilde{E})$ ,  $(\tilde{\delta})$  and  $(\sigma)$  denote magnetic parameter, Prandtl number, thermophoresis parameter, Lewis number, radiation parameter, Eckert number, heat generation variable, Brownian motion parameter, non-dimensional fluid parameter, dimensionless activation energy parameter, temperature ratio parameter and non-dimensional chemical reaction parameter respectively.

Coefficient of skin friction and Nusselt and Sherwood numbers are presented in to definitions given below

$$\tilde{C}_{fx} = \frac{2 \tilde{\tau}_w|_{y=0}}{\rho U_w^2}, \quad (5.12)$$

$$\tilde{N}_{ux} = \frac{x \tilde{q}_w|_{y=0}}{k(\tilde{T}_w - \tilde{T}_\infty)}, \quad (5.13)$$

$$\tilde{S}_{hx} = \frac{x \tilde{q}_m|_{y=0}}{D_B(\tilde{C}_w - \tilde{C}_\infty)}. \quad (5.14)$$

where

$$\tilde{\tau}_w = \mu \frac{\partial u}{\partial y} - k_0 \left( u \frac{\partial^2 u}{\partial x \partial y} - 2 \frac{\partial u}{\partial x} \frac{\partial u}{\partial y} \right), \quad (5.15)$$

$$\tilde{q}_w = -k \frac{\partial \tilde{T}}{\partial y} - \frac{16\sigma^* \tilde{T}_\infty^3}{3k^*} \frac{\partial \tilde{T}}{\partial y}, \quad (5.16)$$

$$\tilde{q}_m = D_B \frac{\partial \tilde{C}}{\partial y}. \quad (5.17)$$

Equation (5.7) and (5.12)-(5.17) give

$$\text{Re}_x^{0.5} \tilde{C}_{fx} = 2[1 + K_0 \check{f}'(0)] \check{f}''(0), \quad (5.18)$$

$$\text{Re}_x^{-0.5} \tilde{N}_{ux} = - \left( 1 + \frac{4}{3} R_d \right) \check{\theta}'(0), \quad (5.19)$$

$$\text{Re}_x^{-0.5} \tilde{S}_{hx} = -\check{\phi}'(0), \quad (5.20)$$

in which  $\text{Re}_x = \frac{x U_w}{\nu}$  depicts local Reynold's number.

### 5.2.1 Entropy generation examination

Irreversibility analysis for nanofluid flow of Walter's-B fluid with Arrhenius activation energy is main interest. Thermal radiation, viscous dissipation and MHD effects are implemented for entropy generation minimization. Relevant expression satisfies

$$\tilde{S}_{gen}''' = \underbrace{\frac{k}{\tilde{T}^2} \left[ 1 + \frac{16\sigma^* \tilde{T}_\infty^3}{3kk^*} \right] \left( \frac{\partial \tilde{T}}{\partial y} \right)^2}_{\text{heat transfer irreversibility}} + \underbrace{\frac{1}{\tilde{T}} \tilde{\Phi}}_{\text{viscous dissipation irreversibility}} + \underbrace{\frac{\sigma B_0^2 \tilde{u}^2}{\tilde{T}}}_{\text{Joule heating irreversibility}} + \underbrace{\frac{RD}{\tilde{C}_\infty} \left( \frac{\partial \tilde{C}}{\partial y} \right)^2 + \frac{RD}{\tilde{T}_\infty} \left( \frac{\partial \tilde{T}}{\partial y} \right) \left( \frac{\partial \tilde{C}}{\partial y} \right)}_{\text{Diffusive irreversibility}} \quad (5.21)$$

$$\tilde{\Phi} = k_0 \left[ \frac{\partial u}{\partial x} \left( \frac{\partial u}{\partial y} \right)^2 + u \frac{\partial u}{\partial y} \frac{\partial^2 u}{\partial x \partial y} + v \frac{\partial u}{\partial y} \frac{\partial^2 u}{\partial y^2} + 2 \left( \frac{\partial u}{\partial y} \right)^2 \frac{\partial v}{\partial y} \right], \quad (5.22)$$

From Eqs. (5.16) and Eq. (5.17) one obtain

$$\tilde{S}_{gen}''' = \underbrace{\frac{k}{\tilde{T}^2} \left[ 1 + \frac{16\sigma^* \tilde{T}_\infty^3}{3kk^*} \right] \left( \frac{\partial \tilde{T}}{\partial y} \right)^2}_{\text{heat transfer irreversibility}} + \underbrace{\frac{k_0}{\tilde{T}} \left[ \frac{\partial u}{\partial x} \left( \frac{\partial u}{\partial y} \right)^2 + u \frac{\partial u}{\partial y} \frac{\partial^2 u}{\partial x \partial y} + v \frac{\partial u}{\partial y} \frac{\partial^2 u}{\partial y^2} + 2 \left( \frac{\partial u}{\partial y} \right)^2 \frac{\partial v}{\partial y} \right]}_{\text{viscous dissipation irreversibility}} + \underbrace{\frac{RD}{\tilde{C}_\infty} \left( \frac{\partial \tilde{C}}{\partial y} \right)^2 + \frac{RD}{\tilde{T}_\infty} \left( \frac{\partial \tilde{T}}{\partial y} \right) \left( \frac{\partial \tilde{C}}{\partial y} \right)}_{\text{Diffusive irreversibility}} + \underbrace{\frac{\sigma B_0^2 \tilde{u}^2}{\tilde{T}}}_{\text{Joule heating irreversibility}} \quad (5.23)$$

Entropy minimization in dimensionless form is

$$\begin{aligned} \tilde{N}_G &= (1 + R_d) \text{Re}_x \tilde{\theta}'^2 + \frac{K_0 Br \text{Re}_x}{\tilde{\Omega}} \tilde{f} \tilde{f}'' \tilde{f}''' + \text{Re}_x \zeta \left( \frac{\tilde{\xi}}{\tilde{\Omega}} \right)^2 \tilde{\phi}'^2 \\ &+ \text{Re}_x \zeta \left( \frac{\tilde{\xi}}{\tilde{\Omega}} \right) \tilde{\theta}' \tilde{\phi}' + \frac{\text{Re}_x M Br}{\tilde{\Omega}} \tilde{f}'^2, \end{aligned} \quad (5.24)$$

$$\begin{aligned} Br &= \frac{\mu U_w^2}{k \Delta \tilde{T}}, & \tilde{\Omega} &= \frac{\Delta \tilde{T}}{\tilde{T}_\infty}, & \zeta &= \frac{RD \tilde{C}_\infty}{k}, & \tilde{\xi} &= \frac{\Delta \tilde{C}}{\tilde{C}_\infty} \\ \tilde{N}_G &= \frac{S_G''' \tilde{T}_\infty^2 x^2}{k (\Delta \tilde{T})^2}, \end{aligned} \quad (5.25)$$



where  $(\check{N}_G)$ ,  $(\check{\zeta})$ ,  $(Br)$ ,  $(\check{\xi})$  and  $(\check{\Omega})$  denote total entropy rate, diffusion constant, Brinkman number, concentration and temperature difference parameters respectively.

### 5.3 Solution methodology

Series solution of above mentioned systems are obtained via homotopic technique. The suitable initial guesses  $(\check{f}_0, \check{\theta}_0, \check{\phi}_0)$  and corresponding linear operators  $(\tilde{\mathcal{L}}_{\check{f}}, \tilde{\mathcal{L}}_{\check{\theta}}, \tilde{\mathcal{L}}_{\check{\phi}})$  are

$$\check{f}_0(\eta) = 1 - e^\eta, \quad (5.26)$$

$$\check{\theta}_0(\eta) = e^{-\eta}, \quad (5.27)$$

$$\check{\phi}_0(\eta) = e^{-\eta}, \quad (5.28)$$

$$\tilde{\mathcal{L}}_{\check{f}}(\eta) = \frac{d^3 \check{f}}{d\eta^3} - \frac{d\check{f}}{d\eta}, \quad \tilde{\mathcal{L}}_{\check{\theta}}(\eta) = \frac{d^2 \check{\theta}}{d\eta^2} - \check{\theta}, \quad \tilde{\mathcal{L}}_{\check{\phi}}(\eta) = \frac{d^2 \check{\phi}}{d\eta^2} - \check{\phi}, \quad (5.29)$$

$$\tilde{\mathcal{L}}_{\check{f}} \left[ \hat{X}_1 + \hat{X}_2 e^\eta + \hat{X}_3 e^{-\eta} \right] = 0, \quad (5.30)$$

$$\tilde{\mathcal{L}}_{\check{\theta}} \left[ \hat{X}_4 e^\eta + \hat{X}_5 e^{-\eta} \right] = 0, \quad (5.31)$$

$$\tilde{\mathcal{L}}_{\check{\phi}} \left[ \hat{X}_6 e^\eta + \hat{X}_7 e^{-\eta} \right] = 0. \quad (5.32)$$

with  $\hat{X}_i$  ( $i = 1 - 7$ ) as the arbitrary constants.

### 5.4 Convergence analysis

For this purpose the  $\hbar$ -curves are displayed in Fig. 5.2. The series solutions converge for ranges of auxiliary parameters satisfying  $-1.5 \leq \hbar_{\check{f}} \leq -0.5$ ,  $-1.4 \leq \hbar_{\check{\theta}} \leq -0.6$ , and  $-1.8 \leq \hbar_{\check{\phi}} \leq -0.4$ . Table 5.1 includes numerical computations of convergent solutions. Clearly the momentum equation converges at 9<sup>th</sup> order of approximation while 15<sup>th</sup> and 19<sup>th</sup> orders of approximations are sufficient for temperature and concentration.

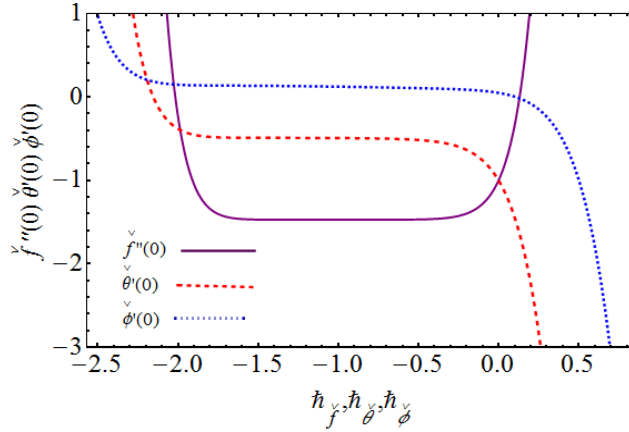


Fig. 5.2:  $\tilde{h}$ -curves for  $\tilde{h}_f$ ,  $\tilde{h}_\theta$  and  $\tilde{h}_\phi$ .

**Table 5.1:** Velocity, temperature and concentration convergence.

Order of approximation	$-\tilde{f}''(0)$	$-\tilde{\theta}'(0)$	$\tilde{\phi}'(0)$
1	1.3500	0.73167	0.077040
9	1.4719	0.49925	0.11297
15	1.4719	0.49195	0.12603
19	1.4719	0.49195	0.12967
30	1.4719	0.49195	0.12967
40	1.4719	0.49195	0.12967

## 5.5 Discussion

Figs. (5.3-5.16) illustrates the velocity, temperature, concentration and entropy generation minimization. Fig. 5.3 presents outcome of  $(M)$  on velocity. For  $(M = 0.1, 0.3, 0.5, 0.7)$  the velocity decays gradually when Lorentz force (opposing force) enhances. In Fig. 5.4, change in velocity is shown for higher dimensionless fluid variable  $(K_0)$ . An increase in  $(K_0 = 0.5, 0.6, 0.7, 0.8)$  yields reduction of velocity. Temperature for  $(N_t)$  variation is shown in Fig. 5.5. Temperature enhances for  $(N_t = 0.5, 1, 1.4, 2.1)$ . As heat transfer occurs from region of hotter region to the cooler part. This process boosts the temperature. Result of higher Brownian motion parameter  $(N_b)$  on temperature is depicted in Fig. 5.6. Temperature rises via higher  $(N_b = 0.7, 0.9, 1.3, 1.7)$ . Variation of Pr on temperature is shown in Fig. 5.7. Thermal dif-

fusivity decays for ( $Pr = 1.1, 1.6, 2.2, 2.6$ ) and so temperature reduces. Fig. 5.8 displays the outcome of Eckert number ( $Ec$ ) on temperature. Temperature is an increasing function of ( $Ec = 0.5, 0.9, 1.3, 1.6$ ). Higher Eckert number give rise to kinetic energy of fluid and consequently fluid temperature enhances. Fig. 5.9 provides description of radiation on temperature. An increase of ( $R_d = 0.2, 0.4, 0.6, 0.8$ ) enhances temperature. Here radiation parameter defines the transfer rate of thermal radiation relative to conductive heat transfer rate. For higher radiation parameter the radiation term dominates over conduction. Hence more heat releases in a system due to radiative heat flux and so temperature increases. Fig. 5.10 gives outcome of ( $\tilde{Q}$ ) on temperature. Temperature increases as ( $\tilde{Q} = 0.1, 1, 1.7, 2.4$ ) generates energy in system. Outcomes of ( $N_t$ ) and ( $N_b$ ) on concentration are sketched in Figs. 5.11 and 5.12. Opposite trend are observed in case of higher ( $N_t = 0.5, 0.9, 1.3, 1.7$ ) and ( $N_b = 0.6, 0.9, 1.6, 2.7$ ) for concentration. Variation in fluids concentration against dimensionless chemical reaction parameter ( $\sigma$ ) is pictured in Fig. 5.13. Increasing ( $\sigma = 0.5, 0.9, 1.25, 1.55$ ) lead to reduction of concentration. Fig. 5.14 provides impact of activation energy parameter ( $\hat{E}$ ) on concentration. It can be seen through figure that concentration rises for higher ( $\hat{E} = 0.2, 1.5, 2.1, 2.9$ ).

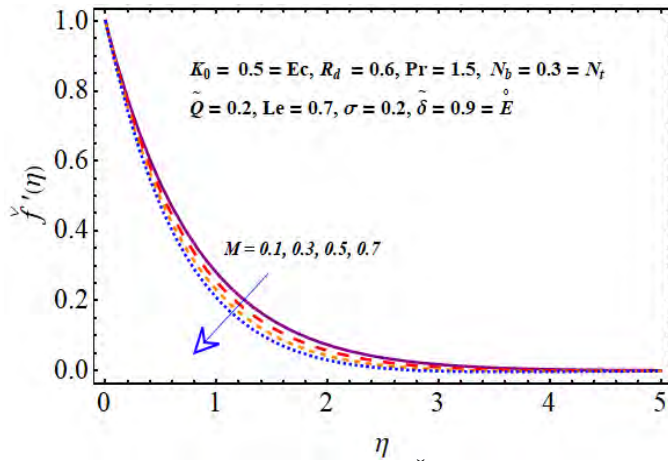


Fig. 5.3: Variation of  $\check{f}(\eta)$  via  $M$

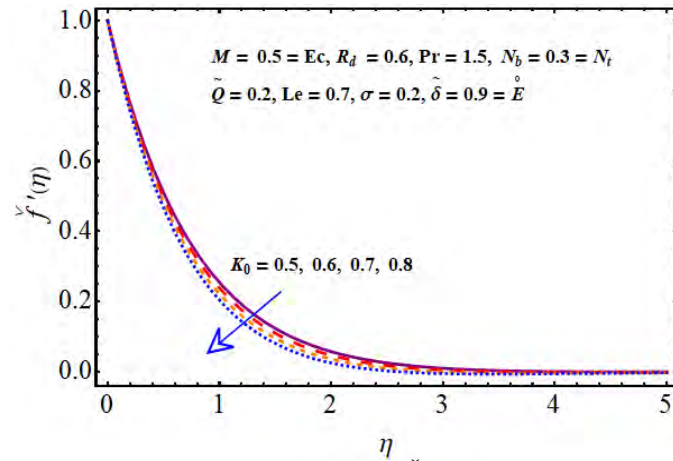


Fig. 5.4: Impact for  $\check{f}(\eta)$  via  $K_0$

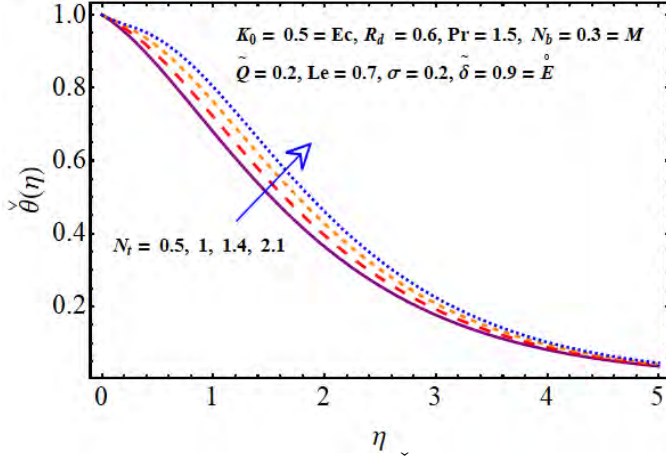


Fig. 5.5: Impact for  $\check{\theta}(\eta)$  via  $N_t$

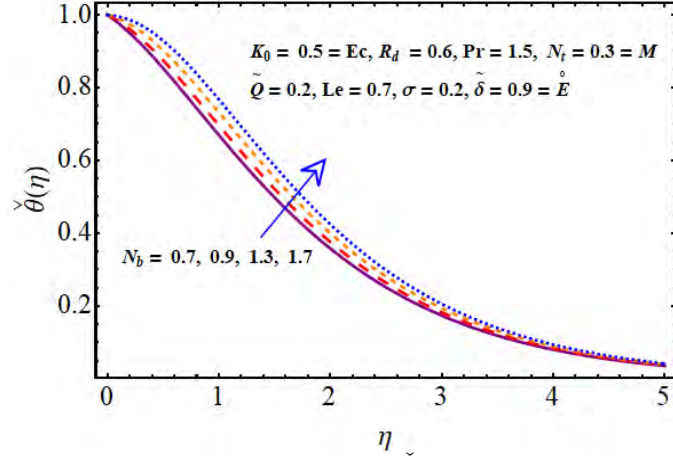


Fig. 5.6: Impact for  $\check{\theta}(\eta)$  via  $N_b$

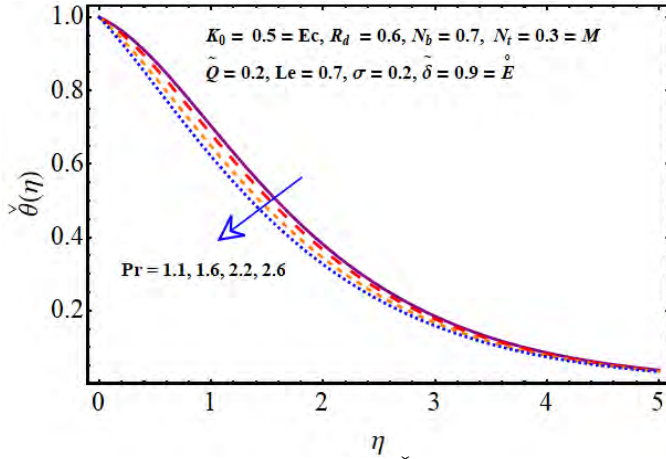


Fig. 5.7: Impact for  $\check{\theta}(\eta)$  via  $Pr$

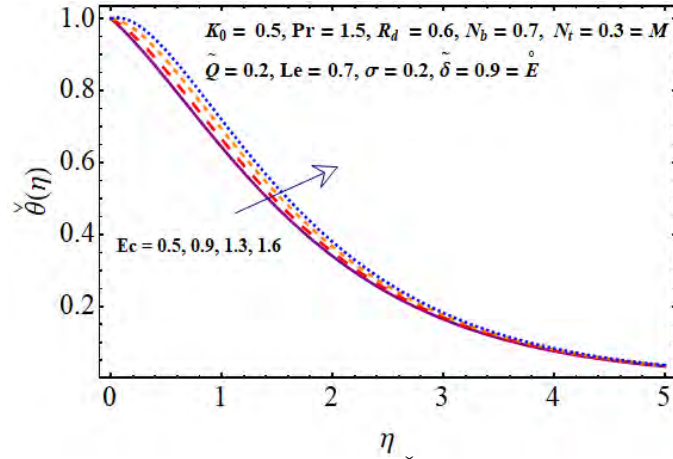


Fig. 5.8: Impact for  $\check{\theta}(\eta)$  via  $Ec$

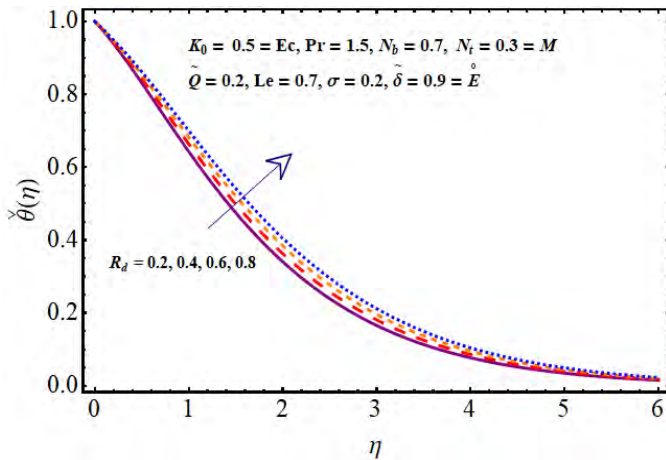


Fig. 5.9: Influence of  $R_d$  on  $\check{\theta}(\eta)$

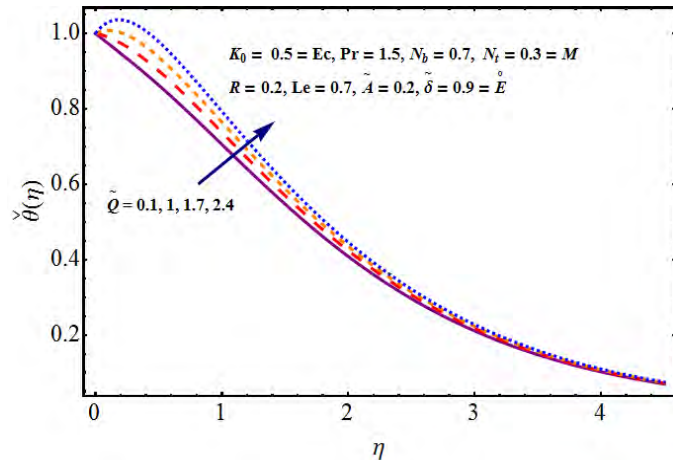


Fig. 5.10: Influence of  $\tilde{Q}$  on  $\check{\theta}(\eta)$

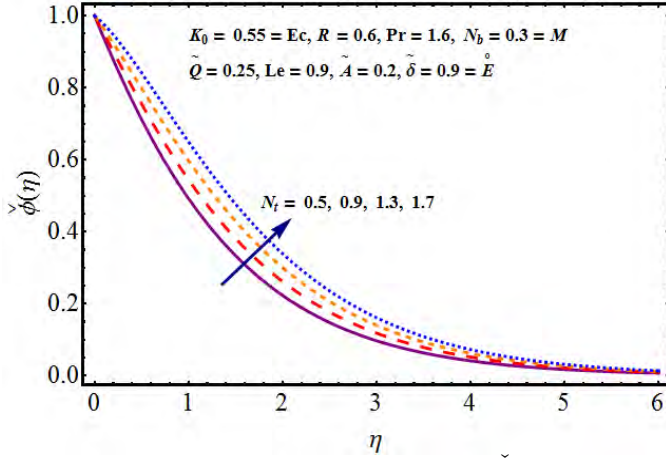


Fig. 5.11: Influence of  $N_t$  on  $\check{\phi}(\eta)$

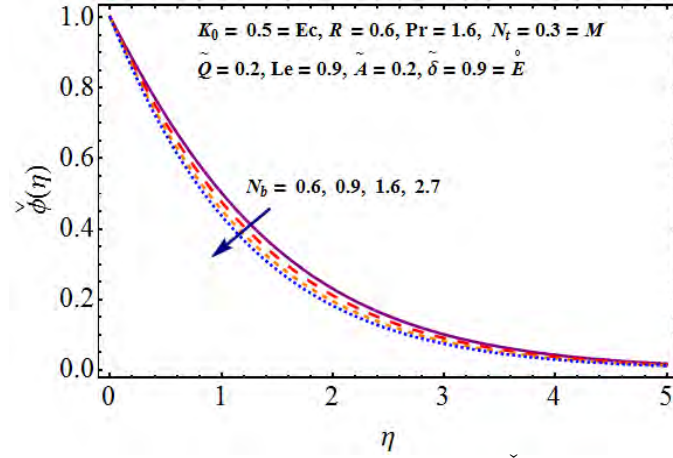


Fig. 5.12: Influence of  $N_b$  on  $\check{\phi}(\eta)$

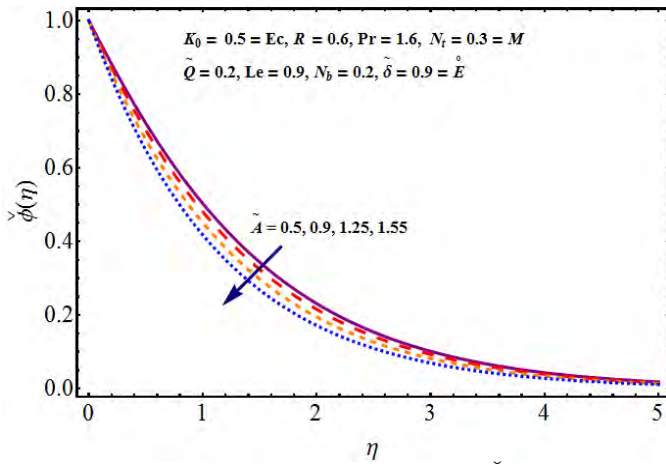


Fig. 5.13: Influence of  $\sigma$  on  $\check{\phi}(\eta)$

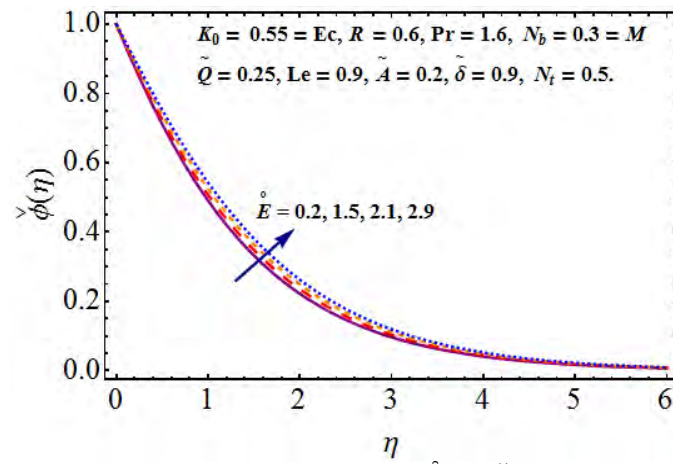


Fig. 5.14: Influence of  $\hat{E}$  on  $\check{\phi}(\eta)$

Influences of  $M$  and  $K_0$  on  $\text{Re}_x^{0.5} \tilde{C}_{fx}$  are disclosed in Fig. 5.15. It is clear that  $\text{Re}_x^{0.5} \tilde{C}_{fx}$  increases for higher  $M$  and  $K_0$ . Fig. 5.16 depicts  $Ec$  and  $R$  on  $\text{Re}_x^{-0.5} \tilde{N}_{ux}$ . Higher values of  $R$  and  $Ec$  decay  $\text{Re}_x^{-0.5} \tilde{N}_{ux}$ . Variations of  $\hat{E}$  and  $\sigma$  on  $\text{Re}_x^{-0.5} \tilde{S}_{hx}$  are shown in Fig. 5.17. ( $\text{Re}_x^{-0.5} \tilde{S}_{hx}$ ) is decreasing function of  $\hat{E}$  and  $\sigma$ .

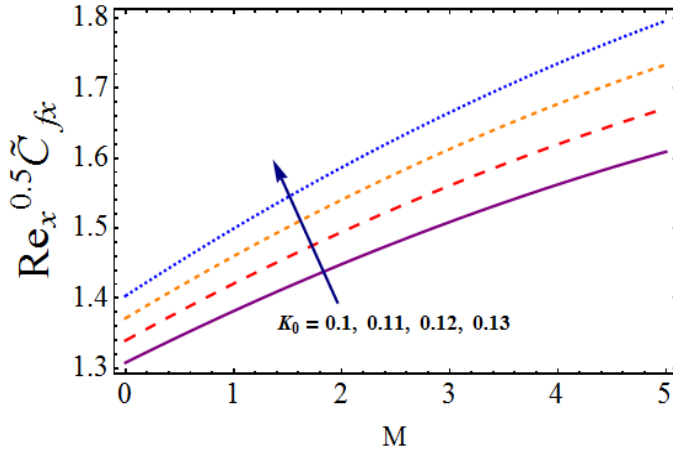


Fig. 5.15: Variations of  $M$  and  $K_0$  on  $\text{Re}_x^{0.5} \tilde{C}_{fx}$ .

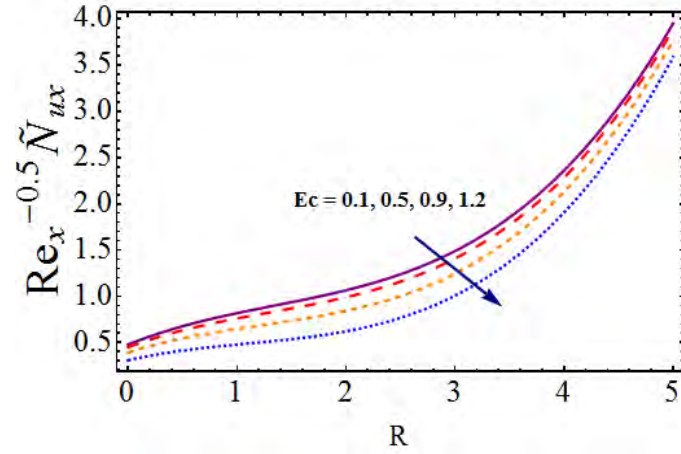


Fig. 5.16: Variations of  $R$  and  $Ec$  on  $\text{Re}_x^{-0.5} \tilde{N}_{ux}$ .

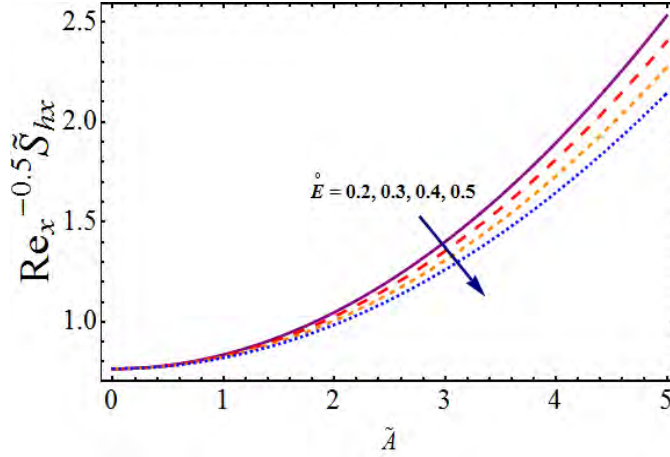


Fig. 5.17: Variations of  $\sigma$  and  $\hat{E}$  on  $\text{Re}_x^{-0.5} \tilde{S}_{hx}$ .

### 5.5.1 Entropy rate analysis

Fig. 5.18 elucidates the outcome of  $M$  on  $N_G(\eta)$ . Clearly  $N_G(\eta)$  increases for larger  $M$ . Consequences of Brinkman number  $Br$  on  $N_G(\eta)$  are disclosed in Fig. 5.19.  $N_G(\eta)$  enhances by higher  $Br$ . Infact irreversibility occurs in fluid friction by higher  $Br$ . Fig. 5.20 indicates effectiveness of  $K_0$  on  $N_G(\eta)$ . An increase in  $N_G(\eta)$  is noticed for  $K_0$ . Figs. 5.21 and 5.22 portrayed Reynolds number  $Re$  and temperature difference parameter  $\xi$  on  $N_G(\eta)$ . For higher  $Re$  and  $\xi$  the entropy generation minimization increases. Here heat transfer dominates in comparison to fluid friction and magnetic field for higher  $\xi$ .

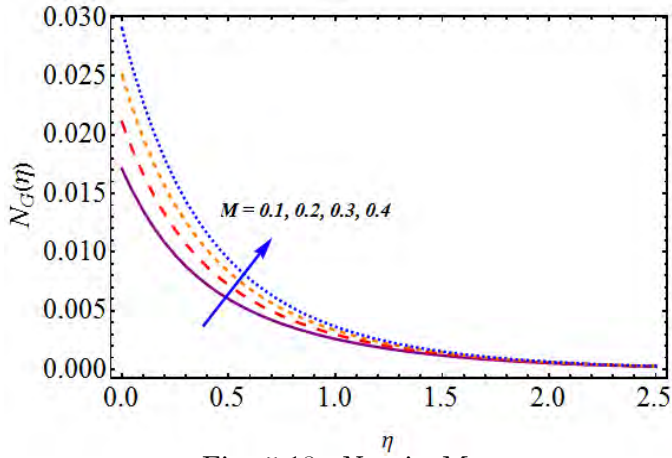


Fig. 5.18:  $N_G$  via  $M$ .

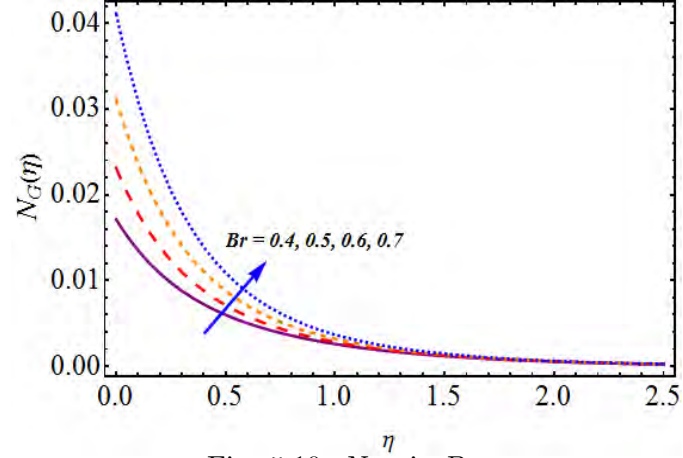


Fig. 5.19:  $N_G$  via  $Br$ .

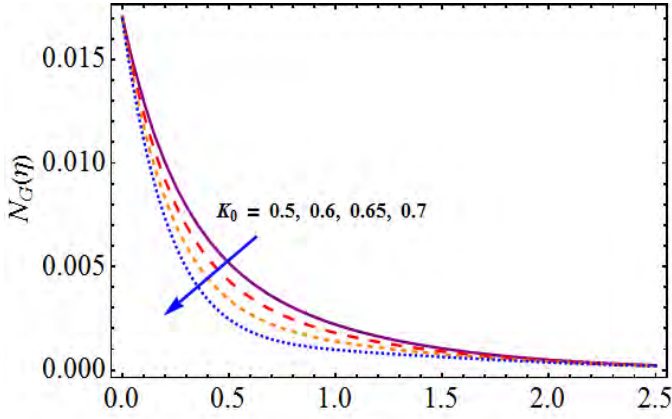


Fig. 5.20:  $N_G$  via  $K_0$

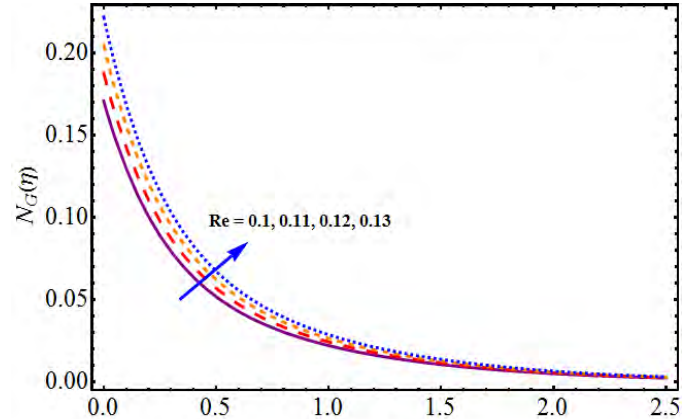


Fig. 5.21:  $N_G$  via  $Re$

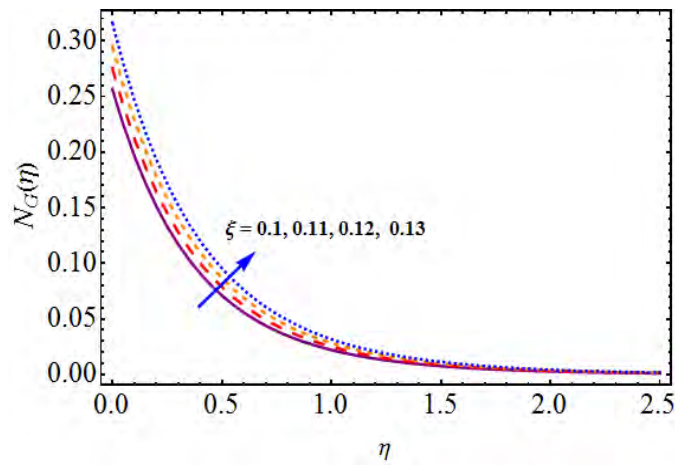


Fig. 5.22:  $N_G$  via  $\xi$

## 5.6 Conclusions

Major findings are summarized as follows

- Qualitative effect of concentration and temperature are opposite for higher thermophoresis parameter.
- Temperature has similar behavior for radiation and Eckert number.
- An enhancement of temperature is possible for Brownian motion and heat/generation parameter.
- Concentration by an activation energy parameter is increased.
- Decrease in mass transfer rate is noticed.
- Behavior of total entropy rate for Reynolds number and temperature difference parameter is similar.
- Total entropy rate against Brinkman number and magnetic field has increasing trend.



## Chapter 6

# Characteristics of activation energy on Darcy-Forchheimer flow with zero mass flux condition

### 6.1 Introduction

This chapter focus on consequences of activation energy on magneto-nanoparticles considering zero mass flux condition. Fluid flow over permeable sheet is analyzed by using Darcy-Forchheimer model. Additionally, the significance of thermal radiation is discussed. Aspects of thermophoresis and Brownian motion are also observed. Influences of convective and zero mass flux conditions at boundary are introduced. System of partial differential equations are converted in to ordinary differential equations by employing transformation technique. Formulated system is solved numerically and the involved parameters discussed through graphs. Heat flux and skin friction coefficient are also computed.

### 6.2 Formulation

Darcy-Forchheimer flow of magnetic nanofluid with activation energy is discussed here. Fluid motion occurs due to porous sheet lying at  $y = 0$ . Fluid is confined to the region  $y > 0$ . Sheet is stretched linearly with velocity  $U_w(x) = ax$  in which  $a$  being the stretching rate.  $(T_f)$  is

the fluids temperature while  $(T_\infty)$  represents the temperature far away from surface. Magnetic field  $(B_0)$  is applied perpendicularly to the fluid motion. Influence of electric field is neglected. Moreover, impact of activation energy and chemical reaction is also examined. Convective and zero mass flux condition at boundary are imposed. Thermal radiation and heat generation mechanism are analyzed in heat flow. We set

$$\frac{\partial \tilde{u}}{\partial x} + \frac{\partial \tilde{v}}{\partial y} = 0, \quad (6.1)$$

$$\tilde{u} \frac{\partial \tilde{u}}{\partial x} + \tilde{v} \frac{\partial \tilde{u}}{\partial y} = v \frac{\partial^2 \tilde{u}}{\partial y^2} - \frac{\check{\sigma} B_0^2}{\rho} \tilde{u} - \frac{v}{k^\dagger} \tilde{u} - \check{F} \tilde{u}^2, \quad (6.2)$$

$$\tilde{u} \frac{\partial \tilde{T}}{\partial x} + \tilde{v} \frac{\partial \tilde{T}}{\partial y} = \frac{\check{k}}{(\rho c_p)_f} \frac{\partial^2 \tilde{T}}{\partial y^2} + \frac{1}{(\rho c_p)_f} \frac{16\sigma^* \tilde{T}_\infty^3}{3k^*} \frac{\partial^2 \tilde{T}}{\partial y^2} + \frac{Q_0}{(\rho c_p)_f} (\tilde{T} - \tilde{T}_\infty) \quad (6.3)$$

$$+ \tau \left[ D_B \frac{\partial \tilde{T}}{\partial y} \frac{\partial \tilde{C}}{\partial y} + \frac{D_{\tilde{T}}}{\tilde{T}_\infty} \left( \frac{\partial \tilde{T}}{\partial y} \right)^2 \right], \quad (6.4)$$

$$\tilde{u} \frac{\partial \tilde{C}}{\partial x} + \tilde{v} \frac{\partial \tilde{C}}{\partial y} = D_B \left( \frac{\partial^2 \tilde{C}}{\partial y^2} \right) + \frac{D_{\tilde{T}}}{\tilde{T}_\infty} \left( \frac{\partial^2 \tilde{T}}{\partial y^2} \right) - K_r^2 (\tilde{C} - \tilde{C}_\infty) \left[ \frac{\tilde{T}}{\tilde{T}_\infty} \right]^n \exp \left[ \frac{-E_a}{k_1 \tilde{T}} \right], \quad (6.5)$$

subject to the conditions

$$\begin{aligned} \tilde{u} &= U_w = ax, \quad \tilde{v} = 0, \quad -\check{k} \frac{\partial \tilde{T}}{\partial y} = \check{h}_f (\tilde{T}_f - \tilde{T}), \quad D_B \frac{\partial \tilde{C}}{\partial y} + \frac{D_{\tilde{T}}}{\tilde{T}_\infty} \left( \frac{\partial \tilde{T}}{\partial y} \right) \quad \text{at } y = 0 \quad (6.6) \\ \tilde{u} &\rightarrow 0, \quad \tilde{T} \rightarrow \tilde{T}_\infty \quad \tilde{C} \rightarrow \tilde{C}_\infty \quad \text{as } y \rightarrow \infty \end{aligned}$$

Here  $(\tilde{u}, \tilde{v})$  are representation of velocity components in  $(x, y)$  directions,  $(B_0)$  is the magnetic field,  $(\check{\sigma})$  denotes the electrical conductivity,  $(k^\dagger)$  stands for porous medium permeability,  $(\check{F} = \frac{\check{C}_b}{x\sqrt{k^\dagger}})$  denotes the inertia coefficient,  $(\check{C}_b)$  depicts the drag coefficient,  $(k)$  the thermal conductivity,  $(c_p)$  the specific heat,  $(\sigma^*)$ ,  $(k^*)$  denotes the Stefan-Boltzmann constant, mean absorption coefficient,  $(Q_0)$  the heat generation coefficient,  $(k_1)$ ,  $(D_B)$ ,  $(n)$ ,  $(K_r)$ ,  $(E_a)$ ,  $(\check{h}_f)$  and  $(D_{\tilde{T}})$  depicts the Boltzmann constant, Brownian diffusion coefficient, the dimensionless constant or rate constant having the range  $-1 < n < 1$ , chemical reaction parameter, activation energy, heat transfer coefficient and thermophoretic diffusion coefficient.

Considering

$$\begin{aligned}\psi &= \sqrt{av}xf(\eta), & \eta &= \sqrt{\frac{a}{v}}y \\ \theta(\eta) &= \frac{\tilde{T} - \tilde{T}_\infty}{\tilde{T}_f - \tilde{T}_\infty}, & \phi(\eta) &= \frac{\tilde{C} - \tilde{C}_\infty}{\tilde{C}_\infty},\end{aligned}\quad (6.7)$$

the problems can be reduced in to the following forms

$$\check{f}''' - \check{f}'^2 + \check{f}\check{f}'' - M\check{f}' - \tilde{\lambda}_e\check{f}' - \tilde{F}_r\check{f}'^2 = 0, \quad (6.8)$$

$$(1 + R_d)\check{\theta}'' + \text{Pr}\check{f}\check{\theta}' + \text{Pr}N_b\check{\theta}'\check{\phi}' + \text{Pr}N_t(\check{\theta}')^2 + \text{Pr}\tilde{Q}\check{\theta} = 0, \quad (6.9)$$

$$\check{\phi}'' + \frac{N_t\check{\theta}''}{N_b} + Sc\check{f}\check{\phi}' - Sc\sigma(1 + \tilde{\delta}\theta)^n \exp\left[\frac{-\dot{E}}{1 + \tilde{\delta}\theta}\right]\check{\phi} = 0, \quad (6.10)$$

$$\begin{aligned}\check{f}'(\eta) &= 1, & \check{f}(\eta) &= 0 & \check{\theta}'(\eta) &= -\tilde{B}_i(1 - \check{\theta}(\eta)), & N_b\check{\phi}'(\eta) + N_t\check{\theta}'(\eta) &= 1 & \text{at } \eta = 0, \\ \check{f}'(\eta) &\rightarrow 0, & \check{\theta}(\eta) &\rightarrow 0, & \check{\phi}(\eta) &\rightarrow 0 & \text{when } \eta &\rightarrow \infty.\end{aligned}\quad (6.11)$$

where

$$\begin{aligned}M &= \frac{\tilde{\sigma}B_0^2}{\rho a}, & R_d &= \frac{16\sigma^*\tilde{T}_\infty^3}{3kk^*}, & \text{Pr} &= \frac{\mu c_p}{k}, & N_b &= \frac{\tau D_B C_\infty}{v_f}, \\ N_t &= \frac{\tau D_T (T_w - T_\infty)}{T_\infty v_f}, & \tilde{Q} &= \frac{Q_0}{a\rho c_p}, & Sc &= \frac{v_f}{D_B}, & \dot{E} &= \frac{-E_a}{k_1\tilde{T}_\infty}, \\ \tilde{\delta} &= \frac{(\tilde{T}_w - \tilde{T}_\infty)}{\tilde{T}_\infty}, & \sigma &= \frac{K_r^2}{a}, & \tilde{B}_i &= \frac{\check{h}_f}{\check{k}}\sqrt{\frac{v}{a}}, & \tilde{\lambda}_e &= \frac{v_f}{ak^\dagger}, & F_r &= \frac{\tilde{C}_b}{\sqrt{k^\dagger}}.\end{aligned}$$

In above definitions the parameters  $(M)$ ,  $(\text{Pr})$ ,  $(N_t)$ ,  $(Sc)$ ,  $(R_d)$ ,  $(\tilde{B}_i)$ ,  $(\tilde{Q})$ ,  $(N_b)$ ,  $(\tilde{\lambda}_e)$ ,  $(\tilde{F}_r)$ ,  $(\dot{E})$ ,  $(\tilde{\delta})$  and  $(\sigma)$  denote magnetic parameter, Prandtl number, thermophoresis parameter, Schmidt number, radiation parameter, Biot number, heat generation parameter, Brownian motion parameter, porosity parameter, dimensionless inertia parameter, dimensionless activation energy parameter, temperature ratio parameter and non-dimensional chemical reaction parameter respectively.

Coefficient of skin friction and Nusselt are represented in to definitions given below

$$\tilde{C}_{fx} = \frac{2 \tilde{\tau}_w|_{y=0}}{\rho U_w^2}, \quad (6.12)$$

$$\tilde{N}_{ux} = \frac{x \tilde{q}_w|_{y=0}}{\tilde{k}(\tilde{T}_w - \tilde{T}_\infty)}, \quad (6.13)$$

where

$$\tilde{q}_w = \tilde{k} \frac{\partial \tilde{T}}{\partial y} + \frac{16\sigma^* \tilde{T}_\infty^3}{3k^*} \frac{\partial \tilde{T}}{\partial y}, \quad (6.14)$$

Using equation (6.6),

$$\begin{aligned} \text{Re}_x^{0.5} \tilde{C}_{fx} &= \check{f}''(0), \\ \text{Re}_x^{-0.5} \tilde{N}_{ux} &= -(1 + R_d) \check{\theta}'(0), \end{aligned} \quad (6.15)$$

in which  $\text{Re}_x = \frac{xU_w}{\nu}$  depicts local Reynold's number.

### 6.3 Discussion

This chapter focused on influences of Darcy-Forchheimer flow of magneto-nanoparticles in the presence of activation energy and zero mass flux at stretching surface. Set of governing equations (6.7)-(6.9) along conditions (6.10) solved numerically using ND solve. Impact of involved parameters on velocity, temperature and concentration are discussed through graphs. Fig. 6.1 depicts the effectiveness of ( $M$ ) on  $\check{f}'(\eta)$ . Fluid velocity decays as ( $M = 0.6, 0.8, 1, 1.2, 1.5$ ) rises because this enhance the resistive force and consequently motion of particle reduces. Variation in velocity by increasing ( $\tilde{\lambda}_e$ ) porosity parameter is shown in Fig. 6.2. Velocity decreases as ( $\tilde{\lambda}_e$ ) reaches from (0.6) to (1.5). Fig. 6.3 presents that velocity reduces for larger values of inertia parameter ( $\tilde{F}_r = 0.1, 0.3, 0.7, 1.1, 1.3$ ). Fig. 6.4 exhibits the impact of radiation parameter ( $R_d$ ) on temperature. It is seen that temperature enhances for increasing values of ( $R_d$ ) as higher radiation delivers additional heat to the system. Effect of Prandtl number on temperature is plotted in Fig. 6.5. Decrease in temperature is noticed via ( $\text{Pr}$ ). Fig. 6.6 illustrates the influence of heat generation parameter on temperature. Since heat of fluid increases via ( $\tilde{Q}$ ) so temperature increases. Consequences of thermophoresis and Brownian motion parameter are

sketched in Figs. 6.7 and 6.8. Temperature enhances in both cases. Effect of Biot number ( $\tilde{B}_i$ ) on temperature is sketched in Fig. 6.9. Higher convection resembles to stronger surface temperature. Fig. 6.10 shows the variation in concentration due to change in ( $\tilde{B}_i$ ). Concentration enhances for larger ( $\tilde{B}_i$ ). Impact of activation energy on concentration are displayed in Fig. 6.11. Fluid's concentration increases for increasing ( $\tilde{E}$ ). Fig. 6.12 sketched to see the effectiveness of chemical reaction parameter on ( $\sigma$ ). Concentration is a decaying function for ( $\sigma$ ). Same behavior is observed for Brownian motion parameter in case of concentration (See Fig. 6.13). Characteristics of thermophoresis on ( $N_t$ ) is pictured in Fig. 6.14. Concentration enhances via ( $N_t$ ).

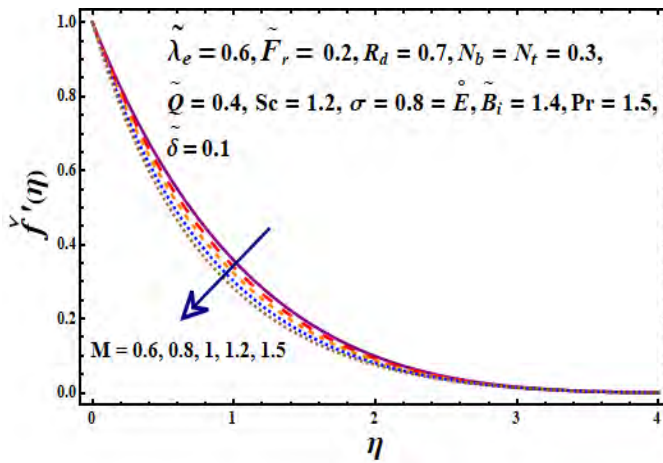


Fig. 6.1: Influence of  $M$  on  $\check{f}'(\eta)$

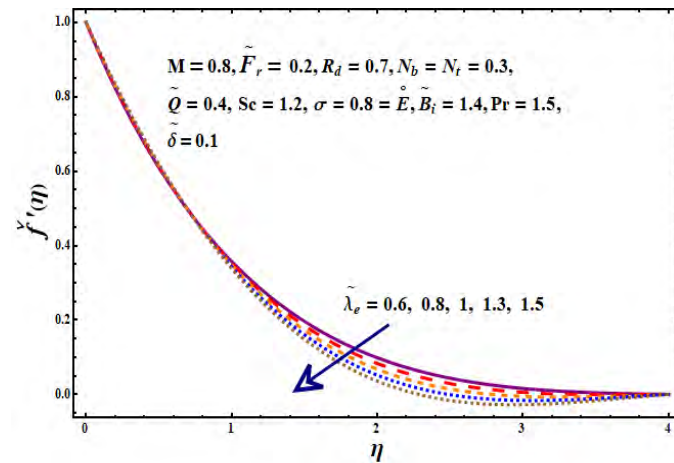


Fig. 6.2: Influence of  $\tilde{\lambda}_e$  on  $\check{f}'(\eta)$

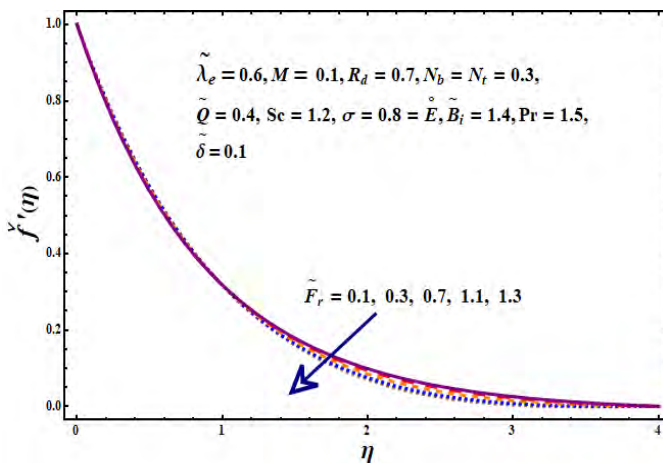


Fig. 6.3: Influence of  $\tilde{F}_r$  on  $\check{f}'(\eta)$

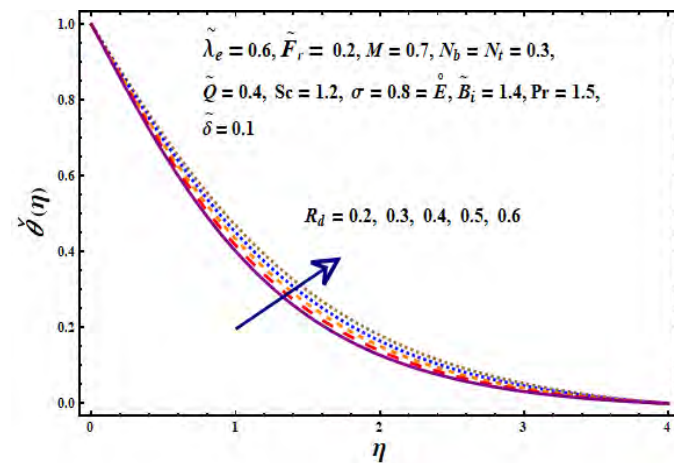


Fig. 6.4: Influence of  $R_d$  on  $\check{\theta}(\eta)$

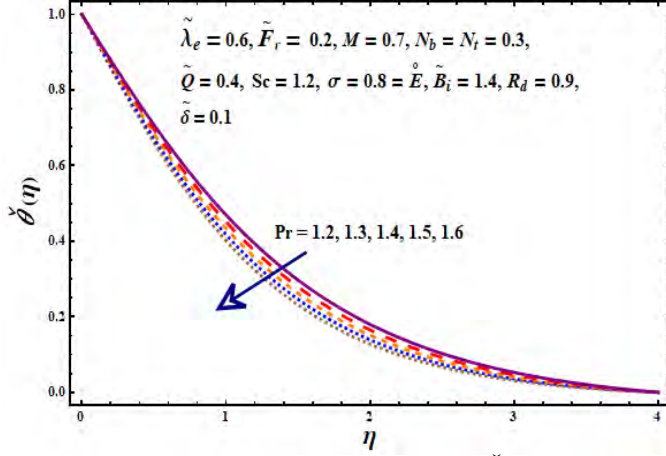


Fig. 6.5: Influence of  $Pr$  on  $\check{\theta}(\eta)$

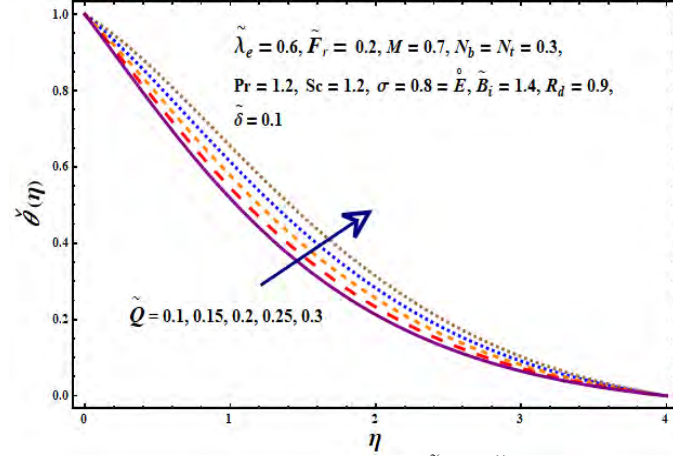


Fig. 6.6: Influence of  $\tilde{Q}$  on  $\check{\theta}(\eta)$

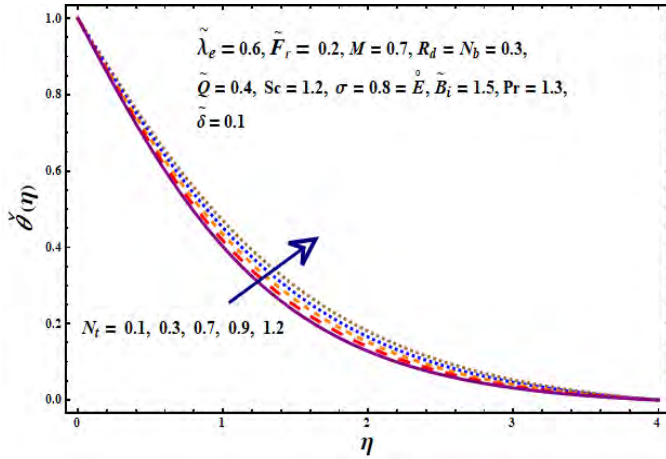


Fig. 6.7: Influence of  $N_t$  on  $\check{\theta}(\eta)$

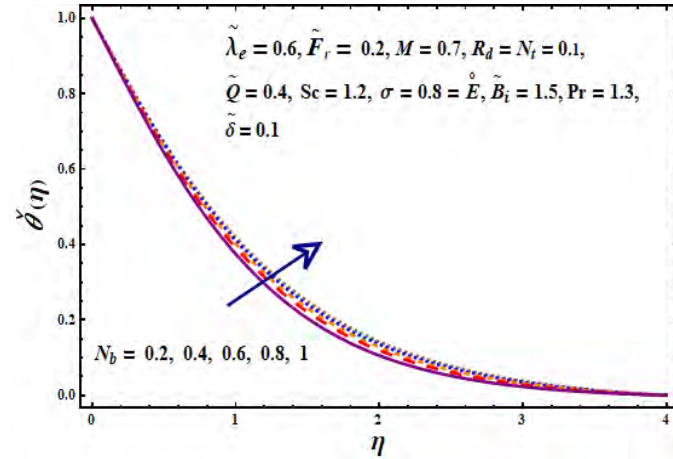


Fig. 6.8: Influence of  $N_b$  on  $\check{\theta}(\eta)$

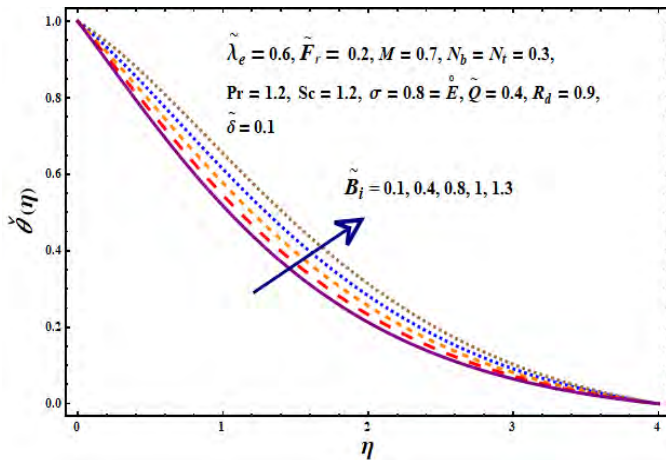


Fig. 6.9: Influence of  $\tilde{B}_i$  on  $\check{\theta}(\eta)$

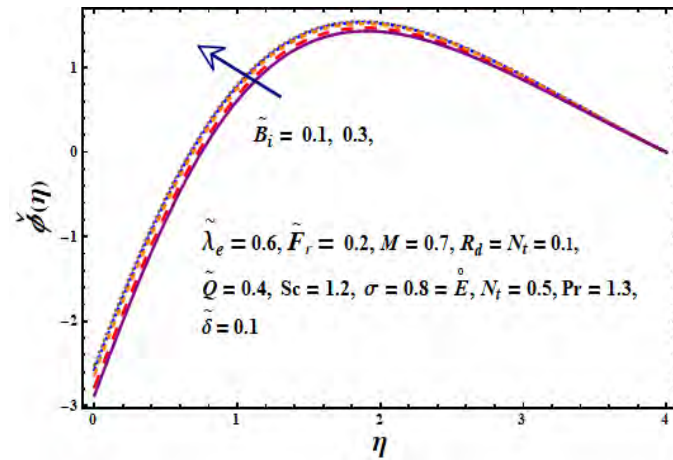


Fig. 6.10: Influence of  $\tilde{B}_i$  on  $\check{\phi}(\eta)$

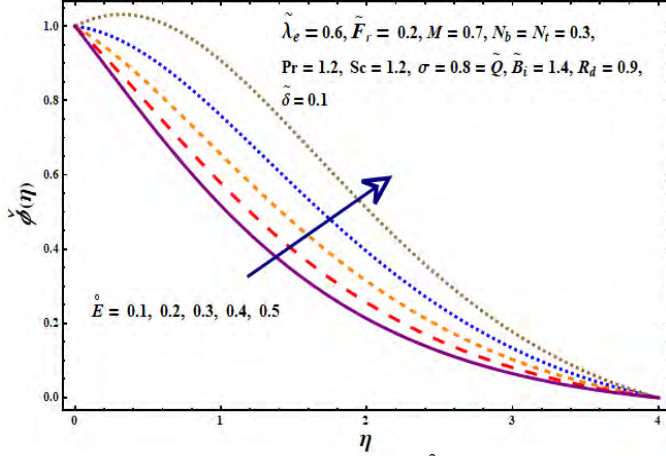


Fig. 6.11: Influence of  $\hat{E}$  on  $\check{\phi}(\eta)$

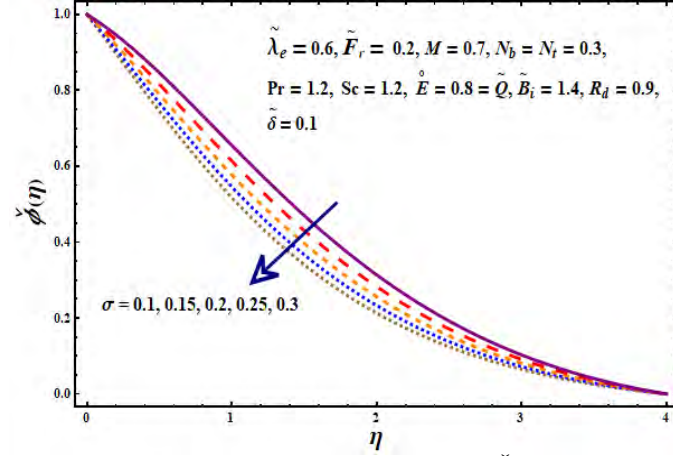


Fig. 6.12: Influence of  $\sigma$  on  $\check{\phi}(\eta)$

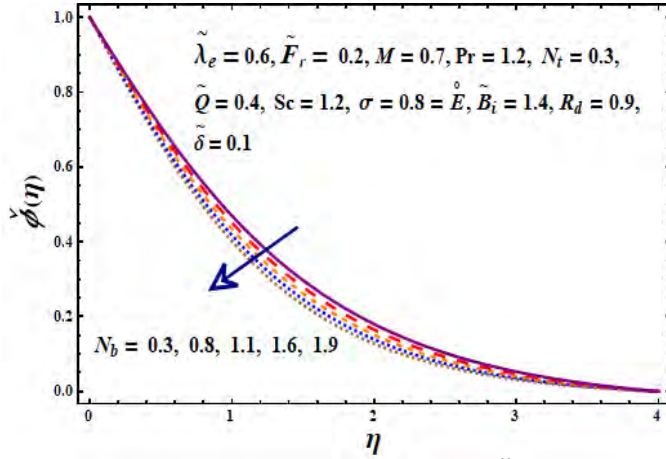


Fig. 6.13: Influence of  $N_b$  on  $\check{\phi}(\eta)$

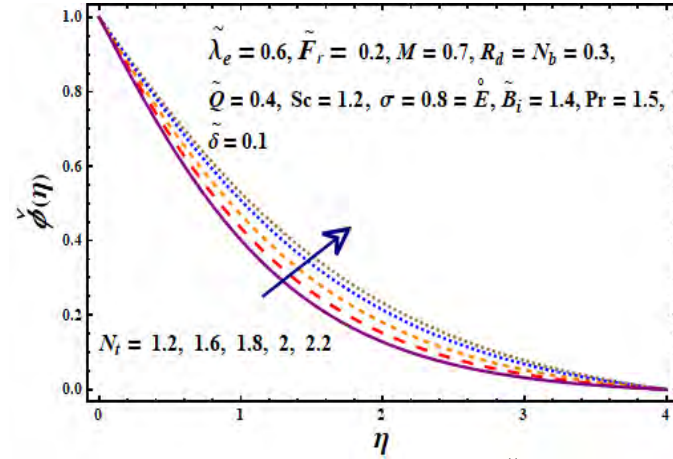


Fig. 6.14: Influence of  $N_t$  on  $\check{\phi}(\eta)$

Table 6.1 is computed in order to show the impact of various parameters ( $\tilde{\lambda}_e$ ,  $\tilde{F}_r$ ,  $M$ ) on skin friction coefficient ( $\check{f}''(0)$ ). Clearly observe that  $\text{Re}_x^{0.5} \tilde{C}_{f_x}$  reduces for ( $\tilde{\lambda}_e$ ,  $\tilde{F}_r$ ) while enhances for magnetic parameter ( $M$ ). Influence of ( $\text{Pr}$ ,  $M$ ,  $N_t$ ,  $N_b$  and  $\tilde{B}_i$ ) on heat transfer coefficient are mentioned in Table 6.2. Local Nusselt number ( $\text{Re}_x^{-\frac{1}{2}} \tilde{N}u_x$ ) reduced for Biot number ( $\tilde{B}_i$ ), Brownian motion ( $N_b$ ) and thermophoresis ( $N_t$ ) while opposite behavior is noticed in case of higher ( $\text{Pr}$ ) and ( $M$ ).

**Table 6.1:** Numerical description of skin friction coefficient for various parameters.

$\tilde{F}_r$	$\tilde{\lambda}_e$	$M$	$\text{Re}_x^{0.5} \tilde{C}_{fx}$
0.1	0.3	1	0.33467
0.15			0.25678
0.2			0.15199
0.25			0.11064
0.1	0.4	1	0.65409
	0.6		0.55129
	0.8		0.34096
	1.2		0.28701
0.1	0.3	1.1	0.12679
		1.3	0.34609
		1.7	0.44672
		1.9	0.55632



**Table 6.2:** Numerical description of Nusselt number for various parameters.

Pr	$M$	$\tilde{B}_i$	$N_b$	$N_t$	$\text{Re}_x^{-\frac{1}{2}} \tilde{N}u_x$
1	0.1	1.1	0.2	0.3	0.345011
	1.5				0.450987
	2				0.620913
1	0.2	1.1	0.2	0.3	0.249200
		0.3			0.289679
		0.4			0.329459
1	0.1	1.2	0.2	0.3	0.278934
		1.3			0.228682
		1.4			0.218732
1	0.1	1.1	0.25	0.3	0.171905
			0.3		0.141098
			0.35		0.115602
1	0.1	1.1	0.2	0.4	0.183450
				0.5	0.165191
				0.6	0.154120

## 6.4 Conclusion

Remarkable results of this chapter are mentioned below

- Velocity of fluid reduces for higher magnetic parameter.
- Temperature of fluid grows while concentration reduces under the influence of Brownian motion parameter.
- As chemical reaction parameter increases, the nanoparticle concentration diminishes.
- Temperature enhances for increasing radiation parameter, heat generation parameter and Biot number.
- Heat transfer rate increases rapidly as Prandtl number and magnetic parameter rises.

- Nanoparticle concentration increases for larger Biot number.

## Chapter 7

# Irreversibility analysis for second grade nanomaterial with zero mass flux at stretching boundary

### 7.1 Introduction

This chapter addresses the impact of entropy generation for steady flow of second grade nanomaterial with thermal radiation. A substantial perspective of this formulation is to analyze the significance of activation energy and chemical reaction under convective and zero mass flux conditions at boundary. Appropriate non-dimensional variable have been employed to get ordinary differential system. Convergent series solution is derived by using homotopic technique. Graphical results of involved pertinent parameters are sketched and discussed thoroughly. Fluid flow is observed through heat transfer rate and coefficient of drag force.

### 7.2 Flow analysis

Two-dimensional incompressible flow of second grade nanofluid is discussed. Energy equation is formulated via Joule heating, heat generation, thermal radiation and viscous dissipation. Influence of activation energy and chemical reaction are accounted. Impacts of Brownian motion and thermophoresis are considered. Sheet at  $y = 0$  is stretched with velocity  $U_w(x) = ax$

along  $x$ -axis.  $(\tilde{T}_w, \tilde{C}_w)$  are constant temperature and concentration while  $(\tilde{C}_\infty, \tilde{T}_\infty)$  is the fluid's ambient temperature and concentration. Magnetic field ( $B_0$ ) is applied in the direction perpendicular to motion of fluid. Effects of electric field are assumed negligible. Irreversibility analysis is done for involved parameters. Convective and zero mass flux condition are taken at boundary. Under such assumptions, the velocity, temperature and concentration equations are

$$\frac{\partial \tilde{u}}{\partial x} + \frac{\partial \tilde{v}}{\partial y} = 0, \quad (7.1)$$

$$\begin{aligned} \tilde{u} \frac{\partial \tilde{u}}{\partial x} + \tilde{v} \frac{\partial \tilde{u}}{\partial y} &= v \frac{\partial^2 \tilde{u}}{\partial y^2} + \frac{\tilde{\alpha}_1}{\rho_f} \left( \frac{\partial}{\partial x} \left( \tilde{u} \frac{\partial^2 \tilde{u}}{\partial y^2} \right) - \frac{\partial \tilde{u}}{\partial y} \frac{\partial^2 \tilde{u}}{\partial x \partial y} + v \frac{\partial^3 \tilde{u}}{\partial y^3} \right) \\ &\quad - \check{\sigma} \frac{B_0^2}{\rho_f} \tilde{u} + g[\beta_{\tilde{T}}(\tilde{T} - \tilde{T}_\infty) + \beta_{\tilde{C}}(\tilde{C} - \tilde{C}_\infty)], \end{aligned} \quad (7.2)$$

$$\begin{aligned} \left( \tilde{u} \frac{\partial \tilde{T}}{\partial x} + \tilde{v} \frac{\partial \tilde{T}}{\partial y} \right) &= \frac{\check{k}}{(\rho c_p)_f} \left( \frac{\partial^2 \tilde{T}}{\partial y^2} \right) + \frac{\mu}{(\rho c_p)_f} \left( \frac{\partial \tilde{u}}{\partial y} \right)^2 + \frac{\tilde{\alpha}_1}{(\rho c_p)_f} \left( \tilde{u} \frac{\partial \tilde{u}}{\partial y} \frac{\partial^2 \tilde{u}}{\partial x \partial y} + \tilde{v} \frac{\partial \tilde{u}}{\partial y} \frac{\partial^2 \tilde{u}}{\partial y^2} \right) \\ &\quad + \tau D_B \left( \frac{\partial \tilde{T}}{\partial y} \right) \left( \frac{\partial \tilde{C}}{\partial y} \right) + \tau \frac{D_{\tilde{T}}}{\tilde{T}_\infty} \left( \frac{\partial \tilde{T}}{\partial y} \right)^2 + \frac{1}{(\rho c_p)_f} \frac{16\sigma^* \tilde{T}_\infty^3}{3k^*} \frac{\partial^2 \tilde{T}}{\partial y^2} + \check{\sigma} \frac{B_0^2}{(\rho c_p)_f} \tilde{u}^2 \\ &\quad \frac{Q_0}{(\rho c_p)_f} (\tilde{T} - \tilde{T}_\infty), \end{aligned} \quad (7.3)$$

$$\tilde{u} \frac{\partial \tilde{C}}{\partial x} + \tilde{v} \frac{\partial \tilde{C}}{\partial y} = D_B \left( \frac{\partial^2 \tilde{C}}{\partial y^2} \right) + \frac{D_{\tilde{T}}}{\tilde{T}_\infty} \left( \frac{\partial^2 \tilde{T}}{\partial y^2} \right) - K_r^2 (\tilde{C} - \tilde{C}_\infty) \left[ \frac{\tilde{T}}{\tilde{T}_\infty} \right]^n \exp \left[ \frac{-E_a}{k_1 \tilde{T}} \right]. \quad (7.4)$$

The boundary conditions are

$$\begin{aligned} \tilde{u} &= U_w = ax, \quad \tilde{v} = 0, \quad -\check{k} \frac{\partial \tilde{T}}{\partial y} = \check{h}_f (\tilde{T}_f - \tilde{T}), \quad D_B \frac{\partial \tilde{C}}{\partial y} + \frac{D_{\tilde{T}}}{\tilde{T}_\infty} \left( \frac{\partial \tilde{T}}{\partial y} \right) \quad \text{at } y = 0 \quad (7.5) \\ \tilde{u} &\rightarrow 0, \quad \tilde{T} \rightarrow \tilde{T}_\infty \quad \tilde{C} \rightarrow \tilde{C}_\infty \quad \text{as } y \rightarrow \infty. \end{aligned}$$

Here  $\tilde{u}$  and  $\tilde{v}$  represents the velocities parallel to the  $x$  and  $y$ -axes,  $v$  the kinematic viscosity,  $(\tilde{\alpha}_1)$  the fluid parameter,  $\rho$  the fluid density,  $c_p$  the specific heat,  $\mu$  the dynamic viscosity,  $D_{\tilde{T}}$  thermophoresis coefficient,  $U_w$  stretching velocity,  $D_B$  Brownian coefficient,  $\tau$  the heat

capacity of nanoparticles,  $\check{\sigma}$  the electrical conductivity and  $\check{k}$  the thermal conductivity. The term  $\left[\frac{\check{T}}{\check{T}_\infty}\right]^n \exp\left[\frac{-E_a}{k_1\check{T}}\right]$  in Eq. (7.4) is called modified Arrhenius function. Further  $k_1 = 8.61 \times 10^{-5} eV/K$  represents the Boltzmann constant,  $n$  being dimensionless constant or rate constant having range  $-1 < n < 1$ ,  $K_r$  the chemical reaction parameter and  $E_a$  termed as activation energy.

We use

$$\begin{aligned}\psi &= \sqrt{av}xf(\eta), & \eta &= \sqrt{\frac{a}{v}}y \\ \check{\theta}(\eta) &= \frac{\check{T} - \check{T}_\infty}{\check{T}_w - \check{T}_\infty}, & \check{\phi}(\eta) &= \frac{\check{C} - \check{C}_\infty}{\check{C}_\infty}.\end{aligned}\quad (7.6)$$

Here  $\psi$  denotes the stream function satisfying  $\tilde{v} = -\frac{\partial\psi}{\partial x}$  and  $\tilde{u} = \frac{\partial\psi}{\partial y}$ . We can write

$$\tilde{u} = ax\check{f}'(\eta) \quad , \quad \tilde{v} = -\sqrt{av}\check{f}(\eta), \quad (7.7)$$

Expressions (7.2)-(7.6) are converted as follows

$$\check{f}''' + \check{f}\check{f}'' - (\check{f}')^2 + \tilde{\alpha}_f(2\check{f}'\check{f}''' - \check{f}\check{f}^{iv} - \check{f}''^2) - M^2\check{f}' + \lambda_1[\check{\theta} + N^*\check{\phi}] = 0, \quad (7.8)$$

$$\begin{aligned}(1 + R_d)\check{\theta}'' + \text{Pr}\check{f}\check{\theta}' + \text{Pr}Ec[\check{f}''^2 + 2\tilde{\alpha}_f\check{f}'\check{f}''^2 - \tilde{\alpha}_f\check{f}\check{f}''\check{f}'''] \\ + \text{Pr}[N_b'\check{\theta}'\check{\phi}' + N_t(\check{\theta}')^2] + \text{Pr}MEc^2(\check{f}')^2 + \text{Pr}\check{Q}\check{\theta} = 0, \end{aligned}\quad (7.9)$$

$$\check{\phi}'' + \frac{N_t}{N_b}\check{\theta}'' + Scf\check{\phi}' - Sc\sigma(1 + \delta\check{\theta})^n \exp\left[\frac{-\dot{E}}{1 + \delta\check{\theta}}\right]\check{\phi} = 0, \quad (7.10)$$

$$\begin{aligned}\check{f}'(\eta) &= 1, & \check{f}(\eta) &= 0 & \check{\theta}'(\eta) &= -\tilde{B}_i(1 - \check{\theta}(\eta)), & N_b\check{\phi}'(\eta) + N_t\check{\theta}'(\eta) &= 1 \quad \text{at } \eta = 0, \\ \check{f}'(\eta) &\rightarrow 0, & \check{\theta}(\eta) &\rightarrow 0, & \check{\phi}(\eta) &\rightarrow 0 & \text{when } \eta \rightarrow \infty.\end{aligned}\quad (7.11)$$

where  $\left(\tilde{\alpha}_f = \frac{a\tilde{\alpha}_1}{\rho v}\right)$  depicts the second grade fluid parameter,  $\left(\lambda_1 = \frac{Gr}{\text{Re}_x^2}\right)$  the mixed convection parameter,  $\left(M^2 = \frac{\check{\sigma}B_0^2x^2}{\mu}\right)$  represents the magnetic parameter,  $\left(Gr = \frac{g\beta_{\check{T}}(\check{T}_w - \check{T}_\infty)x^3}{v^2}\right)$  denotes the Grashof number for temperature and  $\left(Gr^* = \frac{g\beta_C(C_w - C_\infty)x^3}{v^2}\right)$  is the Grashof number for con-

centration, ( $N^* = \frac{Gr^*}{Gr}$ ) the local buoyancy parameter, ( $\sigma = \frac{K_f^2}{a}$ ) the dimensionless chemical reaction parameter, ( $Ec = \frac{U_w^2}{(T_w - T_\infty)c_p}$ ) the Eckert number, ( $Sc = \frac{\nu}{D_B}$ ) is the Schmidt number, ( $\tilde{\delta} = \frac{\tilde{T}_w - \tilde{T}_\infty}{\tilde{T}_\infty}$ ) is called temperature ratio parameter, ( $N_t = \frac{(\rho c)_p D_{\tilde{T}}(\tilde{T}_w - \tilde{T}_\infty)}{\tilde{T}_\infty \nu(\rho c)_f}$ ) the thermophoresis parameter, ( $N_b = \frac{(\rho c)_p D_B C_\infty}{\nu(\rho c)_f}$ ) is the Brownian motion parameter, ( $R_d = \frac{16\sigma^* \tilde{T}_\infty^3}{3kk^*}$ ) is termed as radiation parameter, ( $\tilde{Q} = \frac{Q_0}{a\rho c_p}$ ) dimensionless heat generation parameter, ( $\tilde{B}_i = \frac{\tilde{h}_f}{k} \sqrt{\frac{\nu}{a}}$ ) represents the Biot number and ( $\tilde{E} = \frac{-E_a}{k_1 \tilde{T}_\infty}$ ) is dimensionless activation energy.

### 7.2.1 Physical Quantities of interest

Coefficient of drag force ( $\tilde{C}_{fx}$ ) and rate of heat flux ( $\tilde{N}u_x$ ) can be described as:

$$\tilde{C}_{fx} = \frac{\check{\tau}_w}{\rho U_w^2 x}, \quad \tilde{N}u_x = \frac{x \check{q}_w}{\check{k}(\tilde{T}_w - \tilde{T}_\infty)}. \quad (7.12)$$

$$\begin{aligned} \check{\tau}_w &= \mu \left[ \mu \frac{\partial \tilde{u}}{\partial y} + \tilde{\alpha}_1 \left( \tilde{u} \frac{\partial^2 \tilde{u}}{\partial x \partial y} + 2 \frac{\partial \tilde{u}}{\partial x} \frac{\partial \tilde{u}}{\partial y} + \tilde{v} \frac{\partial^2 \tilde{u}}{\partial y^2} \right) \right] \Big|_{y=0}, \\ \check{q}_w &= -\check{k} \left( \frac{\partial \tilde{T}}{\partial y} \right) - \frac{16\sigma^* \tilde{T}_\infty^3}{3k^*} \frac{\partial \tilde{T}}{\partial y} \Big|_{y=0}. \end{aligned} \quad (7.13)$$

In non-dimensional form we obtain

$$\begin{aligned} 0.5 \text{Re}_x^{\frac{1}{2}} \tilde{C}_{fx} &= \check{f}''(0) + \tilde{\alpha}_f 3\check{f}'(0)\check{f}''(0), \\ \text{Re}_x^{\frac{1}{2}} \tilde{N}u_x &= -(1 + R_d)\check{\theta}'(0). \end{aligned} \quad (7.14)$$

in which  $\text{Re}_x = \frac{U_w x}{\nu}$  is Reynold number.

### 7.2.2 Entropy generation analysis:

Entropy minimization equation for second grade fluid is

$$\begin{aligned}
\check{S}_G = & \underbrace{\frac{\check{k}}{\check{T}_\infty^2} \left[ 1 + \frac{16\sigma^* \check{T}_\infty^3}{3\check{k}k^*} \right] \left( \frac{\partial \check{T}}{\partial y} \right)^2}_{\text{Thermal irreversibility}} + \underbrace{\frac{RD}{\check{C}_\infty} \left( \frac{\partial \check{C}}{\partial y} \right)^2 + \frac{RD}{\check{T}_\infty} \left( \frac{\partial \check{T}}{\partial y} \right) \left( \frac{\partial \check{C}}{\partial y} \right)}_{\text{Diffusive irreversibility}} \\
& + \underbrace{\frac{\mu}{\check{T}_\infty} \left[ \left( \frac{\partial \check{u}}{\partial y} \right)^2 + \frac{\check{\alpha}_1}{\mu} \left( \check{u} \frac{\partial \check{u}}{\partial y} \frac{\partial^2 \check{u}}{\partial x \partial y} + v \frac{\partial \check{u}}{\partial y} \frac{\partial^2 \check{u}}{\partial y^2} \right) \right]}_{\text{Fluid friction irreversibility}} \\
& + \underbrace{\check{\sigma} \frac{B_0^2}{\check{T}_\infty} \check{u}^2}_{\text{Joule dissipation irreversibility}}. \tag{7.15}
\end{aligned}$$

Basically entropy generation number is the ratio of actual entropy rate ( $\check{S}_G$ ) to the characteristic entropy rate ( $\check{S}_0$ ) so entropy generation number can be written as

$$\begin{aligned}
\check{N}_G = \frac{\check{S}_G}{\check{S}_0} = & \text{Re}_x (1 + R_d) (\check{\theta}')^2 + \text{Re}_x \left( \frac{\check{\xi}}{\check{\Omega}} \right)^2 \check{\zeta} (\check{\phi}')^2 + \text{Re}_x \check{\zeta} \left( \frac{\check{\xi}}{\check{\Omega}} \right) \check{\theta}' \check{\phi}' \\
& + \frac{\text{Re}_x}{\check{\Omega}} Br [\check{f}''^2 + \check{\alpha}_f \check{f}' \check{f}''^2 - \check{\alpha}_f \check{f} \check{f}'' \check{f}'''] + M^2 \frac{Br}{\check{\Omega}} (\check{f}')^2, \tag{7.16}
\end{aligned}$$

in which  $\left( \check{S}_0 = \frac{\check{k}(\Delta \check{T})}{\check{T}_\infty^2 x^2} \right)$  is characteristic entropy rate,  $\left( \check{\zeta} = \frac{RD\check{C}_\infty}{k} \right)$  the diffusion constant,  $\left( Br = \frac{\mu U_w^2}{k \Delta T} \right)$  is Brinkman number,  $\left( \check{\xi} = \frac{\Delta \check{C}}{\check{C}_\infty} \right)$  and  $\left( \check{\Omega} = \frac{\Delta \check{T}}{\check{T}_\infty} \right)$  the concentration and temperature differences respectively.

Bejan number is defined as

$$Be = \frac{\text{Thermal irreversibility} + \text{Diffusive irreversibility}}{\text{Total entropy rate}}. \tag{7.17}$$

In non-dimensionalized form it can be represented as

$$\begin{aligned}
Be = & \frac{\text{Re}_x (1 + R_d) (\check{\theta}')^2 + \text{Re}_x \left( \frac{\check{\xi}}{\check{\Omega}} \right)^2 \check{\zeta} (\check{\phi}')^2 + \text{Re}_x \check{\zeta} \left( \frac{\check{\xi}}{\check{\Omega}} \right) \check{\theta}' \check{\phi}'}{\text{Re}_x (1 + R_d) (\check{\theta}')^2 + \text{Re}_x \left( \frac{\check{\xi}}{\check{\Omega}} \right)^2 \check{\zeta} (\check{\phi}')^2 + \text{Re}_x \check{\zeta} \left( \frac{\check{\xi}}{\check{\Omega}} \right) \check{\theta}' \check{\phi}'} \\
& + \frac{\text{Re}_x}{\check{\Omega}} Br [\check{f}''^2 + \check{\alpha}_f \check{f}' \check{f}''^2 - \check{\alpha}_f \check{f} \check{f}'' \check{f}'''] + M^2 \frac{Br}{\check{\Omega}} (\check{f}')^2. \tag{7.18}
\end{aligned}$$

### 7.3 Solutions by homotopy analysis method

Series solutions of involved systems is obtained via homotopic analysis. Suitable initial assumptions  $(\check{f}_0, \check{\theta}_0, \check{\phi}_0)$  and associated linear operators  $(\tilde{\mathcal{L}}_{\check{f}}, \tilde{\mathcal{L}}_{\check{\theta}}, \tilde{\mathcal{L}}_{\check{\phi}})$  are

$$\check{f}_0(\eta) = 1 - e^{-\eta}, \quad (7.19)$$

$$\check{\theta}_0(\eta) = \frac{\tilde{B}_i}{1 + \tilde{B}_i} e^{-\eta}, \quad (7.20)$$

$$\check{\phi}_0(\eta) = - \left( \frac{N_t}{N_b} \right) \frac{\tilde{B}_i}{1 + \tilde{B}_i} e^{-\eta}, \quad (7.21)$$

$$\tilde{\mathcal{L}}_{\check{f}}(\eta) = \frac{d^3 \check{f}}{d\eta^3} - \frac{d\check{f}}{d\eta}, \quad \tilde{\mathcal{L}}_{\check{\theta}}(\eta) = \frac{d^2 \check{\theta}}{d\eta^2} - \check{\theta}, \quad \tilde{\mathcal{L}}_{\check{\phi}}(\eta) = \frac{d^2 \check{\phi}}{d\eta^2} - \check{\phi}, \quad (7.22)$$

$$\tilde{\mathcal{L}}_{\check{f}} \left[ \check{F}_1 + \check{F}_2 \eta + \check{F}_3 e^\eta \right] = 0, \quad (7.23)$$

$$\tilde{\mathcal{L}}_{\check{\theta}} \left[ \check{F}_4 e^\eta + \check{F}_5 e^{-\eta} \right] = 0, \quad (7.24)$$

$$\tilde{\mathcal{L}}_{\check{\phi}} \left[ \check{F}_6 e^\eta + \check{F}_7 e^{-\eta} \right] = 0. \quad (7.25)$$

with  $\check{F}_i$  ( $i = 1 - 7$ ) denote the arbitrary constants.

### 7.4 Convergence

This section tends to find the convergence region. Fig. 7.1 presented the  $\hbar$ -curves. Clearly the series solutions converge for ranges of auxiliary parameters satisfying  $-0.8 \leq \hbar_{\check{f}} \leq -0.1$ ,  $-0.95 \leq \hbar_{\check{\theta}} \leq -0.2$  and  $-1.0 \leq \hbar_{\check{\phi}} \leq -0.15$ . Clearly the momentum equation converges at 19<sup>th</sup> order of approximation while 18<sup>th</sup> and 25<sup>th</sup> orders of approximations are required for temperature and concentration.



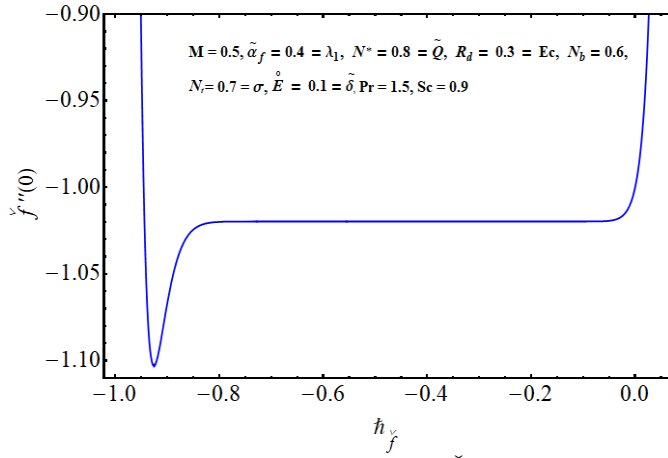


Fig. 7.1:  $\tilde{h}$ -curve for  $\check{f}''(0)$

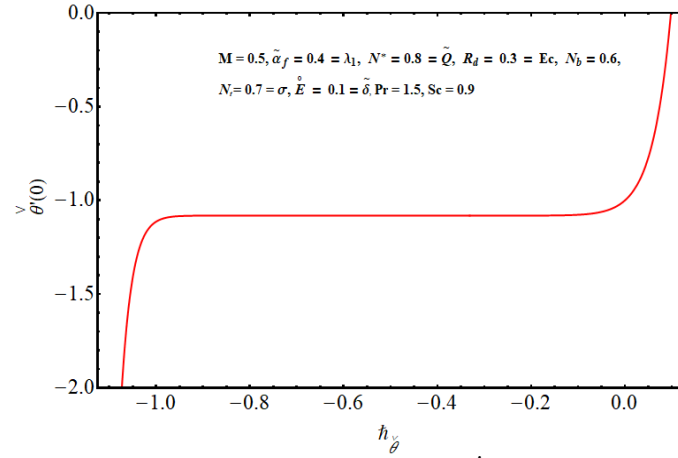


Fig. 7.2:  $\tilde{h}$ -curve for  $\check{\theta}'(0)$

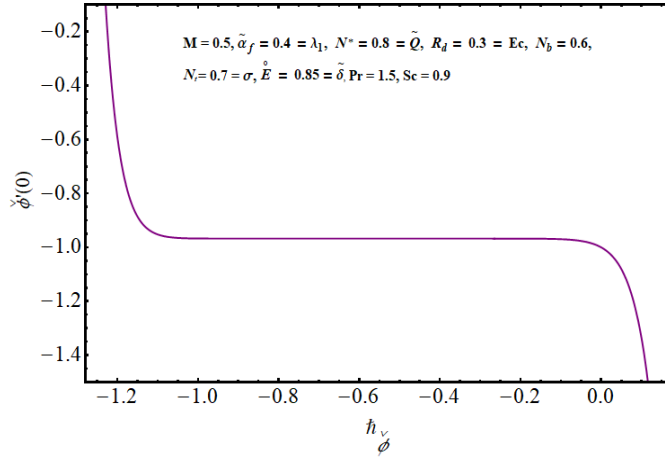


Fig. 7.3:  $\tilde{h}$ -curve for  $\check{\phi}'(0)$

**Table 7.1:** Values for convergence analysis.

Order of approximation	$-\check{f}''(0)$	$-\check{\theta}'(0)$	$-\check{\phi}'(0)$
1	0.3500	0.73167	0.07704
9	0.4719	0.49925	0.11298
15	0.5892	0.87805	0.12643
18	0.9856	1.19195	0.15667
19	1.0252	1.19195	0.89654
25	1.0252	1.19195	0.95786

## 7.5 Analysis

In this section the effectiveness of involved variables on velocity, temperature, concentration, drag surface coefficient, heat transfer rate and irreversibility mechanism are discussed in detail. Fig. 7.4 indicates the impact of magnetic parameter on velocity. Velocity decays as ( $M = 0.1, 0.3, 0.5, 0.6$ ). Higher  $M$  lead to reduction in fluids velocity due to resistive force named as Lorentz force. Consequences of dimension less second grade fluid parameter is sketched in Fig. 7.5.  $f'(\eta)$  is an increasing function of ( $\tilde{\alpha}_f$ ). Impact of mixed convective parameter ( $\lambda_1$ ) and buoyancy parameter ( $N^*$ ) on  $f'(\eta)$  are presented in Figs. 7.6 and 7.7. Velocity enhances in both cases.

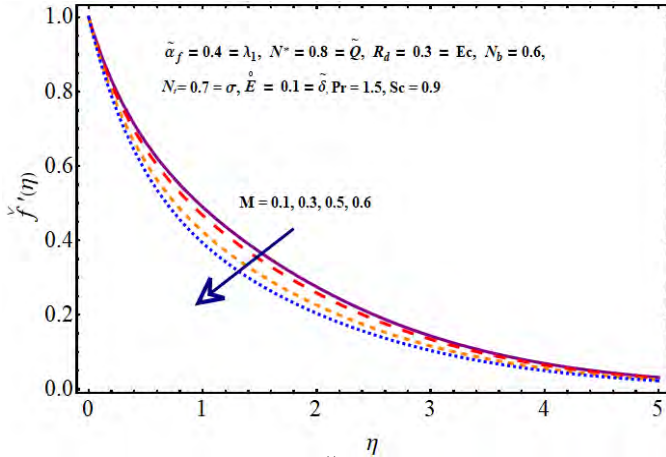


Fig. 7.4:  $f'(\eta)$  via  $M$ .

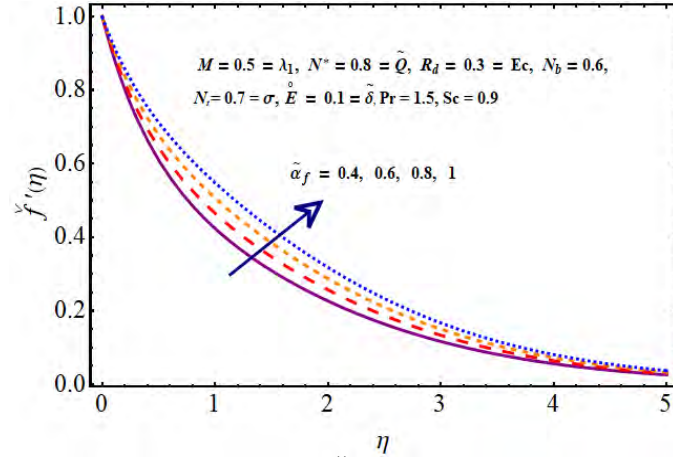


Fig. 7.5:  $f'(\eta)$  via  $\tilde{\alpha}_f$

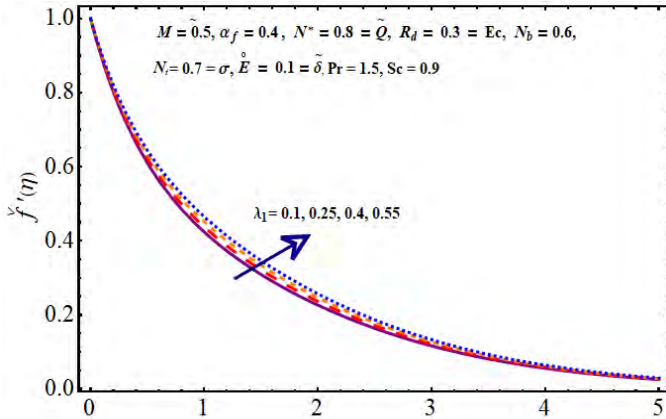


Fig. 7.6:  $f'(\eta)$  via  $\lambda_1$

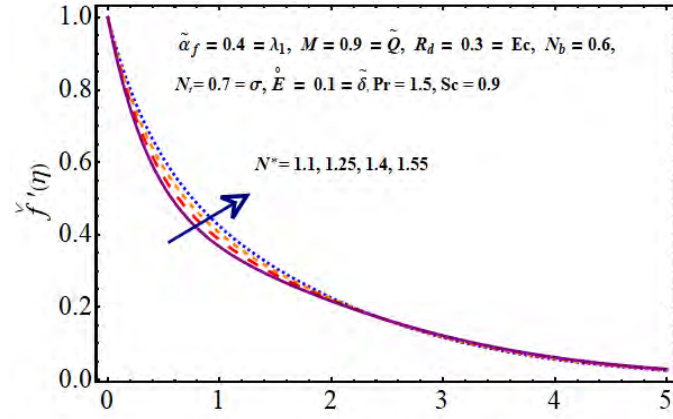


Fig. 7.7:  $f'(\eta)$  via  $N^*$

Characteristics of magnetic parameter on temperature are displayed in Fig. 7.8. Temperature increases as  $M$  ranges from 1 to 1.6. Fig. 7.9 discloses the effect of radiation parameter on temperature. Due to increment in  $(R_d)$ , the thermal field enhanced. Fig. 7.10 exhibits the relation of Eckert number ( $Ec$ ) with temperature. More  $Ec$  rises fluids temperature. Because Eckert number is ratio of difference in enthalpy to kinetic energy of fluid. Here higher  $Ec$  leads to reduction in fluids motion so heat of system enhances. Fig. 7.11 addresses that temperature decays for larger  $Pr$ . Figs. 7.12 and 7.13 display the effects of  $(N_t)$  and  $(N_b)$  on  $(\theta(\eta))$ . Temperature increases for both parameters as the difference between initial and ambient temperature rises. Kinetic motion of nanoparticles increases and gradually more heat added in the setup. Heat generation parameter ( $\tilde{Q}$ ) enhances nanomaterial thermally as sketched in Fig. 7.14. Variation in chemical reaction parameter ( $\sigma$ ) is presented in Fig. 7.15. Concentration of nanomaterial decreases for  $(\sigma)$ . Impact of dimensionless activation energy ( $\hat{E}$ ) is pictured in Fig. 7.16. Solutal concentration rises for larger  $(\hat{E})$ .

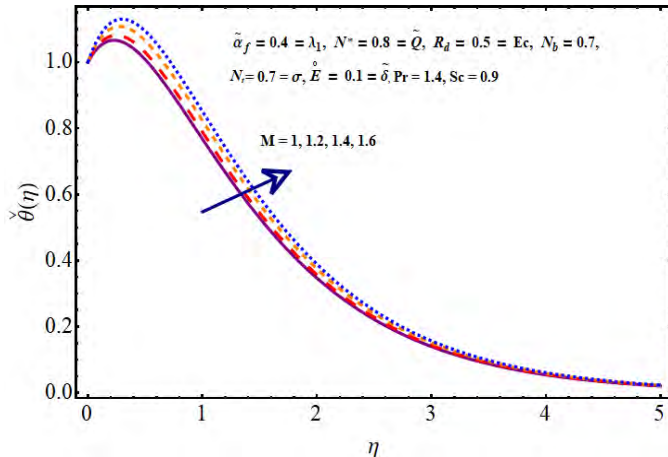


Fig. 7.8:  $\check{\theta}(\eta)$  via  $M$

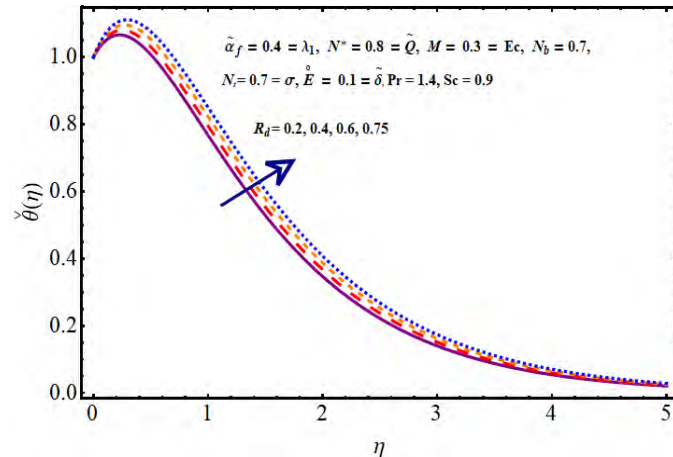


Fig. 7.9:  $\check{\theta}(\eta)$  via  $R_d$

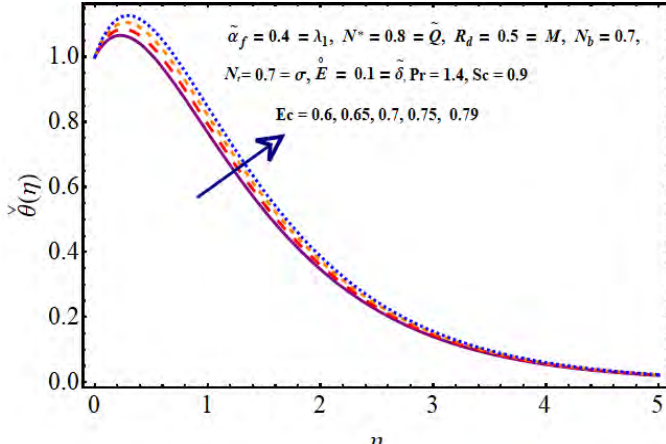


Fig. 7.10:  $\check{\theta}(\eta)$  via  $Ec$

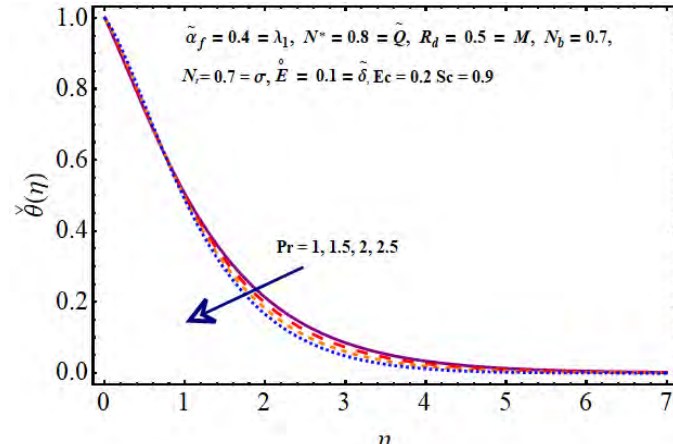


Fig. 7.11:  $\check{\theta}(\eta)$  via  $Pr$

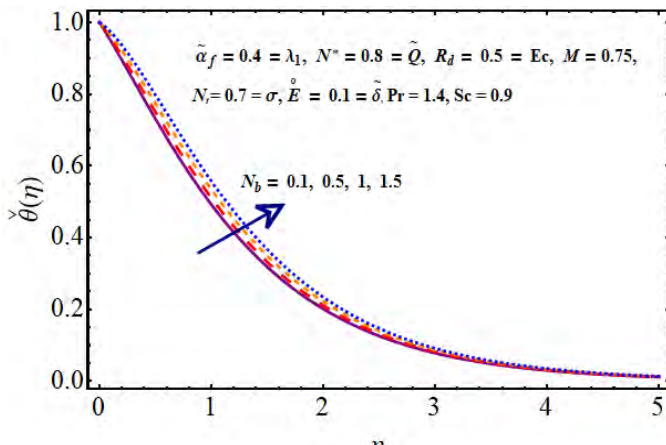


Fig. 7.12:  $\check{\theta}(\eta)$  via  $N_b$

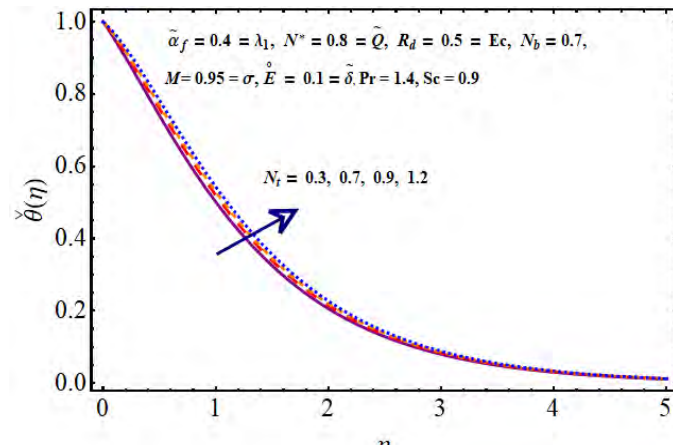


Fig. 7.13:  $\check{\theta}(\eta)$  via  $N_t$

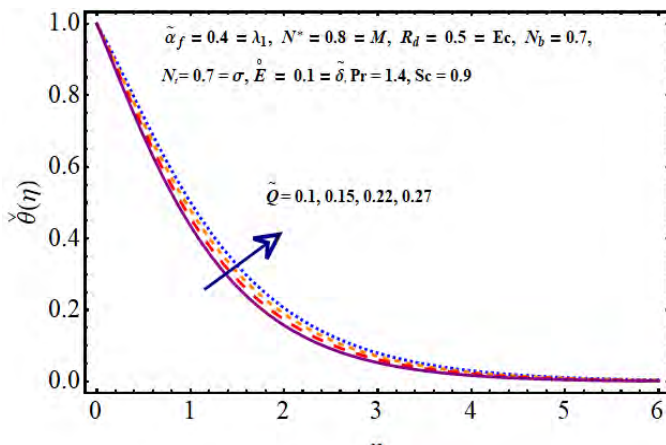


Fig. 7.14:  $\check{\theta}(\eta)$  via  $\tilde{Q}$

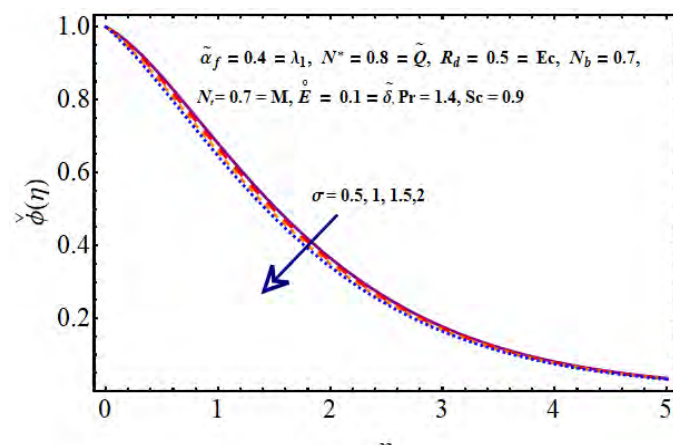


Fig. 7.15:  $\check{\phi}(\eta)$  via  $\sigma$

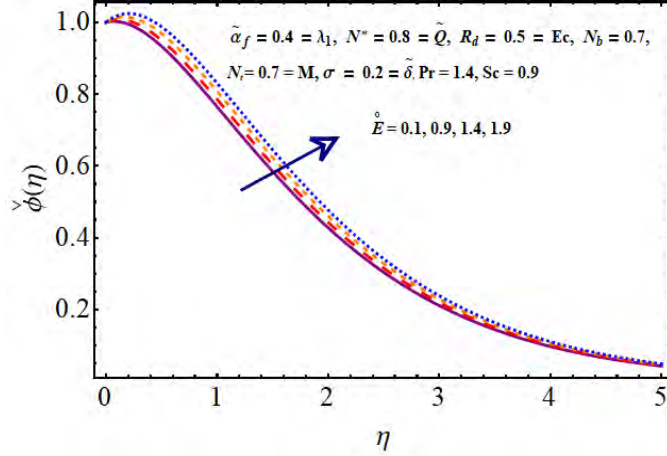


Fig. 7.16:  $\check{\phi}(\eta)$  via  $\hat{E}$

Fig. 7.17 shows the outcome of  $M$  on entropy rate ( $\check{N}_G$ ). Irreversibility rate enhances as values of applied magnetic field increases ( $M = 0.1, 0.4, 0.6, 0.8$ ). Influence of concentration difference ( $\check{\xi}$ ) on ( $\check{N}_G$ ) are pictured in Fig. 7.18. It is noticed that entropy higher for larger ( $\check{\xi}$ ). Brinkman number ( $Br$ ) also boosted the irreversibility rate as shown in Fig. 7.19. As larger ( $Br$ ) reduces thermal process so entropy increases. Effect of Prandtl number ( $Pr$ ) on ( $\check{N}_G$ ) are sketched in Fig. 7.20. ( $\check{N}_G$ ) increases as ( $Pr$ ) varies from 1.2 to 2.3. Consequences of ( $\check{\xi}$ ) and ( $Br$ ) on ( $\check{N}_G$ ) are presented in Figs. 7.21 and 7.22. Opposite effect are noticed for both parameters. Features of  $Re_x$  on ( $\check{N}_G$ ) are reported in Fig 7.23. Irreversibility rises as  $Re_x$  increases from 1.1 to 1.9.

Table 7.1 is drawn to verify the effects of ( $\tilde{\alpha}_f, \lambda_1, N^*$ ) on drag friction coefficient ( $Re_x^{0.5} \check{C}_{fx}$ ). Drag force decreases for ( $\lambda_1, N^*$ ) while it enhances for second grade fluid parameter ( $\tilde{\alpha}_f$ ). Effects of different variables on heat transfer rate are reflected in Table 7.2. It is clear that heat transfer

of fluid enhances for  $(Pr, \tilde{B}_i)$  while decays for  $(\tilde{\alpha}_f, \tilde{Q})$ .

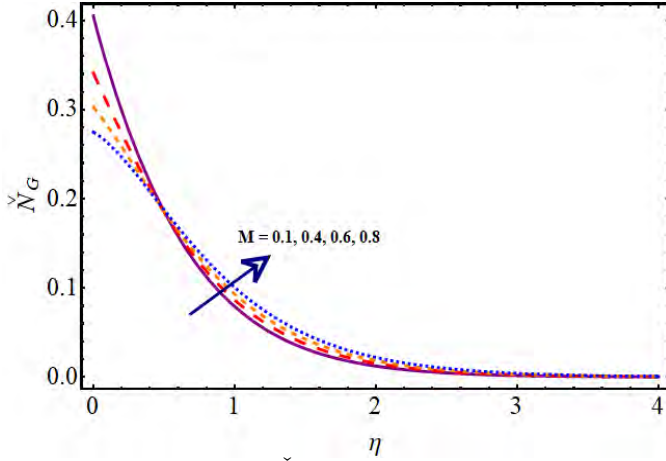


Fig. 7.17:  $\check{N}_G$  variations via  $M$

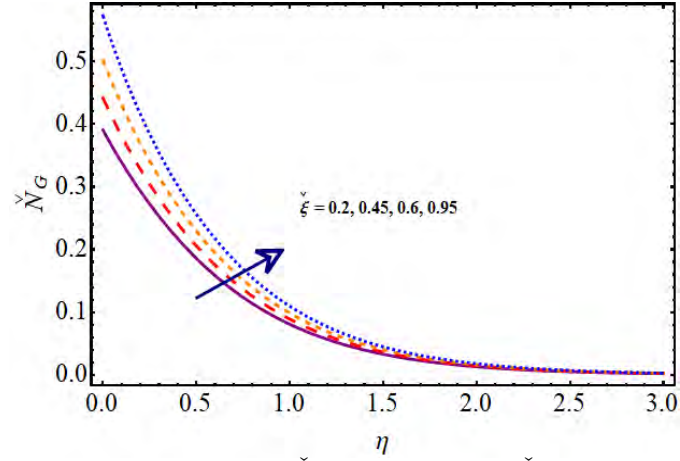


Fig. 7.18:  $\check{N}_G$  variations via  $\check{\xi}$

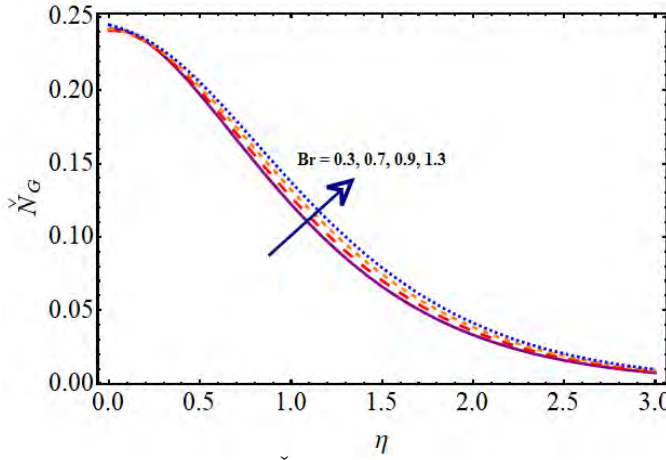


Fig. 7.19:  $\check{N}_G$  variations via  $Br$

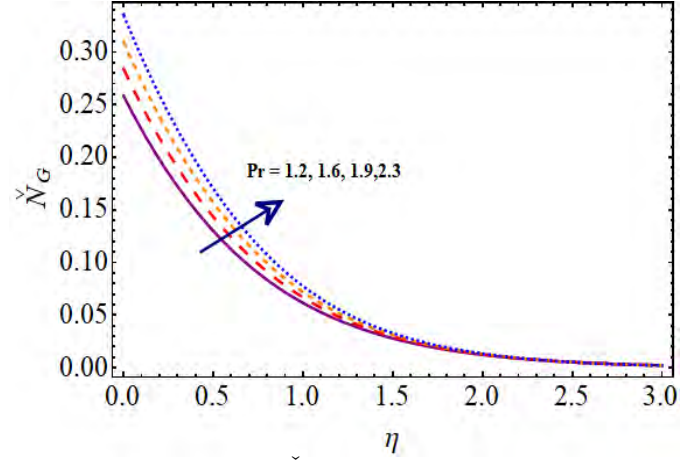


Fig. 7.20:  $\check{N}_G$  variations via  $Pr$

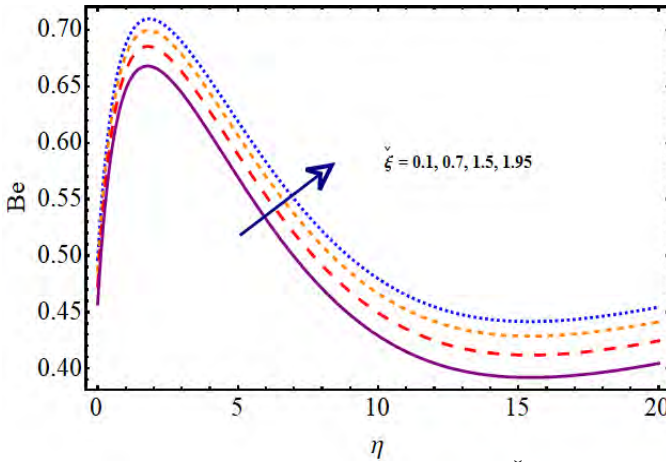


Fig. 7.21:  $Be$  variations via  $\check{\xi}$

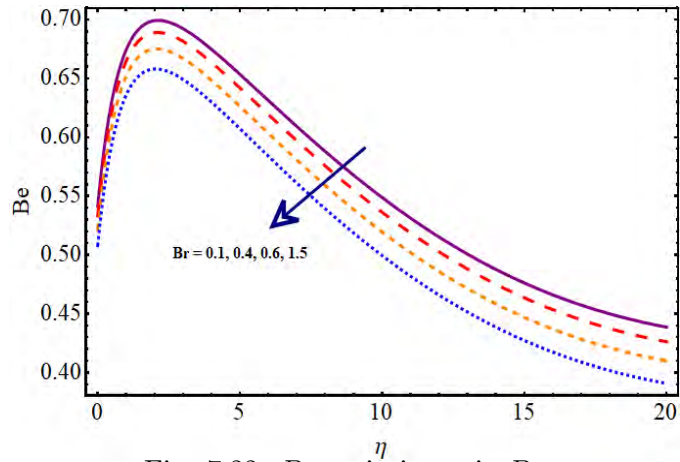


Fig. 7.22:  $Be$  variations via  $Br$

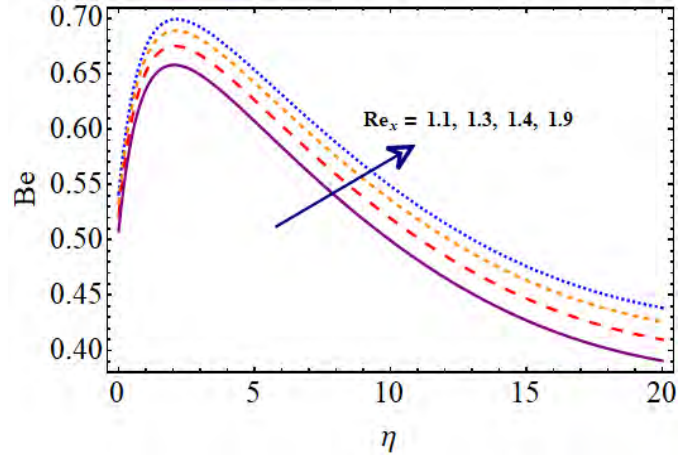


Fig. 7.23:  $Be$  variations via  $Re_x$

**Table 7.1:** Numerical description of skin friction coefficient for various parameters.

$\tilde{\alpha}_f$	$\lambda_1$	$N^*$	$\text{Re}_x^{0.5} \tilde{C}_{fx}$
0.1	0.3	1	0.45902
0.15			0.34781
0.2			0.16478
0.25			0.11894
0.1	0.4	1	0.55690
	0.6		0.45231
	0.8		0.33467
	1.2		0.22891
0.1	0.3	1.1	0.11348
		1.3	0.34729
		1.7	0.45981
		1.9	0.52390



**Table 7.2:** Nusselt number description.

Pr	$\tilde{\alpha}_f$	$\tilde{B}_i$	$Ec$	$\tilde{Q}$	$Re_x^{-\frac{1}{2}} \tilde{N}u_x$
1	0.1	1.1	0.2	0.3	0.21348
1.5					0.34908
2					0.67129
1	0.2	1.1	0.2	0.3	0.98763
	0.3				0.56230
	0.4				0.32764
1	0.1	1.2	0.2	0.3	0.45239
		1.3			0.12569
		1.4			0.09345
1	0.1	1.1	0.25	0.3	0.98673
			0.3		0.63489
			0.35		0.34986
1	0.1	1.1	0.2	0.4	0.17893
				0.5	0.16583
				0.6	0.14908

## 7.6 Conclusion

Key findings are summarized below:

- Radiation and Eckert number leads to temperature enhancement.
- For higher heat/generation absorption and Brownian motion parameters the temperature of fluid motion gets enhanced.
- An enhancement for concentration of fluid through activation energy parameter is noticed.
- Decay in mass transfer rate is found for higher chemical reaction parameter.
- Impact of Brinkman number and temperature difference parameter on total entropy rate is similar.

- Higher Brinkman and Reynold numbers lead to an increment in Bejan number.

# Bibliography

- [1] A. R. Bestman, Radiative heat transfer to flow of a combustible mixture in a vertical pipe, *Int. J. Energy Res.* 15(1991) 179 – 184.
- [2] K. A. Maleque, Effects of binary chemical reaction and activation energy on MHD boundary layer heat and mass transfer flow with viscous dissipation and heat generation/absorption, *ISRN Thermodyn.* (2013)284637.
- [3] M. Mustafa, J. A. Khan, T. Hayat and A. Alsaedi, Buoyancy effects on the MHD nanofluid flow past a vertical surface with chemical reaction and activation energy, *Int. J. Heat and Mass Transf.* 108(2017)1340 – 1346.
- [4] D. Viju, R. Gautam and R. Vinu, Application of the distributed activation energy model to the kinetic study of pyrolysis of *Nannochloropsis oculata*, *Algal Research* 35(2018)168–177.
- [5] A. Ambekar and J. J. Yoh, Chemical kinetics of multi-component pyrotechnics and mechanistic deconvolution of variable activation energy, *Proceedings Combustion Inst.* 37(2019)3193 – 3201.
- [6] L. Ahmad and M. Khan, Importance of activation energy in development of chemical covalent bonding in flow of Sisko magneto-nanofluids over a porous moving curved surface, *Int. J. Hydrogen Energy* 44(2019)10197 – 10206.
- [7] S. Jabeen, T. Hayat, S. Qayyum and A. Alsaedi, Significance of activation energy in stratified flow of tangent hyperbolic fluid, *Int. J. Num. Methods for Heat & Fluid Flow* 29(2019)2932 – 2947.

- [8] T. Hayat, R. Riaz, A. Aziz and A. Alsaedi, Influence of Arrhenius activation energy in MHD flow of third grade nanofluid over a nonlinear stretching surface with convective heat and mass conditions, *Physica A: Stat. Mech. App.* 549(2020)124006.
- [9] R. Muhammad, M. I. Khan, M. Jameel and N. B. Khan, Fully developed Darcy-Forchheimer mixed convective flow over a curved surface with activation energy and entropy generation, *Comp. Meth. Prog. Bio.* 188(2020)105298.
- [10] S. Naz, M. M. Gulzar, M. Waqas, T. Hayat and A. Alsaedi, Numerical modeling and analysis of non-Newtonian nanofluid featuring activation energy, *App. Nanosci.* 10(2020)3183 – 3192.
- [11] R. Cortell, Fluid flow and radiative nonlinear heat transfer over a stretching sheet, *J. King Saud. Univ. Sci.* 26(2014)161 – 167
- [12] Z. Shah, A. Dawar, P. Kumam, W. Khan and S. Islam, Impact of nonlinear thermal radiation on MHD nanofluid thin film flow over a horizontally rotating disk, *Appl. Sci.* 9(2019)1533
- [13] M. M. Bhatti, M. Sheikholeslami, A. Shahid, M. Hassan and T. Abbas, Entropy generation on the interaction of nanoparticles over a stretched surface with thermal radiation, *Colloids and Surfaces A: Phys. Eng. Asp.* 5(2019)368 – 376
- [14] H. Waqas, S. Khan, M. M. Bhatti and M. Imran, Significance of bioconvection in chemical reactive flow of magnetized Carreau–Yasuda nanofluid with thermal radiation and second-order slip, *J. Therm. Analysis and Calorimetry* 140(2020)1293 – 1306
- [15] M. Sheikholeslami, T. Hayat and A. Alsaedi, MHD free convection of Al<sub>2</sub>O<sub>3</sub>–water nanofluid considering thermal radiation: A numerical study, *Int. J. Heat and Mass Trans.* 96(2016)513 – 524
- [16] S. Qayyum, T. Hayat and A. Alsaedi, Thermal radiation and heat generation/absorption aspects in third grade magneto-nanofluid over a slendering stretching sheet with Newtonian conditions, *Physica B: Cond. Matter*, 537(2018)139 – 149

- [17] M. Mustafa, R. Ahmad, T. Hayat and A. Alsaedi, Rotating flow of viscoelastic fluid with nonlinear thermal radiation: a numerical study, *Neural Comp. App.* 29(2018)493 – 499
- [18] S. K. Asha and G. Sunitha, Thermal radiation and Hall effects on peristaltic blood flow with double diffusion in the presence of nanoparticles, *Case Stu. Therm. Eng.* 17(2020)100560
- [19] J. Gireesha, G. Sowmya, M. I. Khan and H. F. Öztopc, Flow of hybrid nanofluid across a permeable longitudinal moving fin along with thermal radiation and natural convection, *Comp. Meth. Prog. Biom.* 185(2020)105166
- [20] Y. S. Daniel, Z. A. Aziz, Z. Ismail, A. Bahar and F. Salah, Slip role for unsteady MHD mixed convection of nanofluid over stretching sheet with thermal radiation and electric field, *Ind. J. Phy.* 94(2020)195 – 207
- [21] M. Irfan, M. Khan, W. A. Khan, M. Alghamdi and M. ZakaUllah, Influence of thermal-solutal stratifications and thermal aspects of non-linear radiation in stagnation point Oldroyd-B nanofluid flow, *Int. Comm. Heat and Mass Transf.* 116(2020)104636
- [22] M. Waqas, A. S. Dogonchi, S. A. Shehzad, M. I. Khan, T. Hayat and A. Alsaedi, Nonlinear convection and Joule heating impacts in magneto-thixotropic nanofluid stratified flow by convectively heated variable thicked surface, *J. Mol. Liq.* 300(2020)111945
- [23] S. Rehman, N. A. Mir, M. Farooq, M. Rizwan, F. Ahmad, S. Ahmad and B. Ahmad, Analysis of thermally stratified flow of Sutterby nanofluid with zero mass flux condition, *J. Mat. Research and Techn.* 9(2020)1631 – 1639
- [24] M. Bilal and S. Ashbar, Flow and heat transfer analysis of Eyring-Powell fluid over stratified sheet with mixed convection, *J. Egypt. Math. Soc.* 40(2020)100
- [25] M. Ramzan, H. Gul and M. Zahri, Darcy-Forchheimer 3D Williamson nanofluid flow with generalized Fourier and Fick's laws in a stratified medium, *Bull. Pol. Ac.: Tech.* 68(2020) 133116
- [26] I. Jabeen, M. Farooq, N. A. Mir, S. Ahmad and A. Anjum, Optimization of entropy generation in nonlinear stratified Powell–Eyring fluid with convective boundary conditions, *Phys. Scrip.* 95(2020)

- [27] K. Rehman, M. Y. Malik, S. Bilal, I. Zahra and S. A Ghaffar, On both magnetohydrodynamics thermal stratified and dual convection flow field features: A Computational Study, *J. Nanofluids* 8(2019)460 – 465
- [28] F. M. Abbasi, S. A. Shehzad, T. Hayat and M. S. Alhuthali, Mixed convection flow of Jeffrey nanofluid with thermal radiation and double stratification, *J. Hydrodynamics, Ser. B*, 28(2016)840 – 849
- [29] M. Ramzan, M. Bilal and J. D. Chung, Effects of thermal and solutal stratification on Jeffrey magneto-nanofluid along an inclined stretching cylinder with thermal radiation and heat generation/absorption, *Int. J. Mech. Sci.* 132(2017)317 – 324.
- [30] A. M. Rashad, S. Abbasbandy and A. J. Chamkha, Mixed convection flow of a micropolar fluid over a continuously moving vertical surface immersed in a thermally and solutally stratified medium with chemical reaction, *J. Taiwan Inst. Chem. Eng.* 45(2014)2163 – 2169
- [31] P. Forchheimer, Wasserbewegung durch boden, *Zeitschrift Ver. D. Ing.*, 45(1901)1782 – 1788.
- [32] M. Muskat, *The flow of homogeneous fluids through porous media*, Edwards, MI, (1946)
- [33] S. Mukhopadhyay, P. R. De, K. Bhattacharyya and G. C. Layek, Forced convective flow and heat transfer over a porous plate in a Darcy-Forchheimer porous medium in presence of radiation, *Meccanica* 47(2012)153 – 161
- [34] M. A. Sadiq and T. Hayat, Darcy-Forchheimer stretched flow of MHD Maxwell material with heterogeneous and homogeneous reactions, *Neural Comput. & Applic.*, (2017)017 – 3037 – 1
- [35] T. Hayat, M. I. Khan, S. A. Shehzad, M. I. Khan and A. Alsaedi, Numerical simulation of Darcy-Forchheimer flow of third grade liquid with Cattaneo-Christov heat flux model, *Math. Meth. Appl. Sci.*, (2017)4403
- [36] R. S. Saif, T. Muhammad and H. Sadia, Significance of inclined magnetic field in Darcy-Forchheimer flow with variable porosity and thermal conductivity, *Physica A: Stat. Mech. Appl.* 551(2020)124067

- [37] N. Huda, A. Hamid and M. Khan, Impact of Cattaneo-Christov model on Darcy–Forchheimer flow of ethylene glycol base fluid over a moving needle, *J. Mat. Res. Tech.* 9(2020)4139 – 4146
- [38] A. Majeed, A. Zeeshan and F. M. Noori, Numerical study of Darcy-Forchheimer model with activation energy subject to chemically reactive species and momentum slip of order two, *AIP Adv.* 9(2019)045035
- [39] T. Hayat, A. Aziz, T. Muhammad and A. Alsaedi, Numerical simulation for Darcy-Forchheimer 3D rotating flow subject to binary chemical reaction and Arrhenius activation energy, *J. Central South Uni.* 26(2019)1259
- [40] G. Rasool and T. Zhang, Darcy-Forchheimer nanofluidic flow manifested with Cattaneo-Christov theory of heat and mass flux over non-linearly stretching surface, *Plos One*, (2019)0221302
- [41] A. Bejan, A study of entropy generation in fundamental convective heat transfer, *ASME J. Heat Transfer*, 101(4)(1979)718 – 725.
- [42] A. Bejan and J. Kestin, Entropy generation through heat and fluid flow, *J. Appl. Mech.*, 50(1983).
- [43] Y. Liu, Y. Jian and W. Tan, Entropy generation of electromagnetohydrodynamics (EMHD) flow in a curved rectangular microchannel, *Int. J. Heat Mass Transf.*, 127(2018)901 – 913.
- [44] S. Qayyum, M. I. Khan, T. Hayat, A. Alsaedi and M. Tamoor, Entropy generation in dissipative flow of Williamson fluid between two rotating disks, *Int. J. Heat Mass and Transf.*, 127(2018)933 – 942.
- [45] M. Akbarzadeh, S. Rashidi, N. Karimi and R. Ellahi, Convection of heat and thermodynamic irreversibilities in two-phase, turbulent nanofluid flows in solar heaters by corrugated absorber plates, *Adv. Powder Techn.*, 29(2018)2243 – 2254.
- [46] H. K. Bizhaem and A. Abbassi, Numerical study on heat transfer and entropy generation of developing laminar nanofluid flow in helical tube using two-phase mixture model, *Adv. Powder Techn.*, 28(9)(2017), 2110 – 2125.

- [47] S. K. Pal, S. Bhattacharyya and I. Pop, Effect of solid-to-fluid conductivity ratio on mixed convection and entropy generation of a nanofluid in a lid-driven enclosure with a thick wavy wall, *Int. J. Heat and Mass Transf.*, 127(2018)885 – 900.
- [48] M. Sheikholeslami and D.D. Ganji, Entropy generation of nanofluid in presence of magnetic field using lattice Boltzmann method, *Physica A*, 417(2015)273 – 286.
- [49] Y. Wang, Z. Chen and X. Ling, Entropy generation analysis of particle suspension induced by Couette flow, *Int. J. Heat and Mass Transf.*, 90(2015)499 – 504.
- [50] T. Hayat, M. I. Khan, S. Qayyum, M. I. Khan and A. Alsaedi, Entropy generation for flow of Sisko fluid due to rotating disk, *J. Mol. Liq.*, 264(2018)375 – 385.
- [51] S. U. S. Choi, Enhancing Thermal Conductivity of Fluids With Nanoparticles, ASME-Publications-Fed 231(1995)99 – 106
- [52] I. Waini, A. Ishak, I. Pop, Hybrid nanofluid flow and heat transfer over a nonlinear permeable stretching/shrinking surface, *Int. J. Numerical Meth. Heat & Fluid Flow*, (2019)0057
- [53] M. Sheikholeslami, Numerical approach for MHD  $\text{Al}_2\text{O}_3$ -water nanofluid transportation inside a permeable medium using innovative computer method, *Comp. Meth. Appl. Mech. Eng.*344(2019)306 – 318
- [54] E. H. Aly, Dual exact solutions of graphene–water nanofluid flow over stretching/shrinking sheet with suction/injection and heat source/sink: Critical values and regions with stability, *Powder Tech.* 342(2019)528 – 544
- [55] T. Rafiq, M. Mustafa and J. A. Khan, Numerical study of Bödewadt slip flow on a convectively heated porous disk in a nanofluid, *Phys. Scr.* (2019)ab1549.
- [56] S. S. Ghadikolaei, Kh. Hosseinzadeh and D. D. Ganji, Numerical study on magnetohydrodynamic CNTs-water nanofluids as a micropolar dusty fluid influenced by non-linear thermal radiation and Joule heating effect, *Powder Tech.* 340(2018)389 – 399.
- [57] M. Turkyilmazoglu, MHD natural convection in saturated porous media with heat generation/absorption and thermal radiation: closed-form solutions, *Archi. Mech.*, 71(2019)49 – 64.



- [58] M. Ramzan, M. Bilal and J. D. Chung, Effects of thermal and solutal stratification on Jeffrey magneto-nanofluid along an inclined stretching cylinder with thermal radiation and heat generation/absorption, *Int. J. Mech. Sci.* 132(2017)317 – 324
- [59] Y. Ma, R. Mohebbi, M. M. Rashidi and Z. Yang, MHD forced convection of MWCNT–Fe<sub>3</sub>O<sub>4</sub>/water hybrid nanofluid in a partially heated ■-shaped channel using LBM, *J. Therm. Anal. Calorimetry*, 136(2019)1723 – 1735.
- [60] S. Z. Alamri, R. Ellahi, N. Shehzad and A. Zeeshan, Convective radiative plane Poiseuille flow of nanofluid through porous medium with slip: An application of Stefan blowing, *J. Mol. Liq.*, 273(2019)292 – 304.
- [61] K. G. Kumar, B. J. Gireesha, M. R. Krishnamurthy and N. G. Rudraswamy, An unsteady squeezed flow of a tangent hyperbolic fluid over a sensor surface in the presence of variable thermal conductivity, *Results Phys.* 7(2017)3031 – 3036.
- [62] K. Hsiao, Micropolar nanofluid flow with MHD and viscous dissipation effects towards a stretching sheet with multimedia *Int. J. Heat Mass Transf.*, 112(2017)983 – 990.
- [63] T. Hayat, M. Waqas, A. Alsaedi, G. Bashir and F. Alzahrani, Magnetohydrodynamic (MHD) stretched flow of tangent hyperbolic nanoliquid with variable thickness, *J. Mol. Liq.* 229(2017)178 – 184
- [64] S. Qayyum, T. Hayat, S. A. Shehzad and A. Alsaedi, Mixed convection and heat generation/ absorption aspects in MHD flow of tangent-hyperbolic nanoliquid with Newtonian heat/mass transfer, *Rad. Phys. Chem.* 144(2018)396 – 404
- [65] K. Hsiao, To promote radiation electrical MHD activation energy thermal extrusion manufacturing system efficiency by using Carreau-Nanofluid with parameters control method, *Energy*, 130(2017)486 – 499
- [66] M. I. Khan, S. Qayyum, T. Hayat, M. I. Khan, A. Alsaedi and T. A. Khan, Entropy generation in radiative motion of tangent hyperbolic nanofluid in presence of activation energy and nonlinear mixed convection, *Phy. Lett. A*, 382(2018)2017 – 2026
- [67] J. B. J. Fourier, *Theorie Analytique De La Chaleur*, Chez Firmin Didot, Paris (1822).

- [68] C. Cattaneo, Sulla conduzione del calore, *Atti Semin. Mat. Fis. Univ. Modena Reggio Emilia* 3(1948)83 – 101.
- [69] C. I. Christov, On frame indifferent formulation of the Maxwell-Cattaneo model of finite speed heat conduction, *Mech. Res. Commun.*, 36(2009)481 – 486.
- [70] T. Hayat, S. Qayyum, M. Imtiaz and A. Alsaedi, Flow between two stretchable rotating disks with Cattaneo-Christov heat flux model, *Results Phys.* 7(2017)126 – 133.
- [71] J. Sui, L. Zheng and X. Zhang, Boundary layer heat and mass transfer with Cattaneo–Christov double-diffusion in upper-convected Maxwell nanofluid past a stretching sheet with slip velocity, *Int. J. Thermal Sci.*, 104(2016)461 – 468.
- [72] F. M. Abbasi, T. Hayat, S. A. Shehzad and A. Alsaedi, Impact of Cattaneo-Christov heat flux on flow of two-types viscoelastic fluid in Darcy-Forchheimer porous medium, *Int. J. Numer. Meth. Heat Fluid Flow* 27(2017)1955 – 1966.
- [73] S. Saleem, M. Awais, S. Nadeem, N. Sandeep and M. T .Mustafa, Theoretical analysis of upper-convected Maxwell fluid flow with Cattaneo–Christov heat flux model, *Chinese J. Phys.*, 55(2017)1615 – 1625.
- [74] P. K. Kundu, T. Chakraborty and K. Das, Framing the Cattaneo–Christov heat flux phenomena on CNT- based Maxwell nanofluid along stretching sheet with multiple slips, *Arab. J. Sci. Eng.*, (2017)2786 – 6.
- [75] M. Mustafa, An analytical treatment for MHD mixed convection boundary layer flow of Oldroyd-B fluid utilizing non-Fourier heat flux model, *Int. J. Heat Mass Trans.*, 113(2017)1012 – 1020.
- [76] T. Hayat, T. Muhammad and A. Alsaedi, On three-dimensional flow of couple stress fluid with Cattaneo–Christov heat flux, *Chinese J. Phys.*, 55(2017)930 – 938.
- [77] S. J. Liao, *Homotopy Analysis Method in Nonlinear Differential Equations*, Springer, Heidelberg, Germany, 2012.
- [78] S. J. Liao, Notes on the homotopy analysis method: Some definitions and theorems, *Comm. Nonlinear Sci. Num. Simulation* 14(2009)983 – 997.

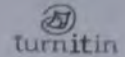
- [79] M. Sheikholeslami, M. Hatami and D. D. Ganji, Micropolar fluid flow and heat transfer in a permeable channel using analytical method, *J. Mol. Liq.* 194(2014)30 – 36
- [80] M. Turkyilmazoglu and I. Pop, Exact analytical solutions for the flow and heat transfer near the stagnation point on a stretching/shrinking sheet in a Jeffrey fluid, *Int. J. Heat Mass Transf.* 57(2013)82 – 88.
- [81] T. Hayat, M. I. Khan, M. Farooq, T. Yasmeen and A. Alsaedi, Stagnation point flow with Cattaneo-Christov heat flux and homogeneous-heterogeneous reactions, *J. Mol. Liq.* 220(2016)49 – 55.
- [82] S. Abbasbandy, E. Shivanian and K. Vajravelu, Mathematical properties of h-curve in the frame work of the homotopy analysis method, *Comm. Nonlinear Sci. Num. Simulation* 16 (2011)4268 – 4275.
- [83] J. Sui, L. Zheng, X. Zhang and G. Chen, Mixed convection heat transfer in power law fluids over a moving conveyor along an inclined plate, *International Journal of Heat and Mass Transfer*, 85(2015)1023 – 1033.
- [84] T. Hayat, S. Qayyum, M. Imtiaz and A. Alsaedi, Impact of Cattaneo-Christov heat flux in Jeffrey fluid flow with homogeneous-heterogeneous reactions, *Plos One*, 11(2016)e0148662
- [85] S. Jabeen, T. Hayat, A. Alsaedi and M. Sh. Alhodaly, Consequences of activation energy and chemical reaction in radiative flow of tangent hyperbolic nanoliquid, *Sci. Iran.* 26(2019)3928 – 3937.
- [86] M. Turkyilmazoglu, Convergence accelerating in the homotopy analysis method: A new approach, *Adv. Applied Math. Mech.* 17(2018) in press.
- [87] A. Jafarimoghaddam, On the homotopy analysis method (HAM) and homotopy perturbation method (HPM) for a nonlinearly stretching sheet flow of Eyring-Powell fluids, *Eng. Sci. Technol. Int. J.* 22(2019)439 – 451.
- [88] H. Y. Martínez and J. F. G. Aguilar, A new modified definition of Caputo—Fabrizio fractional-order derivative and their applications to the Multi Step Homotopy Analysis Method (MHAM), *J. Comp. Appl. Math.* 346(2019)247 – 260

- [89] M. Imtiaz, A. Kiran, T. Hayat and A. Alsaedi, Axisymmetric flow by a rotating disk with Cattaneo-Christov heat flux, *J. Braz. Soc. Mec. Sci. Eng.*, 41(2019)149
- [90] S. Noeiaghdam, E. Zarei and H. B. Kelishami, Homotopy analysis transform method for solving Abel's integral equations of the first kind, *Ain Shams Eng. J.* 7(2016)483 – 495.

Turnitin Originality Report

Computational Analysis for Non-linear Flow Problems with Activation Energy  
Sumaira Jabeen .

by



From DRSM (DRSM L)

- Processed on 31-Aug-2021 08:39 PKT
- ID: 1638642363
- Word Count: 17040

Similarity Index  
19%  
Similarity by Source

Internet Sources:  
12%  
Publications:  
12%  
Student Papers:  
5%

*3/2/2021*  
*7/2/2021*  
**Focal Person (Turnitin)**  
Quaid-i-Azam University  
Islamabad

**sources:**

- 1 1% match (Internet from 29-Aug-2008)  
<http://hal.physast.uga.edu/~jss/1120L/data/CCJD/Lab%20%232/Jupiter25empty.fit>
  - 2 1% match (Internet from 22-Feb-2014)  
[http://iisonline.org/files/uploads/2012/06/220\\_YAO-Kitty\\_and\\_Tony\\_for\\_ShinIIS\\_Yi\\_Kitty\\_Yao\\_v2.pptx](http://iisonline.org/files/uploads/2012/06/220_YAO-Kitty_and_Tony_for_ShinIIS_Yi_Kitty_Yao_v2.pptx)
  - 3 1% match (Internet from 06-Sep-2019)  
<https://link.springer.com/article/10.1007%2Fs13204-019-01064-8>
  - 4 < 1% match (student papers from 18-Jul-2018)  
[Submitted to Higher Education Commission Pakistan on 2018-07-18](#)
  - 5 < 1% match (student papers from 14-May-2018)  
[Submitted to Higher Education Commission Pakistan on 2018-05-14](#)
  - 6 < 1% match (student papers from 01-Mar-2018)  
[Submitted to Higher Education Commission Pakistan on 2018-03-01](#)
  - 7 < 1% match (student papers from 20-Sep-2017)  
[Submitted to Higher Education Commission Pakistan on 2017-09-20](#)
  - 8 < 1% match (student papers from 27-Feb-2021)  
[Submitted to Higher Education Commission Pakistan on 2021-02-27](#)
  - 9 < 1% match (student papers from 30-Jul-2018)  
[Submitted to Higher Education Commission Pakistan on 2018-07-30](#)
- < 1% match (student papers from 12-Nov-2013)